Tero Ahonen

MONITORING OF CENTRIFUGAL PUMP OPERATION BY A FREQUENCY CONVERTER

Thesis for the degree of Doctor of Science (Technology) to be presented with due permission for public examination and criticism in the Auditorium 1382 at Lappeenranta University of Technology, Lappeenranta, Finland on the 27th of May, 2011, at noon.

Acta Universitatis
Lappeenrantaensis 427

Supervisor Professor Jero Ahola
Department of Electrical Engineering
Institute of Energy Technology
Lappeenranta University of Technology
Lappeenranta, Finland

Reviewers Dr. Gunnar Hovstadius
Gunnar Hovstadius Consulting Llc
Westport, USA

Dr. Michal Orkisz
ABB Corporate Research Center
Krakow, Poland

Opponent Professor Sirkka-Liisa Jämsä-Jounela
Laboratory of Process Control and Automation
Department of Biotechnology and Chemical Technology
School of Chemical Technology
Aalto University School of Science and Technology
Espoo, Finland

ISBN 978-952-265-075-7
ISBN 978-952-265-076-4 (PDF)
ISSN 1456-4491

Lappeenrannan teknillinen yliopisto
Digipaino 2011

ABSTRACT

Tero Ahonen

Monitoring of centrifugal pump operation by a frequency converter

Lappeenranta 2011

134 p.

Acta Universitatis Lappeenrantaensis 427

Diss. Lappeenranta University of Technology

ISBN 978-952-265-075-7, ISBN 978-952-265-076-4 (PDF), ISSN 1456-4491

Centrifugal pumps are widely used in industrial and municipal applications, and they are an important end-use application of electric energy. However, in many cases centrifugal pumps operate with a significantly lower energy efficiency than they actually could, which typically has an increasing effect on the pump energy consumption and the resulting energy costs. Typical reasons for this are the incorrect dimensioning of the pumping system components and inefficiency of the applied pump control method. Besides the increase in energy costs, an inefficient operation may increase the risk of a pump failure and thereby the maintenance costs. In the worst case, a pump failure may lead to a process shutdown accruing additional costs.

Nowadays, centrifugal pumps are often controlled by adjusting their rotational speed, which affects the resulting flow rate and output pressure of the pumped fluid. Typically, the speed control is realised with a frequency converter that allows the control of the rotational speed of an induction motor. Since a frequency converter can estimate the motor rotational speed and shaft torque without external measurement sensors on the motor shaft, it also allows the development and use of sensorless methods for the estimation of the pump operation. Still today, the monitoring of pump operation is based on additional measurements and visual check-ups, which may not be applicable to determine the energy efficiency of the pump operation.

This doctoral thesis concentrates on the methods that allow the use of a frequency converter as a monitoring and analysis device for a centrifugal pump. Firstly, the determination of energy-efficiency- and reliability-based limits for the recommendable operating region of a variable-speed-driven centrifugal pump is discussed with a case study for the laboratory pumping system. Then, three model-based estimation methods for the pump operating location are studied, and their accuracy is determined by laboratory tests. In addition, a novel method to detect the occurrence of cavitation or flow recirculation in a centrifugal pump by a frequency converter is introduced. Its sensitivity compared with known cavitation detection methods is evaluated, and its applicability is verified by laboratory measurements for three different pumps and by using two different frequency converters.

The main focus of this thesis is on the radial flow end-suction centrifugal pumps, but the studied methods can also be feasible with mixed and axial flow centrifugal pumps, if allowed by their characteristics.

Keywords: Centrifugal pump, frequency converter, sensorless methods, condition monitoring, diagnostics

UDC 621.671: 621.376.3

ACKNOWLEDGEMENTS

This research project has been carried out during the years 2007–2011 in the LUT Institute of Energy Technology (LUT Energy) at Lappeenranta University of Technology, where I work as a researcher. The project has been funded by ABB Oy and Lappeenranta University of Technology.

I am grateful to my supervisor, Professor Jero Ahola, for his valuable comments, ideas and feedback concerning this thesis and my other scientific publications, which has improved my written output. Especially, I'd like to thank for the support given during the finalisation stage of this thesis.

I thank my reviewers, Dr. Gunnar Hovstadius and Dr. Michal Orkisz. Your feedback and comments have improved the contents of my work, and also made it a better thesis during its finalisation stage. Yet, there are still measurements to be done for the future publications.

I wish to thank Mr. Juha Kestilä and Mr. Matti Kauhanen, who have provided me an opportunity for this research project. Discussions with you have given good ideas for my work, and kept also the practical point of view on my mind during this project. In addition, the guidance and feedback given by Dr. Markku Niemelä and Dr. Julius Luukko is appreciated. I would also like to thank Dr. Hanna Niemelä for her effort to revise the language of this thesis.

During the research project, I have had a pleasure to work with fellow researchers, who have helped me to realise ideas from discussions into actual tests and consequently into scientific papers. Especially, I'd like to thank Mr. Jussi Tamminen and Dr. Risto Tiainen for their help with the laboratory measurements and pilot tests that have been carried out for this project. Mr. Juha Viholainen also deserves thanks for his comments and work concerning our common scientific publications. I would also like to thank all other personnel at our university, who have somehow helped me during my research. For instance, Mr. Erkki Nikku and Mr. Jouni Ryhänen deserve thanks for their help with laboratory devices. Special thanks go, however, to friends, who have ensured that I have remembered to take all the allowed coffee breaks at work.

The financial support provided by Walter Ahlström Foundation, Lauri and Lahja Hotinen Fund, Ulla Tuominen Foundation and Neles Oy 30-year Anniversary Foundation is gratefully appreciated. The product and installation support provided by Sähköliike Tilli & Hakulinen Oy is also greatly valued.

Furthermost, I thank my parents, Pirjo and Aulis, for their support and encouragement throughout my studies.

Lappeenranta, April 2011

Tero Ahonen

For Comfort

For Solace

For Maarit

CONTENTS

ABBREVIATIONS AND SYMBOLS

Roman letters

A	area
E	energy
F	frequency
H	head
M	number of samples
P	pump shaft power, power
R	reliability factor
T	torque
Q	flow rate
Z	vertical distance
d	diameter
g	acceleration due gravity
k	coefficient for the dynamic head, coefficient, discrete-time index
n	rotational speed, speed, discrete-time index
p	pressure
u	peripheral velocity
v	flow velocity
x	discrete-time estimate

Greek letters

Δ	difference
η	efficiency, characteristic life
ρ	density
μ	dynamic viscosity

Subscripts

1	published value, inlet
2	actual value
A	available
AC	alternating component
BEP	best efficiency point
DC	direct component
MEAS	measured
N	normal
NPSH	net positive suction head
QP	values from the pump *QP* characteristic curve
R	required
RMS	root mean square
T, req	torque required by the pump

c	cut-off
d	impeller diameter, discharge
dt	drive train
dyn	dynamic
f	friction losses
in	input power to the pumping system
m	motor
mat	impeller material
n	nominal, rotational speed, value at the nominal speed of the pump
sys	system curve
p	constant pressure
q	specific, relative flow rate
req	required value
s	specific, suction, sampling
ss	suction specific
st	static
total	total
v	vapour

Acronyms

AC	Alternating Component
AOR	Allowable Operating Region
BEP	Best Efficiency Point
BPF	Blade Pass Frequency
DC	Direct Component
EU	European Union
HI	Hydraulic Institute
LCC	Life Cycle Costs
MTBF	Mean Time Between Failures
NI	National Instruments
NPSH	Net Positive Suction Head
POR	Preferred Operating Region
PSD	Power Spectral Density
RI	Reliability Index
RMS	Root Mean Square
SE	Suction Energy
SG	Specific Gravity
VSD	Variable Speed Drive, Variable-Speed-Driven

1 INTRODUCTION

This doctoral thesis discusses the usage of a frequency converter in the condition and operation monitoring of a pumping system comprising a centrifugal pump, an electric motor and a frequency converter. The main objective of this thesis is to present methods that allow the use of a frequency converter as a monitoring and analysis device for the pumping system. The thesis focuses on radial flow end-suction centrifugal pumps that are commonly used in industrial and municipal pumping applications, and with which the laboratory tests have been carried out. However, the methods studied in the thesis can also be applied to other centrifugal pump types, such as mixed and axial flow pumps, if allowed by their characteristics. In this chapter, background and motivation of the study are given. Also the scientific contributions and the outline of the thesis are introduced.

1.1 Background of the study

Fluid transfer is required in countless applications, starting from the everyday use of water. This has created a need for devices that can transfer the fluid without the natural help of gravity. Consequently, pumps are nowadays widely used in industrial and municipal applications, and they are a notable end-use application of electric energy. In the United States, pumping systems account for a quarter of the total electricity consumption in the industrial electric motor systems (DoE, 1998). According to Almeida (2003), the situation is almost equal in the European Union (EU), where 22 % of the industrial motor electricity consumption is caused by pumps (Fig. 1.1). As electric motors are responsible for 69 % of the total electricity consumption in industry, pumps account for 15 % of the total electricity consumption in the European industry (Almeida, 2003).

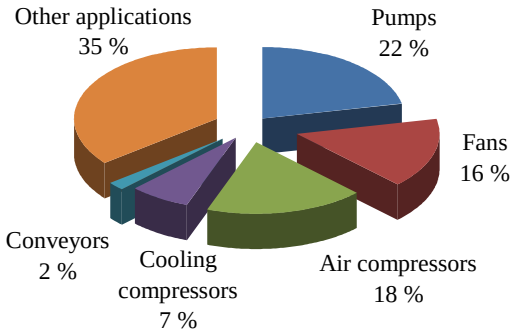

Fig. 1.1: Estimated distribution of the motor electricity consumption according to the end-use in the EU industry. Pumps account for 22 % of the motor electricity consumption in the EU industry (Almeida, 2003).

In many cases, pumps operate with a notably lower efficiency than they could, which has an increasing effect on the pump energy consumption. As the social awareness of environment has increased the public interest in energy efficiency, and pumps often have a notable energy savings potential, optimisation of the pump energy consumption has become a widely studied topic (see e.g. DoE, 1998; Hovstadius, 2005; Binder, 2008). In (DoE, 1998), one of the key findings has been that the major fluid systems (including pumps, fans and air compressors) represent up to 62 % of potential savings in the electricity consumption of industrial electric motor systems. Mentioned actions to realise this savings potential are the improvement of the process system in which the pump is located, the improvement of the pump dimensioning and

the use of a speed control method instead of the throttle or by-pass control method. Hovstadius (2005) has introduced results on how retrofitting pumping systems with frequency converters in a petrochemical company has brought electricity savings of 14 million kWh per annum. However, he has also pointed out that the speed control is not always the most energy efficient control method for the pump, as a speed-controlled pumping system can have a higher specific energy consumption (kWh/m^3) than a similar system operated with the on-off control method. In the survey of Binder (2008), a speed variability of the German pump applications is considered to offer a saving potential of up to 16 TWh per annum, being approximately 3 % of the total electricity consumption in Germany. For a single pumping system, the savings potential in the energy consumption can be in the range of 5–50 %, if a fixed-speed pumping system is retrofitted with a frequency converter (DoE, 1998; Europump, 2004).

Besides the energy costs, the inefficient operation of the pump may also affect the pumping system reliability, since the mechanical reliability of a pumping system is linked to the efficiency of the pump operation, and a pump failure can cause notable additional costs as a result of the production losses (Ahonen, 2007; Barringer, 2003; Bloch, 2010). Consequently, the energy efficient operation of a pumping system is often the key factor also to lower pumping life cycle costs (LCC) (HI, 1999).

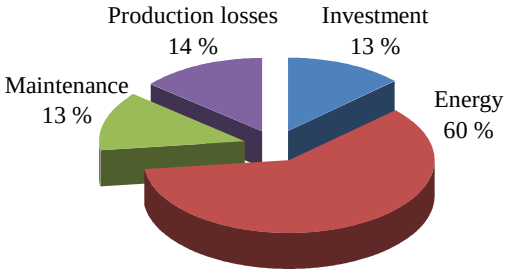

Fig. 1.2: Estimated life cycle cost distribution of an exemplary industrial pumping system comprising a centrifugal pump, an induction motor and a frequency converter (Ahonen, 2007). Commonly, the major proportion of the LCC comes from the energy consumption of the pumping system. In this case, maintenance, production loss and investment costs have been nearly equal.

A typical pumping system consists of a centrifugal pump and an induction motor. Especially in the process industry, a radial flow end-suction centrifugal pump is commonly used because of its simple construction, good reliability, high efficiency and wide range of available capacities (Nesbitt, 2006). In this pump type, the total energy of the fluid is increased by raising the fluid flow velocity with an impeller, which rotates inside the stationary pump casing that transforms the increase in the fluid flow velocity into an increase in the fluid static pressure. Thus, the energy increase can be adjusted by controlling the rotational speed of the pump. In general, the speed control of a centrifugal pump is considered an energy efficient flow control method, as the pump efficiency is not affected by the rotational speed, if the speed change does not alter the relative operating point location of the pump (Europump, 2004; Hovstadius, 2005). However, the speed control of an induction motor requires a variable speed drive (VSD), such as a fluid coupling or a frequency converter into the pumping system.

Without the VSD, the energy increase produced by the pump into the fluid can be controlled by throttling the pump output flow with a valve. This is a traditionally used but an inefficient pump flow control method, as the adjustment of hydraulic losses in the process is utilised to modify the pump flow rate instead of driving the pump with a lower rotational speed and lower power consumption. In addition, the throttling method may more strongly affect the relative pump

operating point location, which can lead to a pump operation with a low efficiency. An example of these two flow control methods is illustrated in Fig. 1.3 with pump and system characteristic curves for the pump head as a function of flow rate. In addition, the shaft power requirement of the pump is shown for both operating points together with the original value. There is a notable difference between the power consumption values, demonstrating the inefficiency of the throttle control method.

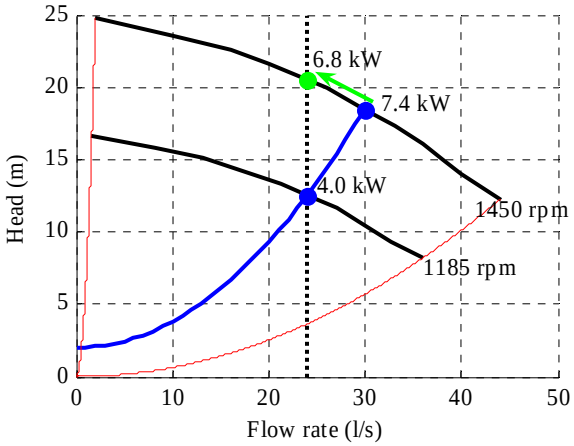

Fig. 1.3: Resulting operating points, when the flow rate is controlled to be 24 l/s either by throttling the flow (indicated by a green arrow and dot) or by adjusting the pump rotational speed (indicated by blue dots). The blue curve represents the system characteristics, and the two thin red curves indicate the edges of the published pump characteristic curves. The flow rate of 24 l/s can be provided with the rotational speed of 1185 rpm instead of throttling the flow when the pump is operating at 1450 rpm. The resulting shaft power requirement of the pump is 6.8 kW for the throttle control method and 4.0 kW for the speed control method, respectively.

Nowadays, owing to their competitive prices and availability for a wide range of motor sizes, frequency converters are the preferred choice for the control of the rotational speed of an induction motor. Frequency converters are also applied in the control of centrifugal pumps, as their prices are competitive with fluid couplings, and they provide an option to drive the pump at rotational speeds above the motor nominal value, if this is allowed by the motor and frequency converter loadability.

In a frequency converter, the frequency and amplitude of the motor supply voltage is adjusted so that the induction motor operates at the desired speed. In general, this is performed by an inverter circuit, which typically consists of insulated gate bipolar transistors. The inverter circuit operation is controlled by a scalar, vector or direct torque control method, which is implemented in the control electronic circuits of the converter. In addition to the control of the motor rotational speed, a frequency converter can estimate the rotational speed and shaft torque of an induction motor without additional measurements from the motor shaft (see e.g. Tiitinen, 1996; Nash, 1997; Vas, 1998; Durán, 2006).

As the performance of microprocessors and embedded systems has greatly increased over the last four decades, implementation of additional functions for monitoring and control of pumping systems has become possible without affecting the price of a frequency converter. To the author's knowledge, frequency converters with sensorless pump monitoring and control functions have been available from Armstrong since 2001, and from Lowara since 2003,

respectively (Armstrong, 2010; Hydrovar, 2003). Nowadays, the sensorless pump control functions have become more common, and for instance ABB and ITT provide frequency converters with a function for the sensorless calculation of the pump flow rate (Hammo, 2005). ITT applies the sensorless flow rate calculation to detect the pump operation with an insufficient or excessive flow rate (Hovstadius, 2001; ITT, 2006). The corresponding protection algorithm can also be found from the frequency converters manufactured by Danfoss (Danfoss, 2009). In addition, a modern frequency converter can be configured to monitor internal and external measurements (e.g. rotational speed, vibration or pressure) and warn the user, if a pre-set threshold value and a time criterion are reached. Another typical example of a monitoring function is the trend-logging of pump and motor operational values, such as the rotational speed and flow rate.

Fig. 1.4: Frequency converters of the laboratory setup used in this study. Modern frequency converters include several pump-related monitoring and control functions, such as the sensorless calculation of the pump flow rate.

However, the scientific research concerning the use of frequency converters with centrifugal pumps has mainly concentrated on the energy efficiency of the speed control method. For instance, the effect of the flow control method on the pump power consumption and the resulting energy costs have been studied in (Carlson, 1999; Hovstadius 2005; Kneip, 2005). New methods for the control of parallel-connected pump systems by a frequency converter have been proposed in (Bartoni, 2008; Ma, 2009; Viholainen, 2009). Research has also been carried out concerning the use of frequency converters in the electric motor diagnostics (Tiainen 2006, 2007; Orkisz, 2008a, 2008b, 2009), but only a few articles have concentrated on the diagnostics of pumping systems by a frequency converter (Stavale, 2001; Discenzo, 2002; Ahonen, 2008a). To the author's knowledge, sensorless estimation accuracy of the pump operating location by a frequency converter has been discussed only by Hammo (2005; 2006) and Ahonen (2009b, 2010b). It is also mentioned in (Europump, 2004), but only in the connection with controlling the pump flow by using the flow rate vs. power characteristic curve. Correspondingly, the discussion concerning the factors that affect the applicability of the sensorless estimation methods is rather limited, as only some general guidelines are given in the manuals of ABB and ITT frequency converters.

1.2 Motivation of the study

Centrifugal pumps are used in a variety of industrial and municipal applications. Typically, centrifugal pumps are a part of a larger system, and hence their reliability may affect the system reliability and productivity. In the worst case, a pump failure may lead to a process shutdown resulting in excessive costs (see Fig. 1.2). For this reason, production-critical pumps are often monitored periodically or continuously with vibration, temperature and other condition monitoring measurements. The pump head and flow rate might also be measured to determine the actual pump operating point location and the resulting efficiency. In addition, production-critical applications can be equipped with backup pumps that are started if the operating pump fails. However in practice, the major part of pumping systems may only have a motor phase current and a process-related measurement, which do not directly indicate the operational efficiency and mechanical reliability of a pump.

Nowadays, there are numerous condition and efficiency monitoring products available for pumping systems, most of which, however, share a common approach: additional measurements are required from the pump. Since the installation of additional measurement sensors may be costly and the sensors can also reduce the pumping system reliability, they are not always the most cost-effective solution for the condition monitoring of a pump. Partially for this reason, the maintenance of pumping systems in paper mills is still often based on regular check-ups, in which the efficiency of pump operation is not typically inspected. Consequently, it is likely that the inefficient or service life decreasing operation of the pump may remain undetected, until it causes a mechanical failure, increasing both the energy and maintenance costs of the pump. This problem can occur both with the fixed-speed and variable-speed-driven (VSD) centrifugal pumps: although the speed control method is generally considered as an energy efficient control approach, the actual operating point locations of a VSD pump may well be found in regions with a lower pump efficiency and higher risk for a mechanical failure of the pump, which may remain undetected by visual check-ups.

If the pumping system is equipped with a frequency converter, it can be utilised as a monitoring device of a centrifugal pump. As discussed in (Ahonen, 2008a), a frequency converter already provides a hardware with standard measurement and communication interfaces, which can be utilised to monitor the pump operation and to transfer the analysis results from the converter to the process control system. Often the frequency converter may be connected to a communication system, allowing the readout of converter estimates without additional configuration.

Besides the feasible hardware, also software consisting of algorithms and analysis methods is required to determine the pump operating point location and possibly the occurrence of adverse events, which may lead to a pump failure. The motivation of this study has arisen from the lack of previous scientific research concerning the use of a frequency converter in the condition and operation monitoring of a pumping system. Although there are already commercial products with monitoring and protection algorithms available, only a few scientific articles have been published concerning the sensorless calculation of the pump flow rate. Correspondingly, the sensorless diagnostics of centrifugal pump operation by a frequency converter has been previously discussed only in few papers (Ahonen, 2008a, 2010c).

In this thesis, methods related to the analysis of pumping system operation by a frequency converter are studied in order to allow the wider use of a frequency converter as a monitoring and analysis device of a centrifugal pump. With the studied methods, the energy efficiency of pumping system operation and the occurrence of service life decreasing events can be

automatically determined. Compared with the previous research, this thesis firstly studies the use of generic energy-efficiency- and reliability-based criteria in the determination of the recommendable operating region of a VSD centrifugal pump. Although the concept of the recommendable operating region for a centrifugal pump and the factors limiting this operating region are well-known in the literature (see e.g. ANSI/HI, 1997; Gülich, 2008), to the author's knowledge, determination of this operating region especially for a variable-speed-driven pump has not been previously studied. The most probable reason for this is the difficulty of setting the actual limit values between different operating regions, requiring extensive research on the topic. Correspondingly, estimation of the pump operating point location by a frequency converter is already known in the literature and in commercial applications (ITT, 2006), but only a few publications with test results are available concerning the accuracy of different estimation methods (Hammo, 2005, 2006; Ahonen 2009b, 2010b). In addition, there is no detailed publication available concerning the factors that affect the estimation accuracy of the methods for the pump operating point location, which is the reason why the topic is discussed in this thesis. Correspondingly, this thesis studies the detection of cavitation or flow recirculation occurrence by a frequency converter and without additional sensors, which has not been previously discussed in scientific publications.

1.3 Objectives of the study

The main objective of this study is to present and research methods that allow the use of a frequency converter as a monitoring and analysis device of a centrifugal pump. These methods utilise the estimates for the rotational speed, shaft torque and power of the induction motor connected to the pump. This study is focused on radial flow end-suction centrifugal pumps that are commonly used in process industry, but the methods can also be applied to other centrifugal pump types, such as mixed and axial flow pumps, if allowed by their characteristic curves and other properties.

The objective of this study has not been the implementation of the methods into an existing frequency converter, but rather their demonstration and analysis by laboratory measurements. The studied methods are closely related to each other, providing first the basic information on the operating region, in which the pump should be driven. Related to this, estimation methods for the pump operating point location are studied. Moreover, factors that may limit their applicability in practice are introduced. Together with the limits for the recommendable operating region, recommendability of the pump operation can be assessed on the basis of the estimated pump operating point location. In addition, a method to detect the occurrence of cavitation or flow recirculation by a frequency converter is studied to determine whether a frequency converter could also be applied in the detection of service life decreasing events occurring in the pump.

With the methods introduced in this study, the energy efficiency of the pump operation and the occurrence of service life decreasing events can be automatically determined by a frequency converter and without additional measurements. For instance, an analysis system could be constructed on the basis of studied methods to determine the general quality of the instantaneous pump operation. An example of such an analysis system is illustrated in Fig. 1.5, in which the analysis of the pumping system operation is carried out by utilising the methods discussed in this thesis. The generation of an analysis system is not discussed in this thesis, but its need is considered in the suggestions for future work.

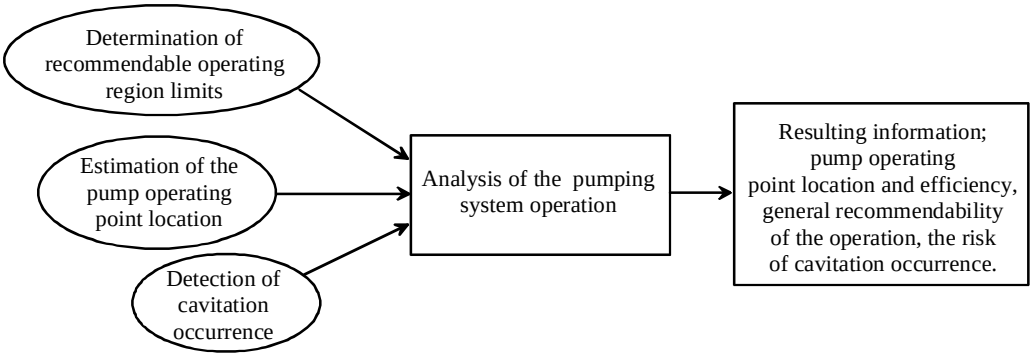

Fig. 1.5: Block diagram of an exemplary analysis system for a pumping system. This thesis discusses the methods that are required to determine the recommendable operating region of a VSD centrifugal pump, to estimate the present operating point location of a centrifugal pump, and to detect the occurrence of service life decreasing events in the pumping system (e.g. the occurrence of cavitation). Together the studied methods provide basic information for the analysis of the pumping system operation.

1.4 Scientific contributions

The main scientific contributions of this thesis include the following:

- The use of generic energy-efficiency- and reliability-based criteria in the determination of the recommendable operating region of a VSD centrifugal pump is studied. Relative specific energy consumption of a pumping system is proposed as the main variable for the energy-efficiency-based determination of the recommendable operating region. It is shown by a laboratory case study how the limits could be determined for the pump.

- An analysis of three known model-based estimation methods (i.e., *QH*, *QP* and system curve methods) for the pump operating point location is provided. Factors that may affect the accuracy of these methods are addressed. The methods are evaluated by laboratory measurements with a radial flow centrifugal pump. Pilot tests are also carried out with the *QP*-curve-based estimation method.

- A novel method to detect the occurrence of cavitation or flow recirculation by a frequency converter is proposed, which can be regarded as the main novelty of this thesis. The method is based on the estimates available for the rotational speed and shaft torque of the motor. The known methods to detect cavitation are tested in comparison with the proposed method.

- The effects of cavitation on the rotational speed and shaft torque estimates provided by the frequency converter are determined by laboratory measurements for three different pumps. Also the effect of a frequency converter on the estimation results is evaluated by using two different frequency converters in the laboratory measurements.

- The feasibility of the proposed method to detect flow recirculation is shown by the results of the conducted laboratory measurements.

The author has also published research results related to the subjects covered in the doctoral thesis in the following publications:

1) J. Ahola, T. Ahonen and J. Tamminen, "Diagnostics of Electrical Drive Systems," in *Proceedings of the 3rd International Seminar on Maintenance, Condition Monitoring and Diagnostics*, Oulu, Finland, 29–30 September 2010, pp. 109–119, (Ahola, 2010).

2) T. Ahonen, J. Tamminen, J. Ahola and J. Kestilä, "Novel Method for Detecting Cavitation in Centrifugal Pump with Frequency Converter," in *Proceedings of the 7th International Conference on Condition Monitoring and Machinery Failure Prevention Technologies (CM and MFPT 2010)*, Stratford-upon-Avon, UK, 22–24 June 2010, pp. 1–13, (Ahonen, 2010c).

3) T. Ahonen, J. Tamminen, J. Ahola, J. Viholainen, N. Aranto and J. Kestilä, "Estimation of Pump Operational State with Model-Based Methods," *Energy Conversion and Management*, Vol. 51, Iss. 6, June 2010, pp. 1319–1325, (Ahonen, 2010b).

4) T. Ahonen, J. Tamminen, J. Ahola and J. Kestilä, "Sensorless Pump Operation Estimation," in *Proceedings of the 13th European Conference on Power Electronics and Applications (EPE 2009)*, Barcelona, Spain, 8–10 September 2009, pp. 1–10, (Ahonen, 2009b).

5) T. Ahonen, J. Ahola, J. Tamminen and J. Kestilä, "Consideration of Recommended Operating Region for Inverter-Driven Pumps," in *Proceedings of the 6th International Conference on Condition Monitoring and Machinery Failure Prevention Technologies (CM and MFPT 2009)*, Dublin, Ireland, 23–25 June 2009, pp. 951–962, (Ahonen, 2009a).

6) N. Aranto, T. Ahonen and J. Viholainen, "Energy Audits: University Approach with ABB," in *Proceedings of the 6th International Conference on Energy Efficiency in Motor Driven Systems (EEMODS '09)*, Nantes, France, 14–17 September 2009, (Aranto, 2009).

7) J. Viholainen, J. Kortelainen, T. Ahonen, N. Aranto and E. Vakkilainen, "Energy Efficiency in Variable Speed Drive (VSD) Controlled Parallel Pumping," in *Proceedings of the 6th International Conference on Energy Efficiency in Motor Driven Systems (EEMODS '09)*, Nantes, France, 14–17 September 2009, (Viholainen, 2009).

8) T. Ahonen, R. Tiainen, J. Viholainen, J. Ahola and J. Kestilä, "Pump Operation Monitoring Applying Frequency Converter," in *Proceedings of the 19th International Symposium on Power Electronics, Electrical Drives, Automation and Motion (SPEEDAM 2008)*, Ischia, Italy, 11–13 June 2008, pp. 184–189, (Ahonen, 2008a).

9) T. Ahonen, J. Ahola, J. Kestilä, R. Tiainen and T. Lindh, "Life Cycle Cost Analysis of Inverter-Driven Pumps," in *Proceedings of the 20th International Congress on Condition Monitoring and Diagnostic Engineering Management (COMADEM 2007)*, Faro, Portugal, 13–15 June 2007, pp. 397–405, (Ahonen, 2007).

T. Ahonen has been the primary author in publications 2–5 and 8–9. The background research and test measurements for publications 2–5 have been carried out together by T. Ahonen and Mr. J. Tamminen. Background research for publications 8 and 9 was done together by T. Ahonen and Dr. R. Tiainen. T. Ahonen was in the major role in the writing of the publications 2–5 and 8–9, with the help of the co-authors.

For publications 1, 6 and 7, T. Ahonen has participated in the background research and writing of the article.

The author is also designated as a co-inventor in the following patent applications considering the subjects presented in this doctoral thesis:

US Patent application 13/024,705 "Method in Connection with a Pump Driven with a Frequency Converter and a Frequency Converter". Application filed 10 February 2011, (Ahonen, 2011).

EU Patent application 10153168.9-1267 "Method in Connection with a Pump Driven with a Frequency Converter and a Frequency Converter". Application filed 10 February 2010, (Ahonen, 2010a).

US Patent application 12/628,669 "Method and System for Detecting Cavitation of Pump and Frequency Converter". Application filed 1 December 2009, (Ahonen, 2009c).

EU Patent application 08171028.7-2315 "Method and System for Detecting Cavitation of Pump and Frequency Converter". Application filed 9 December 2008, (Ahonen, 2008b).

1.5 Outline of the thesis

This doctoral thesis studies the estimation of a radial flow centrifugal pump operation utilising the information available from a frequency converter. Firstly, the theoretical background concerning variable-speed-driven centrifugal pumps is given, and the use of generic energy-efficiency- and reliability-based criteria in the determination of the recommendable operating region of a VSD centrifugal pump is studied. Then, three model-based methods applicable to the estimation of the pump operating point location are discussed. Their applicability is evaluated by laboratory measurements. A novel method to detect the occurrence of cavitation or flow recirculation in a centrifugal pump is introduced. Its sensitivity for cavitation detection is evaluated together with known detection methods. The feasibility of the proposed method is evaluated by laboratory measurements with three different pumps and two different frequency converters.

The rest of the thesis is divided into the following chapters:

Chapter 2 is devoted to the basic theory of variable-speed-driven pumps. The parts of a pumping system are introduced. The use of generic energy-efficiency- and reliability-based criteria in the determination of the recommendable operating region of a VSD centrifugal pump is investigated. It is shown by a case study for the laboratory pumping system how the limits of the recommendable operating region could be determined.

Chapter 3 addresses model-based methods for the estimation of the operating point location of a centrifugal pump. The methods presented in this chapter utilise information from a frequency converter. Factors affecting the accuracy and feasibility of the estimation methods are reviewed. Model-based methods are evaluated by laboratory tests for a radial flow centrifugal pump. Results from two pilot installations are also introduced.

Chapter 4 discusses methods to detect the occurrence of cavitation or flow recirculation in a centrifugal pump. A novel method to detect the occurrence of cavitation or flow recirculation by a frequency converter is proposed. The method is based on the monitoring of rotational

speed and shaft torque estimates provided by the converter. Sensitivity of the proposed method is compared with other published methods for cavitation detection. The method is also evaluated by laboratory measurements for three different centrifugal pumps.

Chapter 5 is the concluding chapter of this doctoral thesis. It provides the conclusions and suggestions for future work.

2 OPERATION OF VARIABLE-SPEED-DRIVEN PUMPS

In this chapter, theory concerning variable-speed-driven pumps is discussed. The parts of a typical pumping system are introduced. The use of generic energy-efficiency- and reliability-based criteria in the determination of the recommendable operating region of a VSD centrifugal pump is investigated with a case study for the laboratory pumping system.

2.1 Parts of a typical pumping system

A variable-speed-driven (VSD) pump typically refers to a centrifugal pump that is driven by an electric motor and a frequency converter, which enables the speed adjustment of the pump-motor combination. A typical structure of such a pumping system is illustrated in Fig. 2.1, where the centrifugal pump is located in a process system consisting of pipes, tanks and valves. An electric motor is directly connected to the pump with a shaft coupling. A frequency converter is typically located in a separate facility with an electric supply. In addition, a pumping system may be equipped with measurement sensors that are used for control and monitoring purposes.

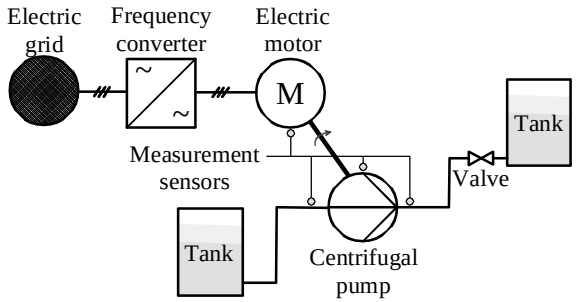

Fig. 2.1: Structure of a pumping system located in a process system. A centrifugal pump and an electric motor may be equipped with measurement sensors for control and monitoring purposes.

In a **centrifugal pump**, the energy of the fluid is increased by increasing the flow velocity with a rotating impeller, which generates the fluid flow. The impeller is located inside the pump casing, in which the increased flow velocity of the fluid is converted into increased static pressure. Centrifugal pumps can be divided into different categories depending on their impeller and casing designs and the direction of the resulting fluid flow. The most common pump type is a single-volute end-suction radial flow pump that is often simply referred to as a radial flow centrifugal pump. A typical construction of this pump type is illustrated in Fig. 2.2. In the radial flow centrifugal pump, the impeller has radial vanes, which lead the incoming flow from the pump suction into the outer edge of the impeller and further into the volute casing. The impeller is connected to the pump shaft, which is supported by ball and roller bearings. The shaft also has a sealing system around it, which prevents uncontrolled leakage of the pumped fluid outside the pump. This pump type is widely used especially in the process industry, and hence this thesis focuses on single-volute end-suction radial flow pumps (Nesbitt, 2006).

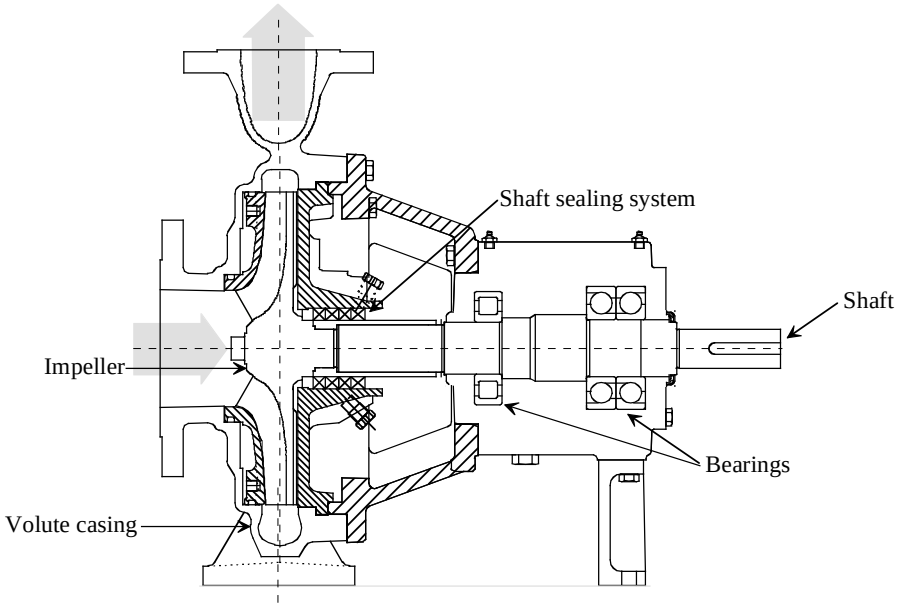

Fig. 2.2: Cross-section of a single-volute end-suction radial flow centrifugal pump (Sulzer, 2006a). The direction of flow is illustrated with grey arrows from the suction to the discharge side of the pump.

The most typical electric motor type applied to a centrifugal pump is an **induction motor** because of its simple construction, good reliability and a fairly good efficiency (Karassik, 1998). In addition, the rotational speed of an induction motor can be controlled accurately enough with a frequency converter: in the pumping applications, there is typically no need for accurate control of rotational speed, which favours the use of an induction motor with the centrifugal pump.

An induction motor consists of a stator core and stator windings located in the motor frame, a rotor connected to the motor shaft, bearings that support the shaft and a ventilation fan connected to the non-driving end of the motor shaft. Typically, nominal values of the torque, rotational speed and shaft power ($T_{m,n}$, $n_{m,n}$ and $P_{m,n}$, respectively) are given for the motor. Manufacturers also publish the motor efficiencies at 75 and 100 percent of the nominal load torque with information on the efficiency class of the motor: in the European Union, the IE classification scheme is now in use, where the IE2 efficiency class is comparable with the old EFF1 efficiency classification and it is identical with the EPact efficiency class applied in the United States (IEC, 2008). The use of higher-efficiency motors with an IE3 or a NEMA Premium efficiency classification will be mandated in both continents to improve the energy efficiency of motor-driven applications (USC, 2007; EC, 2009).

In general, an induction motor is operating at the maximum efficiency, when the load torque is approximately 75 percent of the nominal value $T_{m,n}$. The efficiency of an IE2 or IE3 induction motor typically remains nearly at this level also at lower relative loads, until the relative load torque goes below 25–35 %, and no-load core and copper losses start to decrease the motor efficiency. The same applies also to induction motors having a NEMA Premium efficiency class, which is identical with the IE3 efficiency class applied in Europe (IEC, 2008). As an example, the nominal efficiency of 3–250 kW sized induction motors that have the IE3 efficiency label is in the range of 88–96 % (IEC, 2008).

The motor efficiency will also decrease when it is driven at a low rotational speed because of the larger proportion of constant-valued losses. As the pump load torque curve has a squared relationship with the rotational speed, the resulting motor efficiency may be considerably decreased when a centrifugal pump is driven at a lower speed (Abrahamsen, 2000). Motor efficiencies under varying speeds and loads have also been studied in (Angers, 2009; Burt, 2008; Viholainen, 2009) with similar conclusions. In Fig. 2.3, an example of measurement results for a four-pole 2.2 kW, 14 Nm induction motor has been illustrated, when the motor has been driven with a frequency converter, which produces a constant air-gap flux at partial load torques.

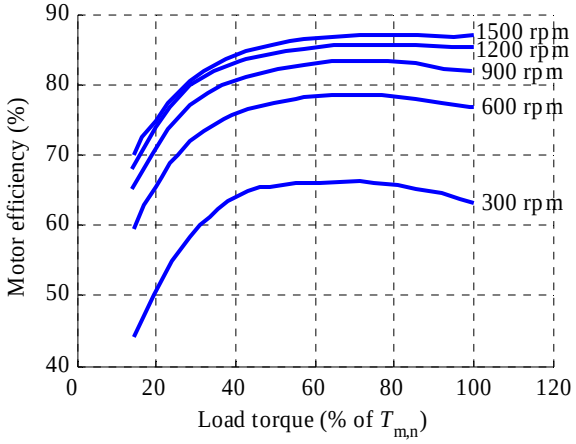

Fig. 2.3: Effect of rotational speed and load torque on the efficiency of a four-pole 2.2 kW induction motor ($T_{m,n}$ = 14 Nm), when it is driven with a frequency converter. A decrease in the rotational speed degrades the motor efficiency. In every case, the motor efficiency reduces considerably, when the relative load torque decreases below 50 percent. In these measurements, an air-gap flux was held constant at partial load torques (Abrahamsen, 2000). It should be noted here that the efficiency curves of larger IE2 and IE3 induction motors are typically flatter, and the critical value of relative load torque, below which the motor efficiency starts to decrease, can be for instance 25–35 %. In Europe these efficiency classes, as the NEMA Premium efficiency class in the United States, become mandatory for new induction motors in years 2011 and 2010, respectively.

A **frequency converter** enables the speed control of an induction motor. A typical frequency converter consists of a rectifier, a dc link capacitor and an inverter, which is controlled based on the required rotational speed of the induction motor. As in the case of induction motors, the efficiency of a frequency converter is affected by the converter size and the amount of required speed and torque. The maximum efficiency of a frequency converter depends on the converter size being in the range of 92–98 %, when the nominal output is 1–400 kW (IEC, 2009a). If the motor is driven at a partial torque or a low rotational speed, this has a decreasing effect on the efficiency of a frequency converter as shown in Fig. 2.4.

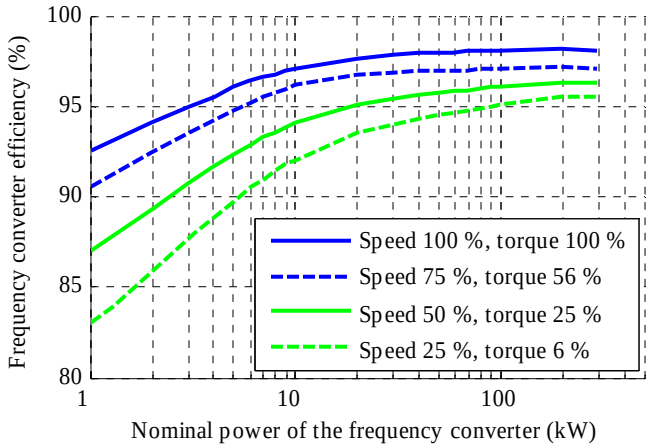

Fig. 2.4: Effect of the converter size, the motor speed and the motor torque on the efficiency of a frequency converter. Operation at a partial speed and load torque decreases the converter efficiency (IEC, 2009a).

The characteristics of a frequency converter also affect the motor efficiency: a frequency converter cannot supply a purely sinusoidal voltage waveform, which results in additional losses in the motor. On the other hand, a frequency converter may contain a flux optimisation function that controls the amount of stator flux in order to minimise the amount of losses in the motor and in the frequency converter, when the motor is driven at a partial load (Abrahamsen, 2000; Bose, 2002; Ghozzi, 2004). For these reasons, the effect of a frequency converter on the motor efficiency should be taken into account by utilising the drive train efficiency term η_{dt}, which is the combined efficiency of the motor and the converter. However, only the nominal efficiency of a frequency converter is typically published, since standards concerning the testing procedure of frequency-converter-driven motors are at the moment in the draft phase (IEC, 2009b).

2.1.1 Basic concepts of centrifugal pumps

Operational characteristics of a centrifugal pump are typically described by characteristic curves for the produced head H, the efficiency η and the shaft power consumption P as a function of flow rate Q at a constant speed n_n (Karassik, 1998). The location of the pump operating point is shown by the pump flow rate Q and the pump head H, which corresponds to the total pressure difference across the pump expressed as the column height of the pumped fluid. The operating point in which the pump efficiency attains its maximum value is called the best efficiency point (BEP) of a centrifugal pump. Depending on the size and design of the pump, the maximum practically attainable efficiency of a centrifugal pump is in the range of 77–88 %, when the Q_{BEP} is 5–50 l/s (Europump, 1999). The efficiency of a centrifugal pump can be calculated, if the operating point location and shaft power consumption of the pump are known with the fluid density ρ:

$$\eta = \frac{\rho \cdot g \cdot Q \cdot H}{P}, \tag{2.1}$$

where g is the acceleration due gravity.

In addition, pump manufacturers publish the flow rate vs. the net positive suction head required ($NPSH_R$) curve, which indicates the required head at the pump suction to avoid the fluid cavitation in a centrifugal pump. Traditionally, an $NPSH_R$ curve is defined by measuring the total suction pressure values, which result in a 3 % decrease in the pump head, when the pump is operating at a constant speed and flow rate (Karassik, 1998). According to (Sulzer, 2000), the published $NPSH_R$ curve may also indicate the minimum allowed flow rate in the continuous use.

The published characteristic curves of a Sulzer APP22-80 centrifugal pump are shown in Fig. 2.5 for four different impeller diameters (210–266 mm) at the 1450 rpm rotational speed. In the case of a 250 mm impeller diameter, the best efficiency point (BEP) of the Sulzer pump is approximately at the 26 l/s flow rate and the 16 m head, which results in a 73 % efficiency value.

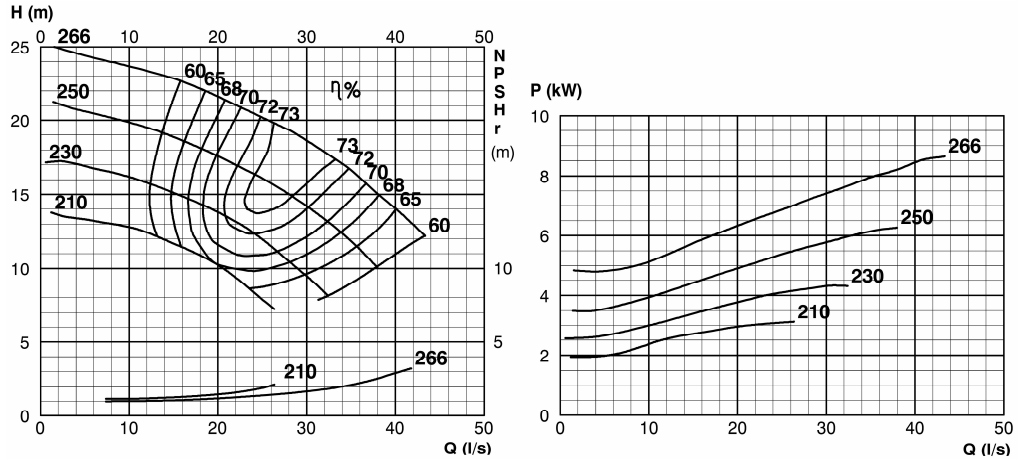

Fig. 2.5: Published characteristic curves of a Sulzer APP22-80 centrifugal pump with four different impeller diameters (Sulzer, 2006b). The flow rate values are given in litres per second (l/s), which is a commonly applied unit of flow rate in the case of centrifugal pumps.

In practice, the efficiency of pump operation is often quantified by the relative flow rate (i.e., Q/Q_{BEP}) and efficiency η of the pump. The pump operation can also be quantified by calculating its specific energy consumption E_s (kWh/m^3), which is especially useful to determine the energy efficiency of different pump flow control methods (Europump, 2004; Hovstadius, 2005). Typically, E_s equals the consumed electric energy per flow volume, which can be determined by

$$E_s = \frac{P_{in}}{Q}, \tag{2.2}$$

where P_{in} is the electric power consumed by the pumping system. Since the magnitude of E_s is affected by the losses in the system, it also encourages designers to minimise these losses already before the purchase of the pump.

If the rotational speed of a centrifugal pump deviates from the nominal value n_n, it affects the pump characteristic curves according to the affinity rules:

$$Q = \left(\frac{n}{n_n} \right) \cdot Q_n \tag{2.3}$$

$$H = \left(\frac{n}{n_n} \right)^2 \cdot H_n \tag{2.4}$$

$$P = \left(\frac{n}{n_n} \right)^3 \cdot P_n \tag{2.5}$$

$$\mathrm{NPSH_R} = \left(\frac{n}{n_n} \right)^2 \cdot \mathrm{NPSH_{R,n}}, \tag{2.6}$$

where n is the present rotational speed of the pump and the subscript $_n$ denotes the operational value at the nominal speed n_n of the pump (Karassik, 1998). According to (Europump, 2004), $\mathrm{NPSH_R}$ has a certain minimum level, so $\mathrm{NPSH_R}$ does not tend to reach zero at a very small rotational speed. The pump efficiency is typically approximated to be independent of rotational speed, and for this reason, the efficiency lines in published pump curves follow the affinity equations (2.3) and (2.4). It should be noted that these rules do not directly predict the pump operating point location at different rotational speeds, as the resulting operating point locations are also affected by the system curve shape.

The actual diameter of the pump impeller may differ from the published characteristic curves. In such a case, the characteristic curves of a centrifugal pump can be converted into the actual impeller diameter with the corresponding scaling laws (Gülich, 2008). If two different pumps with impeller diameters d_1 and d_2 are geometrically similar, the resulting characteristic curves can be approximated by the similarity laws

$$Q_2 = \left(\frac{d_2}{d_1} \right)^3 \cdot Q_1 \tag{2.7}$$

$$H_2 = \left(\frac{d_2}{d_1} \right)^2 \cdot H_1 \tag{2.8}$$

$$P_2 = \left(\frac{d_2}{d_1} \right)^5 \cdot P_1 . \tag{2.9}$$

In practice, the impeller diameter is typically reduced just by trimming the original impeller with no modification of the pump casing. This may alter the impeller geometry, which in turn can have an unexpected effect on the pump performance. For this reason, only empirical equations have been presented for the effect of impeller trimming on the pump performance (Gülich, 2008). A widely used approximation is the linear relationship between the impeller diameter and pump flow rate, resulting in a cubic relationship for the pump power consumption

ratio as a function of the impeller diameter, being similar with (2.5) (Europump, 2004). According to (Sulzer, 1998), the effect of impeller trimming can be approximated by

$$Q_2 = \left(\frac{d_2}{d_1} \right)^k \cdot Q_1 \tag{2.10}$$

$$H_2 = \left(\frac{d_2}{d_1} \right)^k \cdot H_1 , \tag{2.11}$$

where $k = 3$ for relative diameter corrections less than one percent and $k = 2$ for relative diameter corrections over six percents. Consequently, these equations propose that the similarity laws (2.7)–(2.9) may be as applicable to the determination of the pump characteristic curves as other known approximations for the impeller diameter's effect on the pump characteristic curves, although they are originally determined for geometrically similar pumps.

For the comparison of different centrifugal pumps, dimensionless numbers representing the pump operating characteristics have been defined. Specific speed n_q represents the performance of a centrifugal pump regardless of its size. For instance, the impeller geometry and the characteristic curve shapes of a centrifugal pump are affected by the specific speed value as shown in Fig. 2.6. Therefore, n_q can also describe the internal structure of the pump.

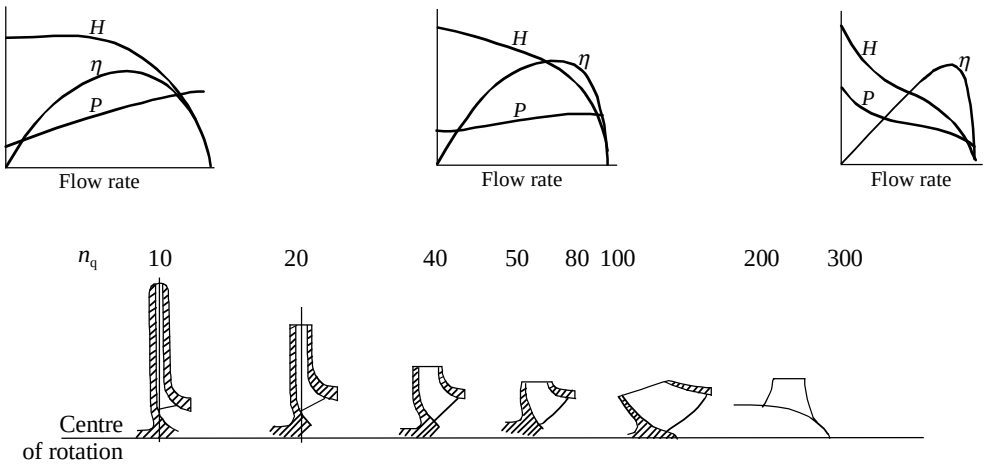

Fig. 2.6: Effect of the pump specific speed n_q on the characteristic curves and the impeller geometry of a centrifugal pump. The direction of flow changes from radial to axial with an increasing specific speed value (Karassik, 1998).

Correspondingly, the suction specific speed n_{ss} represents the suction capability of a centrifugal pump regardless of its size. It also represents the risk of flow recirculation at partial flow rates ($Q < Q_{BEP}$): in general, a higher value of n_{ss} means a higher risk of flow recirculation at a partial flow rate. According to (Bloch, 2010), the magnitude of n_{ss} can also indicate the possible severity of cavitation occurrence in the pump.

Values for specific and suction specific speed are often calculated using inconsistent units, and even the applied equations may vary. In this thesis, the following equations and units are applied:

$$n_{\mathrm{q}} = \frac{n\sqrt{Q}}{H^{0.75}} \tag{2.12}$$

$$n_{\mathrm{ss}} = \frac{n\sqrt{Q}}{\mathrm{NPSH}_{\mathrm{R}}^{0.75}}, \tag{2.13}$$

where the unit of rotational speed is rpm, the flow rate unit is m^3/s, and the head values are in metres. n_q and n_{ss} should be calculated by applying the BEP values of the pump.

When a centrifugal pump is connected to a process system, its present operating point location is determined by the intersection of the pump and system *QH* curves. For this reason, the shape of the system *QH* curve has a direct effect on the operational values of a centrifugal pump at different speeds. In general, the system curve consists of the static head H_{st} and the dynamic head H_{dyn}. The shape of the system curve can typically be described by the following equations:

$$H_{\mathrm{sys}} = H_{\mathrm{st}} + H_{\mathrm{dyn}} \tag{2.14}$$

$$H_{\mathrm{dyn}} = k \cdot Q^2, \tag{2.15}$$

where *k* is the coefficient for the dynamic head.

In the ideal case for a VSD pump, the system curve consists mainly of the dynamic head, and the pump typically operates at its best efficiency point. Then, the operating points can remain close to the pump best efficiency point, although the pump rotational speed would be changed from its typical value. If the system curve has a notable share of static head, a change in the rotational speed can change the operating point into a location with a lower efficiency. For this reason, the speed control method is especially advised for the pumps having a system curve with a small portion of static head (Europump, 2004; Hovstadius, 2005). An example of the resulting operating point locations with two different system curve shapes is given in Fig. 2.7.

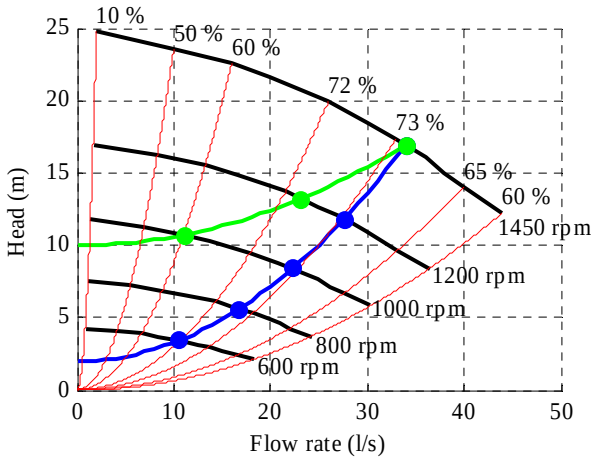

Fig. 2.7: Resulting operating points, when the system curve shape varies and the pump is driven at different rotational speeds. The effect of rotational speed on the pump *QH* curve is taken into account with affinity equations.

2.2 Recommendable operating region of a variable-speed-driven centrifugal pump

It is traditionally advised to drive a centrifugal pump at its best efficiency point in order to optimise the pump energy consumption based on its efficiency. In addition, the risk of cavitation and the amount of hydraulic excitation forces caused by the pressure distribution on the impeller are typically minimised near the BEP, meaning maximised pump reliability in this operating region (Barringer, 2003; Bloch, 2010; Gülich, 2008; Nelik, 2005). Hence, the range around the pump BEP is often called the recommendable or preferred operating region of a centrifugal pump (ANSI/HI, 1997; PSM, 2008). If the pump is driven outside this operating region, the pump efficiency decreases, and it may be susceptible to harmful phenomena as shown in Fig. 2.8. This figure also shows the reliability curve given in (Barringer, 2003) for an ANSI[1] centrifugal pump with the MTBF values for different flow rate regions.

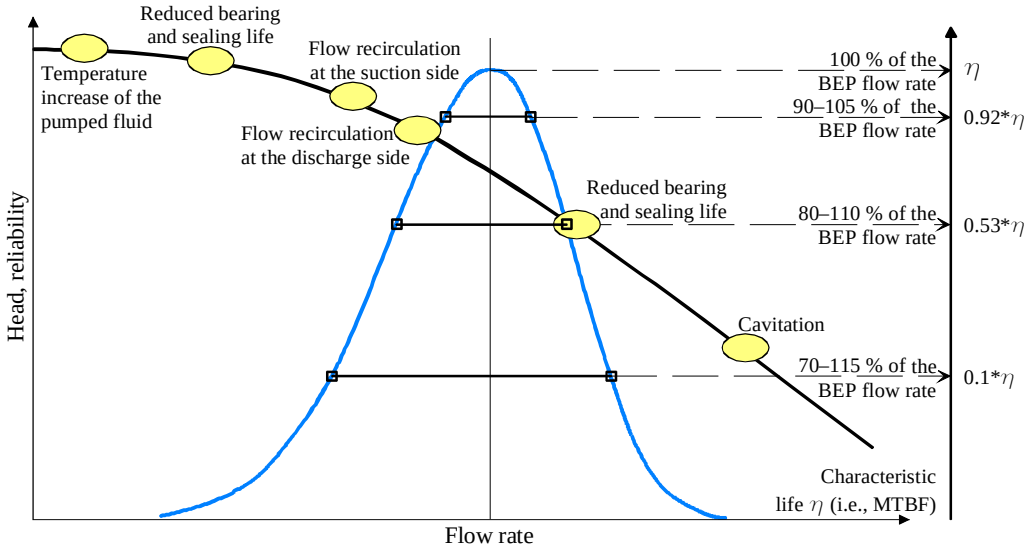

Fig. 2.8: Pump head and reliability curves as a function of flow rate. The head curve is indicated by the black colour, and the reliability curve by the blue colour. In addition, the figure reports the estimated decrease of the pump characteristic life η as a function of relative flow rate and adverse events that may occur, if an ANSI[1] centrifugal pump is driven outside its recommendable operating region at a fixed speed (Barringer, 2003; Karassik, 1998).

The concept of recommendable operating region is discussed in (ANSI/HI, 1997) and (Gülich, 2008). According to (ANSI/HI, 1997), the pump curve can be divided into the preferred and allowable operating region. In the preferred operating region (POR), the service life of a centrifugal pump is not significantly reduced by hydraulic forces, vibration or flow separation. The general guideline for the POR of a typical radial flow and fixed-speed centrifugal pump is 70–120 percent of the BEP flow rate Q_{BEP}. Based on the Barringer's reliability curve shown in Fig. 2.8, this can be considered an optimistic recommendation, as the characteristic life η of an ANSI centrifugal pump may decrease to one tenth of its ideal value within this flow rate region. A better guideline could be for instance 80–110 percent of the BEP, with which the decrease in the pump characteristic life is still half of its ideal value according to Fig. 2.8.

[1] A centrifugal pump built according to the ANSI/ASME B73.1 standard primarily for chemical and process applications (D'Alterio, 2003). In Europe, process pumps are typically built according to the ISO 5199 standard.

An allowable operating region (AOR) is a wider range of flows, in which the service life of a centrifugal pump is not seriously compromised, but the minimum bearing life may be shorter and there is more vibration and noise compared with the operation in POR. Hence, the service life of a centrifugal pump may decrease, if the pump is driven in the allowable operating region. However, operation in the AOR should not cause an immediate failure of a centrifugal pump.

Gülich (2008) has introduced a similar classification with ranges for the continuous and short-term operation. The range of continuous operation allows the use of a centrifugal pump for many thousand hours without damages or excessive wear. This region can be defined for instance by utilising limits for the decrease in the pump efficiency. As the risk of cavitation and the amount of hydraulic excitation forces increase in the operating region with a lower pump efficiency, this approach can exclude those operating points that decrease the pump service life from the allowable range of continuous pump operation. In the range of short-term operation, a centrifugal pump is susceptible to abnormal operating conditions, which may result in premature wear of the pump. However, a centrifugal pump may be driven in this region for a short period of time without a pump failure.

These two guidelines only provide a general view on the operating regions, in which a centrifugal pump should be driven. For this reason, these guidelines may not correctly determine recommendable and allowable operating regions of the pump. In addition, these references and reliability data given in (Barringer, 2003) do not consider the effect of a variable rotational speed on the energy efficiency and reliability of the pump operation, which is why their applicability to VSD centrifugal pumps is doubtful: it is apparent that a variable rotational speed affects the pump mechanical reliability and energy consumption, and therefore, it may be more feasible to drive the pump at a lower rotational speed and slightly off the pump BEP than at a higher rotational speed and exactly in the pump's best efficiency point.

To allow an energy efficient and reliable operation of a VSD centrifugal pump, the limits should be known for operating regions, in which the pump operation can be considered recommendable or at least allowable. To this end, there should be means to determine the energy efficiency and mechanical reliability of the pump in different operating point locations and at different rotational speeds, as these are the key factors affecting the energy, maintenance and possible production loss costs of the pumping LCC. Although these limits cannot prevent the occurrence of unexpected faults, they can further help to select an appropriate pump for the application, and also prevent the pump operation in the operating region with a poor energy efficiency or high risk for a mechanical failure. In addition, threshold values should be available for these operating regions in the form of technical or economical limits. For instance, the limits can be based on vibration-based reliability indices, specific energy consumption or the total LCC of the pump.

In the following, the effect of rotational speed on the pump energy consumption and reliability is studied and laboratory test results are introduced. With the results it is shown that the recommendable operating region of a VSD centrifugal pump can be determined with energy efficiency and reliability-based criteria, and the limits of this operating region are strongly dependent on the rotational speed of the pump. The main focus of this analysis is on the centrifugal pump, although the induction motor and the frequency converter equally affect the total efficiency and reliability of a pumping system, which should also be considered in the analysis.

2.3 Effect of the operating point location on the pump energy consumption

As demonstrated in Fig. 1.3, adjustment of the pump rotational speed is often the most energy efficient method to control the pump output flow. However, this cannot be directly seen from the pump efficiency that may remain unaffected by the rotational speed change. Depending on the pump and system characteristic curves, the pump efficiency may decrease, although the speed decrease would be feasible in the terms of pumping life cycle costs. For this reason, the statement that the pump operation is optimised by driving it in its best efficiency point may not totally hold true for VSD centrifugal pumps, with which the decrease of rotational speed can be a more feasible alternative down to some limit.

For this reason, the energy efficiency of the pump operation should be quantified by calculating its specific energy consumption E_s with (2.2), which shows the pumping system energy consumption per pumped volume. Compared with the sole use of the pump efficiency η, specific energy E_s considers also the effect of rotational speed n, drive train efficiency η_{dt} and system losses on the pumping energy efficiency: the specific energy consumption of the pump has a squared relationship with the rotational speed, when the pump relative flow rate and efficiency stay constant. This can be seen by inserting (2.3) and (2.5) into (2.2):

$$E_s = \frac{P_{in}}{Q} = \frac{P}{\eta_{dt} \cdot Q} = \frac{1}{\eta_{dt}} \cdot \left(\frac{n}{n_n} \right)^2 \cdot \frac{P_n}{Q_n}, \tag{2.16}$$

which determines the pump E_s, when the drive train efficiency η_{dt} is set to 1.

This equation can be further developed, and so the effect of pump efficiency η and static head H_{st} on the pumping system specific energy consumption can be considered (Europump, 2004). By applying (2.1) and dividing the pump head H into its static and dynamic components (i.e., H_{st} and H_{dyn}), E_s can be presented as:

$$E_s = \frac{P}{\eta_{dt} \cdot Q} = \frac{\rho \cdot g \cdot (H_{st} + H_{dyn})}{\eta_{dt} \cdot \eta}. \tag{2.17}$$

This form allows determination of the minimum E_s that is required to transfer the fluid from a place to another based on the system static head and maximum efficiencies of the pump and drive train (Hovstadius, 2007). By comparing the actual specific energy consumption with this or some other base value of E_s, the energy efficiency of pump operation can be expressed as a relative value for the specific energy consumption.

These relationships make the E_s an applicable indicator for the pumping energy efficiency at different rotational speeds and operating point locations: although the decrease in the pump efficiency is linked to the decrease in the pump mechanical reliability at a fixed rotational speed, pump efficiency does not show the effects of rotational speed change, when the relative flow rate stays constant.

2.3.1 Energy-efficiency-based recommendable operating region of a VSD pump

As an example, an E_s value graph has been formed for a Sulzer APP22-80 centrifugal pump having a 255 mm impeller according to its published characteristic curves given in Appendix A, Fig. A.2. The resulting E_s of the pump in different operating point locations is illustrated as

relative values in Fig. 2.9. The chosen base value and also a possible criterion for E_s is 61.1 Wh/m^3, which is consumed at the pump BEP, when the Sulzer pump is driven at the rotational speed of 1450 rpm. The resulting figure shows the operating regions in which the pump E_s exceeds the chosen base value having an increasing effect on the pump energy consumption. For instance, at the 70 % relative flow rate and at 1450 rpm, the relative pump E_s is 1.23, and so at this rotational speed, the HI guideline for the POR seems reasonable. At the rotational speed of 1595 rpm, the corresponding scaled E_s is 1.48, indicating a clearly higher energy consumption.

The figure also shows the operating regions where the pump usage can be considered energy efficient based on the chosen E_s threshold. Compared with the previously introduced guidelines for fixed-speed centrifugal pumps, these results clearly demonstrate how the decrease of the rotational speed extends the recommendable operating region of the pump on the basis of the pump E_s.

It is worth noting that E_s tends to decrease at a fixed rotational speed, when the flow rate increases and the head decreases on the known part of the pump *QH* characteristic curve. For this reason, the E_s criterion primarily results in a minimum recommendable flow rate and maximum recommendable rotational speed limits for this VSD pump. As the decrease of the pump E_s continues also at relative flow rates above the Q_{BEP}, it suggests that the Sulzer pump should be driven in this flow rate region if allowed by the system head requirement, as a lower head results in a lower E_s. This is also noted in (McKinney, 2010), where it is mentioned that a flow rate above the Q_{BEP} could be the most optimal operating point for the existing pump, if the lower specific energy consumption compensates the increase in maintenance costs and possible production loss costs. This kind of head minimisation may require system modifications, such as the opening or removal of the unnecessary control valves from the system. Then, it may also be feasible to replace the existing pump with a more efficient one to further decrease the pump E_s.

In practice, the mechanical reliability of the pump also limits the recommendable operating region of the pump: at flow rates above Q_{BEP} the pump efficiency decreases with an increasing flow rate meaning larger hydraulic losses, and the pump also becomes more prone to the cavitation occurrence because of the increasing NPSH requirement. Correspondingly, operation at partial flow rates increases the risk of the flow recirculation phenomenon. Therefore, determination of the recommendable operating region for a VSD centrifugal pump should also take into consideration factors affecting its mechanical reliability. The recommendable operating region may also be limited for instance by the system static head, the shaft sealing system of the pump, the drive train loadability and other system-related factors, which should also be considered in the analysis, but are not further discussed in this thesis.

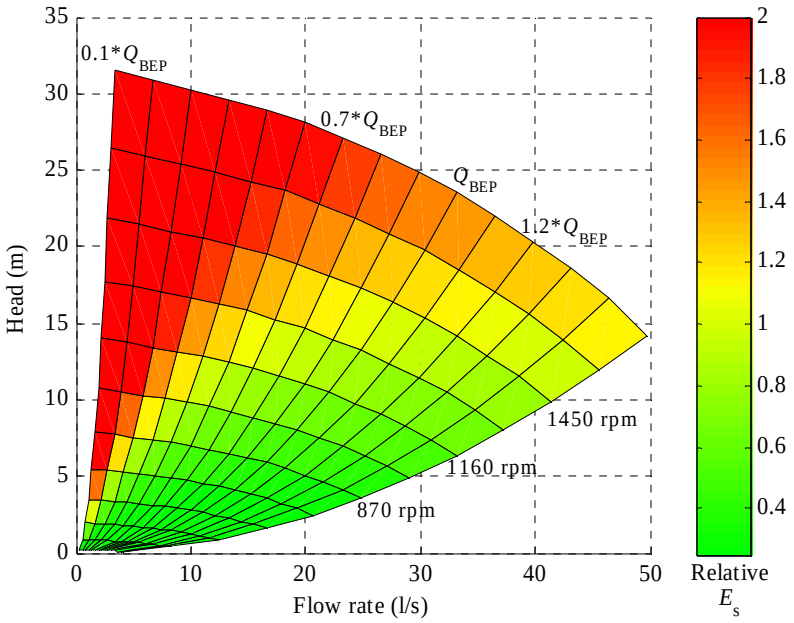

Fig. 2.9: Relative E_s of the Sulzer pump at different operating point locations. The chosen base value for E_s is 61.1 Wh/m^3. Based on the E_s, the recommendable operating region of the pump becomes larger with a decreasing rotational speed. In this case, the E_s criterion for the pump can result in limits for the minimum recommendable flow rate and the maximum recommendable rotational speed.

A possible effect of the drive train efficiency on the pumping energy efficiency has been determined with the efficiency data available for a 11 kW ABB induction motor and an ABB ACS 800 frequency converter, which have been used as the drive train of the Sulzer laboratory pumping system (see Appendix A for more details). The resulting E_s figure for the Sulzer pumping system is illustrated in Fig. 2.10. For the sake of clarity, 61.1 Wh/m^3 is again applied as the base value for E_s. In addition, an exemplary limit for the recommendable operating region is shown in the figure based on the relative E_s threshold of 1.25.

Comparison of Fig. 2.9 and Fig. 2.10 shows that the effect of drive train efficiency is most notable at low rotational speeds and relative flow rates, in which the lower drive train efficiency increases the relative E_s. For instance, at the rotational speed of 870 rpm and at the 30 % relative flow rate, the relative E_s of the pumping system is 1.18, while the relative E_s of the pump is only 0.83. Otherwise the figures are similar, meaning that a decrease in the rotational speed extends the recommendable operating region of the pump on the basis of the pumping system E_s, which results in minimum recommendable flow rate and maximum recommendable rotational speed limits for a VSD pump.

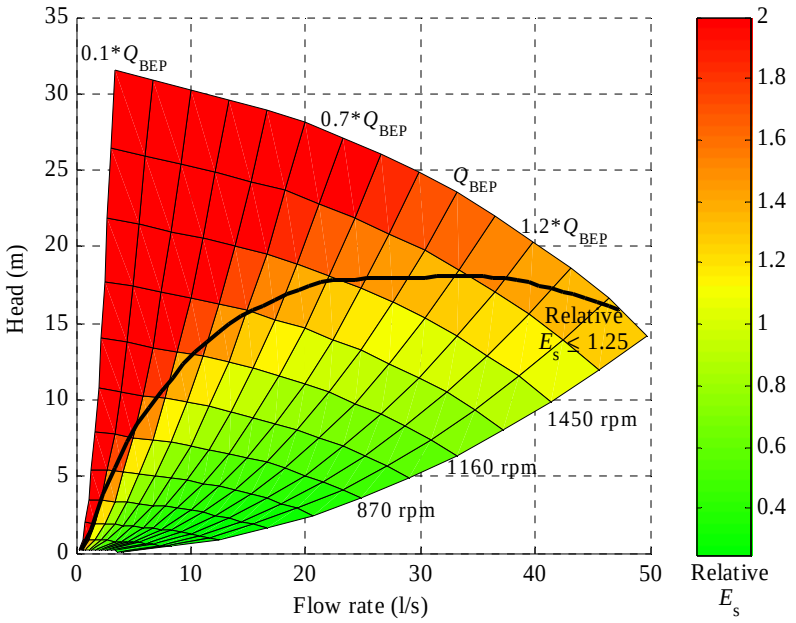

Fig. 2.10: Relative E_s of the Sulzer pumping system including the drive train efficiency at different operating point locations. An exemplary limit for the recommendable operating region is also given in the figure. The chosen base value for E_s is 61.1 Wh/m^3. Compared with Fig. 2.9, the decrease in the drive train efficiency most significantly limits the minimum recommendable flow rate of the pumping system especially at low rotational speeds (e.g. at 870 rpm).

2.4 Effect of the operating point location on the pump mechanical reliability

As shown in Fig. 2.8, the relative flow rate of a centrifugal pump has an effect on its mechanical reliability that can be quantified for instance with the mean time between the failures (MTBF) value. However, only a few papers have been published focusing on the reliability of a centrifugal pump at different rotational speeds and flow rates. The pioneering work has been carried out by Bloch and Geitner, who have proposed a quantitative method to determine the effect of rotational speed, relative flow rate and impeller diameter tip clearance on the pump reliability (Bloch, 1994). It is based on the calculation of the pump reliability index (RI), which is a product of the dimensionless speed (R_n), the relative flow rate (R_q) and the impeller diameter (R_d) reliability factors:

$$\mathrm{RI} = R_n \cdot R_q \cdot R_d \,. \tag{2.18}$$

The scale of the reliability factors is from 0 to 1. A value of one indicates the best condition that can be chosen for the pumping system operation based on the minimum pump vibration magnitude, minimum bearing temperature and other variables, which are related to the service life and mechanical reliability of the pump. Hence, a value of one does not mean an infinite MTBF, but a lower reliability factor is related to the decrease of the pump characteristic life. A value of zero does not directly imply zero reliability, but it indicates the operating conditions that should be avoided. Consequently, reliability indices do not directly indicate the actual reliability (e.g. MTBF) of the pumping system, but they at least allow a comparison of different operating points of the same pump from the reliability point of view.

Bloch and Budris have proposed also another similar index R_{total} for the total hydraulic reliability of the pump that could be used for comparison of different pumping systems (Bloch, 2010). It comprises reliability factors for the rotational speed, relative flow rate, NPSH margin (R_{NPSH}) and impeller material (R_{mat}) of the pump:

$$R_{total} = R_n \cdot R_q \cdot R_{NPSH} \cdot R_{mat} . \tag{2.19}$$

Compared with (2.18), R_{total} takes into account also the cavitation occurrence in the pump, but it does not contain a term for the impeller diameter that remains constant without the change or modification of the impeller. Since the risk of cavitation increases especially at flow rates above the Q_{BEP}, R_{total} should be preferred for the reliability-based determination of the recommendable operating region. Otherwise, both reliability indices are based on the reliability curves originally presented in (Bloch, 1994), which are experimentally studied in (Budris, 2001; Erickson, 2000; Stavale, 2008). Next, the main results of these studies are given for R_n, R_q and R_{NPSH}. It can be well assumed that the impeller material R_{mat} is not changed during the normal pump operation, and hence its effect on the R_{total} can be excluded.

The reliability index for the rotational speed R_n considers the effects of heat generation between the seal faces, heating of the bearing lubricant, seal face wear, bearing wear and abrasive wear on the pump reliability. According to (Bloch, 1994), the effect of these wear- and heating-related factors on the pump reliability is linearly related to the rotational speed, and the index value of one is reached at the zero speed. This has been validated by laboratory measurements in (Erickson, 2000). The linear relationship is also supported by the findings of Budris et al. for 119 process pumps in (Budris, 2001). R_n curves given in these references as a function of relative rotational speed are illustrated in Fig. 2.11.

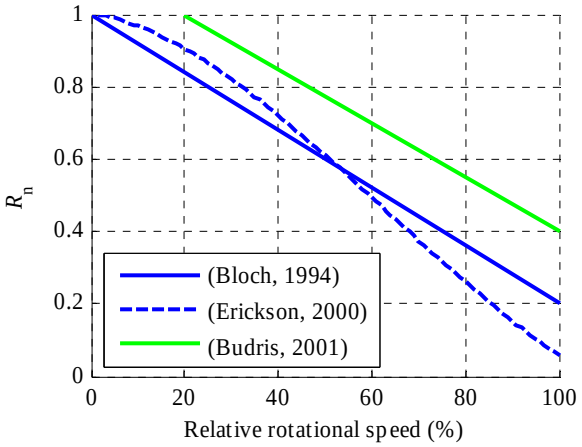

Fig. 2.11: Previously published R_n curves as a function of relative rotational speed. These studies propose the rotational speed reliability factor R_n to be inversely affected by the rotational speed of the pump.

The reliability index of the relative flow rate R_q should be affected both by the relative flow rate and rotational speed of the pump, as the rotational speed strongly affects the pump power consumption and hence the possible vibration magnitude and severity of cavitation phenomenon in the pump. However, this has not been considered in the R_q curves in (Bloch, 1994; Budris, 2001; Erickson, 2000), which are given only at a single rotational speed. Stavale (2008) has published vibration-velocity-based R_q curves for an ANSI centrifugal pump at four

different rotational speeds, which show the extending and increasing effect of a lower rotational speed on the R_q factor (see Fig. 2.12). At the relative rotational speed of 100 %, R_q decreases very steeply, and for instance at the 120 % relative flow rate, R_q is only 0.24. Different from the reliability curve given by Barringer, the maximum values of R_q are reached around the relative flow rate of 70 %, not at the pump BEP. Varying results for the R_q maximum are given in different references: in (Budris, 2001) it is 80 % and in (Bloch, 1994) approximately 95 % of the Q_{BEP}. These results differ from the typical assumption that the pump reliability is maximised at the pump BEP. For radial flow pumps this can be partially explained by the fact that the minimum of radial hydraulic forces and the related vibration may not coincide with the pump BEP, since the design point of the volute casing may differ from the design point of the impeller (Gülich, 2008). A possible reason for these results can also be the location of the energy loss minimum $(1-\eta)\cdot P$ of a centrifugal pump, which may not coincide with the pump Q_{BEP} (Sulzer, 1998). In any case, these references have shown the decrease in R_q at larger relative flow rates, which together with the cavitation occurrence sets limits for the maximum recommendable flow rate and also the rotational speed of the pump.

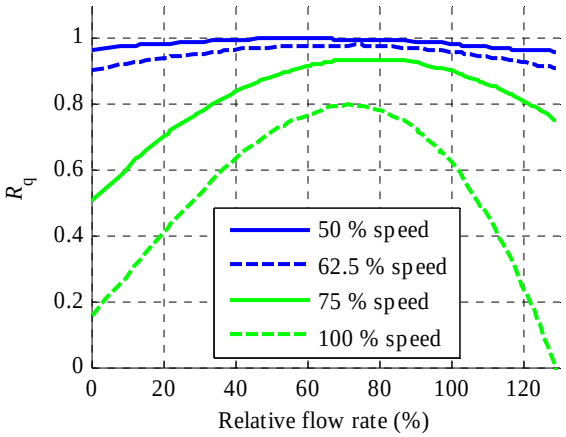

Fig. 2.12: R_q curves as a function of relative flow rate at four different rotational speeds according to (Stavale, 2008). Note that the maximum R_q is attained approximately at the 70 % relative flow rate instead of the Q_{BEP}, which might be caused by the characteristics of the pump volute casing and the location of the pump energy loss minimum.

The reliability index of the NPSH margin ratio R_{NPSH} is based on the suction energy (SE) level of a centrifugal pump, a variable suggested in (Budris, 1997). According to (Bloch, 2010), suction energy is a term for the fluid momentum in the suction eye of the impeller, and it is related to the extent of pressure surges caused by the cavitation phenomenon. The amount of suction energy has an effect on the severity of cavitation, and hence, a higher value of suction energy requires a higher ratio of the available and required NPSH to suppress the harmful occurrence of cavitation. In practice, R_{NPSH} is affected by the SE and $NPSH_A/NPSH_R$ ratios of the pump as shown in Fig. 2.13. Suction energy ratio is a relative value, which determines if a centrifugal pump has a high suction energy rating (i.e., SE > 1; Bloch, 2010). It can be calculated with

$$\mathrm{SE} = \frac{d_1 \cdot n \cdot n_{ss} \cdot \mathrm{SG}}{78760}, \tag{2.20}$$

where d_1 is the impeller inlet diameter in metres and SG is the specific gravity of the fluid. In the case of radial flow centrifugal pumps, the SE ratio is often below one meaning a $R_{NPSH} \approx 1$, if there is a sufficient $NPSH_A/NPSH_R$ ratio to suppress cavitation.

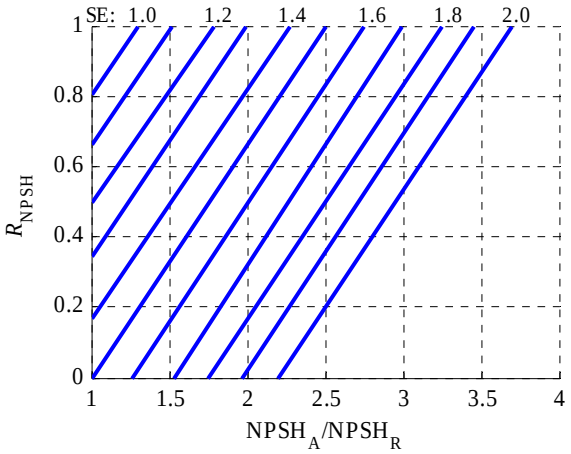

Fig. 2.13: R_{NPSH} can be determined according to the $NPSH_A/NPSH_R$ and SE ratios (Bloch, 2010). In practice, the R_{NPSH} starts to decrease with pumps having an SE ratio above 1. Hence, radial flow centrifugal pumps do not typically pose the problem of a lowered R_{NPSH}, if the NPSH ratio is sufficient to suppress the occurrence of cavitation.

Although the R_{NPSH} is based on a controversial concept of NPSH margin ratios[2], it provides a tool to determine the effect of cavitation occurrence on the pump mechanical reliability. The effect of cavitation occurrence on the recommendable pump operating region can be determined more directly by calculating the pump $NPSH_A/NPSH_R$ ratios in different operating point locations, if the $NPSH_A$-related system characteristics and the required $NPSH_A/NPSH_R$ ratio are known.

To demonstrate the pump mechanical reliability at different operating point locations, R_{total} has been determined using Bloch's curve for the R_n, Stavale's curve for R_q and an assumption that the pump $NPSH_A/NPSH_R$ ratio is sufficient to suppress the occurrence of cavitation (i.e., $R_{NPSH} = 1$). The resulting R_{total} as a function of relative flow rate and rotational speed is shown in Fig. 2.14. In addition, limits for the recommendable operating region are determined according to an arbitrarily chosen R_{total} threshold of 0.15.

The resulting R_{total} figure advises to drive this pump at a lower rotational speed, which is expectable because of the two-fold effect of the rotational speed on the R_{total}. They also show that the pump can be driven at the 100 % rotational speed, but then the flow rate region should be limited between 47 and 92 % of the Q_{BEP}, so the R_{total} would be over 0.15. Because of the arbitrary nature of reliability indices, this level of R_{total} can be still acceptable in the terms of MTBF and maintenance costs of the pump. As a conclusion, this approach may provide rather arbitrary limits for the recommendable operating region, which can be regarded as the weakness of this reliability-index-based approach.

[2] Concerning the required NPSH margins, Hydraulic Institute has published a SE-based and NPSH-margin-related standard in 1998 (ANSI/HI, 1998), but it was withdrawn for a complete revision in 2003. A revised version has not yet been published, describing the difficulty of determining generally applicable guidelines for the NPSH margins. See Chapter 4 and (Henshaw, 2001) for further discussion.

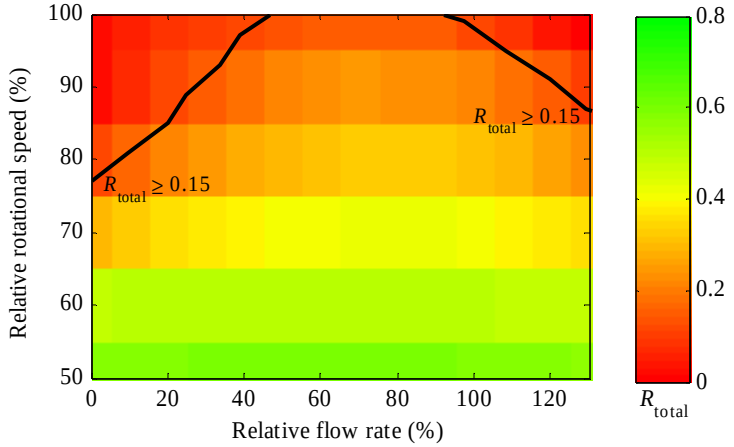

Fig. 2.14: An example of the pump R_{total} as a function of relative flow rate and rotational speed. Also an exemplary R_{total} threshold of 0.15 is shown in the figure. Although this figure is formed for an arbitrary pump, it shows the positive effect of driving the pump at a lower rotational speed, if allowed by pumping-system-related factors such as the system static head.

Alternatively, reliability factors R_n, R_q and R_{NPSH} could be studied separately with individual threshold values. For instance, by choosing the R_n threshold of 0.2 and the R_q threshold of 0.7 for the arbitrary pump, it would have the recommendable operating region shape illustrated in Fig. 2.15. Compared with the R_{total} criterion demonstrated in Fig. 2.14, individual thresholds limit more the recommendable operating region of a centrifugal pump.

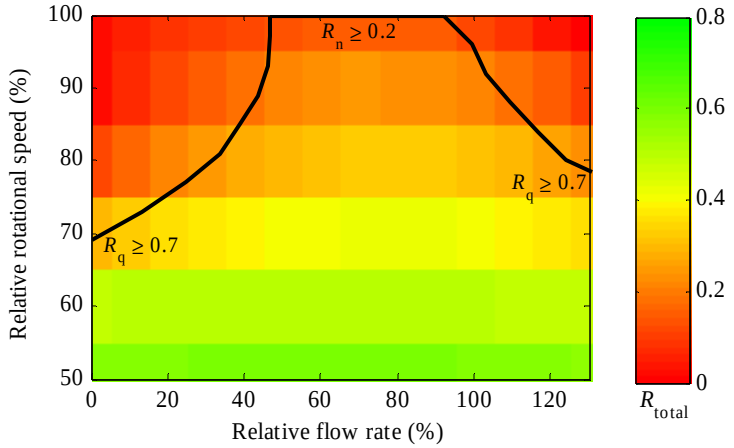

Fig. 2.15: R_n- and R_q-based limits for the recommendable operating region of an arbitrary centrifugal pump. Figure shows also the R_{total} of the pump at different relative flow rates and rotational speeds.

2.4.1 Reliability-based recommendable operating region of a VSD pump

Laboratory measurements were carried out for a Sulzer laboratory pump to determine its R_q curves at different rotational speeds. The pump was driven by an 11 kW ABB induction motor and an ABB ACS 800 frequency converter. The pump was connected to a system consisting of two water tanks, venturi tubes, piping and control valves as shown in Fig. 2.16. The pump was driven at seven different relative flow rates and at five rotational speeds ranging from 1080 to

1620 rpm by adjusting its operation with the frequency converter and control valves. In these operating point locations, the $NPSH_A/NPSH_R$ ratio was at least 3, SE ratio was below 0.5, and there were no signs of cavitation, and thus, cavitation occurrence should have no effect on the measurement results. The relationship of the pump rotational speed and R_n was not tested during these measurements.

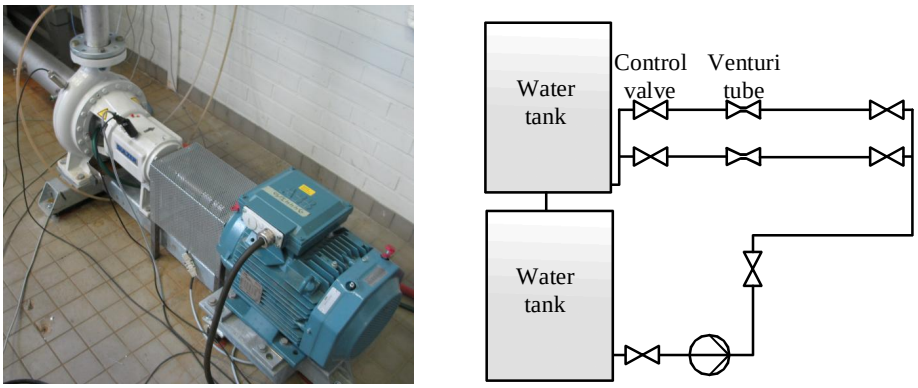

Fig. 2.16: Laboratory pumping system used in the evaluation. It comprises a Sulzer centrifugal pump, an ABB induction motor and an ABB frequency converter (not shown in the figure). The pump is attached to a system consisting of two water tanks and venturi tubes, piping and control valves.

Vibration of the pump was measured in each operating point location by a SKF CMSS786A acceleration sensor that was installed to the location of pump bearings. The measurement data was stored to a computer with a National Instruments (NI) PCI-6032E data acquisition card. Measurements were carried out with a 20 kHz sampling frequency for a time period of five seconds. In addition, the pump has been equipped with pressure sensors for the determination of the pump flow rate and head, as described in Appendix B.

The measured vibration acceleration was numerically integrated into vibration velocity, and R_q values were then determined for the pump based on the measured magnitude of vibration velocity at the pump blade pass frequency (BPF). This was selected as the indicator for the pump reliability, as it should be mainly affected by the pump operation, and it has been used as the R_q indicator in (Erickson, 2000). Calculation of R_q was carried out with the following equation:

$$R_q = 1 - \frac{v}{v_{max}} + C, \tag{2.21}$$

where v is the magnitude of vibration velocity, the subscript $_{max}$ denotes its maximum value, and C is the constant to set the maximum value of R_q to 1.

R_q values of the Sulzer pump are given with their quadratic polynomial curves in Fig. 2.17. Compared with the R_q curves published by Stavale, the resulting curves provide similar conclusions: a decrease in the rotational speed has an increasing effect on the R_q values, and generally the R_q curve shapes become flatter with a lower rotational speed. In addition, the maximum value of R_q is typically attained at the relative flow rate of 70–80 % instead of the Q_{BEP}. This might be partially caused by the location of pump energy loss minimum, which is located around the 90 % relative flow rate. A presumably erroneous exception to the R_q maximum locations is the R_q curve at 1380 rpm, which attains its maximum at the 30 % relative

flow rate. The limited number of measurement points and the scatter of measured vibration velocities have also resulted in a possibly too large R_q maximum value at the 1620 rpm rotational speed. Because of these factors, the use of these R_q curves as an indicator of the recommendable operating region is questionable. However, exemplary limits of the recommendable operating region have been determined for the pump with the R_q threshold of 0.7. This has resulted in relative flow rate limits of 0–110 % at 1380 rpm, 48–98 % at 1560 rpm and 58–103 % at 1620 rpm. Compared with the HI guideline for POR and Barringer's reliability curves, especially the minimum limits of the relative flow rate are smaller, and they are in the region with a higher specific energy consumption. The maximum limits of the relative flow rate, however, are more logical excluding the R_q maximum at the rotational speed of 1620 rpm compared with the R_q maximum at 1560 rpm.

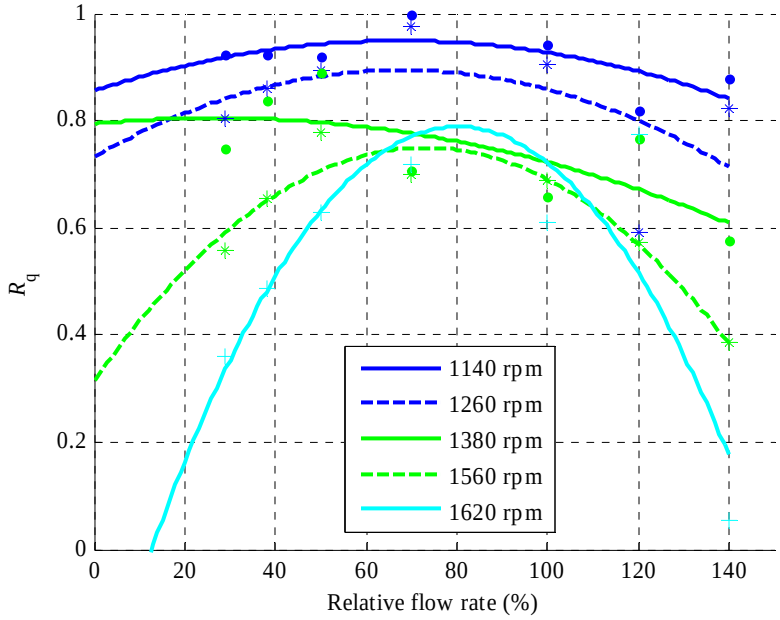

Fig. 2.17: Measurement-based R_q curves as a function of relative flow rate for the Sulzer pump at five different rotational speeds. The maximum R_q is typically attained at the relative flow rate of 70–80 % instead of the Q_{BEP}.

Determination of the Sulzer R_{total} requires the use of an approximate model for R_n, as it has not been determined during the laboratory measurements. Bloch and Geitner's model has been selected for this case with the following equation:

$$R_n = 1 - \frac{n}{1620} \cdot 0.8 \,. \tag{2.22}$$

Based on the measurement-based R_q values, an assumption that $R_{NPSH} = 1$ and (2.22), R_{total} of the Sulzer pump in each measured operating point location was determined. The resulting values with their quadratic polynomial curves are shown in Fig. 2.18. As previously, R_{total} curves show the benefits of driving the pump at a lower rotational speed. However, also these results demonstrate the arbitrary nature of reliability indices and difficulty of selecting appropriate thresholds for R_{total}: for instance, the R_{total} threshold of 0.15 would limit the recommendable operating region to 39–107 % of Q_{BEP} at 1560 rpm. At 1620 rpm, the resulting

limit would be 65–95 % of Q_{BEP}. On the other hand, the same threshold allows the pump usage at all relative flow rates, when the pump rotational speed is 1140–1380 rpm.

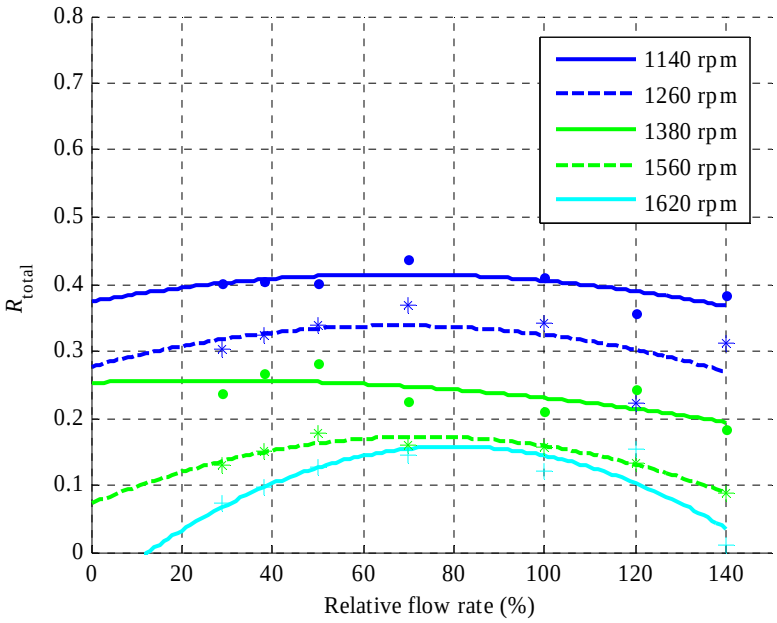

Fig. 2.18: R_{total} curves of the Sulzer pump as a function of relative flow rate at five different rotational speeds. Because of the arbitrary nature of reliability indices, R_{total}-based determination may provide rather arbitrary limits for the recommendable operating region.

Based on these analysis results, R_{total} and R_q-based limits for the recommendable operating region have been added to the Sulzer pump's *QH* characteristic curve. They are illustrated in Fig. 2.19 with the E_s-based limit of the pump recommendable operating region. In this case, the R_{total} criterion has resulted in wider flow rate limits for the recommendable operating region than the R_q criterion of 0.7. R_{total}-based limits are also more logically affected by the rotational speed change than the R_q-based limits. However, these reliability indices do not directly represent the reliability figures of the pump, and therefore the limit values can be rather arbitrary. Consequently, further research should be carried out concerning the applicability of reliability indices in this kind of an application.

In general though, the discussed energy efficiency and reliability-based criteria for this pump have resulted in limits inside which the pump should be driven, so it would not be wasting energy or it would not be prone to a mechanical failure as a result of the higher vibration of the pump. This consideration does not include the possibly limiting effects of the system, fluid characteristics and other factors, but it gives basic information on the recommendable operating region of a VSD centrifugal pump.

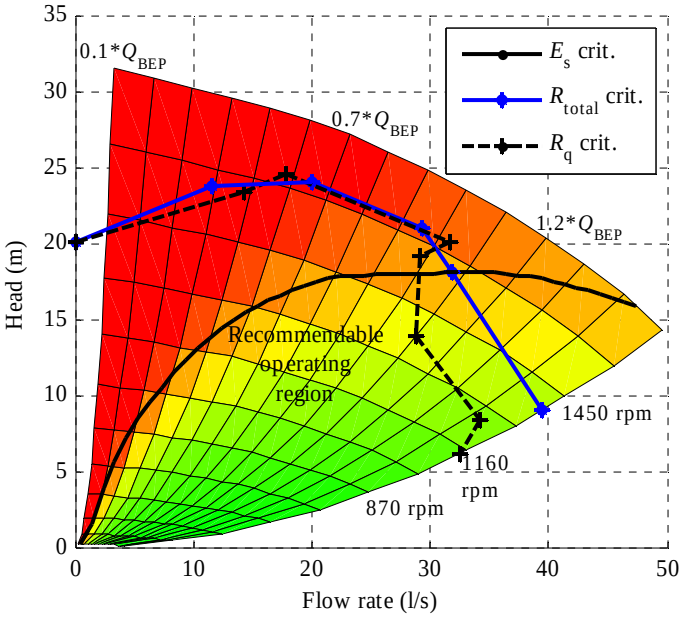

Fig. 2.19: Recommendable operating region of the Sulzer pump based on the energy efficiency and reliability criteria.

2.5 Summary of Chapter 2

In this chapter, theory concerning variable-speed-driven pumps was discussed. Determination of the limits for the recommendable operating region of a VSD centrifugal pump was studied. This study was limited to the pump, and thus, possible limitations set by the fluid, the system and the drive train loadability have not been considered in the analysis.

Firstly, it was shown that the existing guidelines are not designed for variable-speed-driven pumps. It was proposed that limits for the recommendable operating region should be determined according to the pumping energy efficiency (i.e., specific energy consumption E_s) and the pump mechanical reliability in different operating point locations, which can be quantified with non-dimensional reliability indices. Then, determination of the pump recommendable operating region could cover the main factors attributing also to the life cycle costs of the pump.

Applicability of these energy-efficiency- and reliability-based criteria was studied with a laboratory pumping system. This study demonstrated the applicability of the relative E_s as the indicator of pumping energy efficiency and the arbitrary nature of the known reliability indices. The conducted laboratory measurements did not allow a detailed study on the reliability-based determination of the pump recommendable operating region. For this reason, only approximate reliability-based limits have been determined for the Sulzer pump. Correspondingly, only exemplary thresholds have been used in the limit determination of the pump recommendable operating region. Hence in the future, further study is recommended with a number of laboratory and industrial pumping systems concerning the applicability of the reliability-index-based approach for the determination of the recommendable operating region of a VSD centrifugal pump.

3 ESTIMATION OF THE PUMP OPERATING POINT LOCATION

Diagnosis and control of a centrifugal pump operation requires information on the present operating point location of the pump (i.e., the flow rate and head produced by the pump). Typically, a centrifugal pump operation is controlled on the basis of an external process measurement, which may be utilised to determine the location of the pump operating point, if the head or the flow rate produced by the pump is measured. In practice, only the pump output pressure might be measured, and hence additional measurements or alternative estimation methods are required to determine the operating point location.

In this chapter, methods to determine the operational values of a centrifugal pump are discussed. General measurement- and model-based methods are presented. The main focus of this chapter is on the three model-based methods that apply information available from a frequency converter. Factors affecting the accuracy of the model-based methods are discussed. The applicability of the discussed model-based methods is evaluated by laboratory measurements for a radial flow centrifugal pump. A discussion concerning the applicability of model-based methods with other centrifugal pump types is also given. In addition, estimation results of two pilot systems in a paper mill are introduced.

3.1 Measurement-based methods

Operating point location of a centrifugal pump can be directly determined, if the flow rate Q and the head H produced by the pump are known. The flow rate can be measured by various techniques, of which differential pressure and flow velocity methods are typically used. The pump head equals the total pressure difference across the pump, so it can be determined by measuring the static pressure difference and considering the effect of fluid characteristics, velocity head (caused by the fluid velocity difference across the pump) and flow losses between the measurement point and the pump on the resulting values. These direct measurements are the most common way to determine the location of the pump operating point in the manufacturer's QH curve and the hydraulic output power of the pump. Thereby, the pump efficiency η can be determined by measuring the mechanical power consumption of the pump with a combined torque and speed measurement. Alternatively, the pump efficiency can be determined by measuring pressure and temperature changes of the fluid across the pump, which correspond to the ideal compression of the fluid (i.e., an isentropic process) and the effect of internal losses[3] on the pump operation, respectively (ISO, 1987). Hence, a thermodynamic method cannot take into account the effect of mechanical losses on the pump efficiency, which may reduce its applicability with small-sized pumps (Feng, 2004; Sulzer, 1998). Thus, positive results have been shown considering the use of thermodynamic method especially in the efficiency monitoring of large centrifugal pumps ($P_{\text{in}} > 0.5$ MW; Cartwright, 2009).

3.2 Model-based methods

Besides direct measurements for the pump operating point location, it can be determined by adjustable models for the centrifugal pump operation as shown in Fig. 3.1. In that case, operating point location of the pump is calculated by using other measurements or estimates on the pump operation. For the calculation, models are tuned based on the information available on the pump, the pumped fluid and the other parts of the pumping system. Typically, characteristic curves of the pump and basic properties of the pumped fluid are required for the model tuning.

[3] Internal losses comprise events that lead to the heating of the pumped fluid, such as hydraulic losses, disk friction losses, and leakage losses.

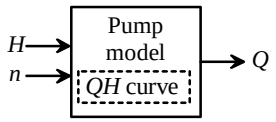

Fig. 3.1: Structure of a model-based estimator. In this case, the pump flow rate Q is calculated based on the measured values for the head H and the rotational speed n, respectively. The model describing the pump operation is tuned with the QH characteristic curve provided by the pump manufacturer.

Compared with the direct measurements, model-based methods are tuned for certain operating conditions and for a certain pumping system, and hence they may provide inaccurate estimation results. On the other hand, they provide an opportunity to estimate the operational state of the pumping system by utilising the internal measurements and estimates of a frequency converter. Next, three different model-based methods for the estimation of the pump operational state are described.

3.2.1 *QH*-curve-based estimation method

In this method, the location of the pump operating point is estimated from the pump QH curve with the calculated pump head and the estimated pump speed value. Since the pump head equals the total pressure difference across the pump expressed as the height of the pumped fluid, it can be measured with a pressure difference sensor or with two separate pressure sensors located at the discharge and suction side of the pump (pressures p_d and p_s, respectively), when the fluid characteristics, velocity head and flow losses between the sensors and corresponding pump flanges are known. In the case of modern frequency converters, an estimate for the pump speed n is readily available without additional measurements. The QH curve estimation method can be divided into four steps, which are illustrated in Fig. 3.2. In addition, the following information is required by the estimation method:

- Pump QH characteristic curve in the numeric form. For unambiguous estimation results, the QH curve should be constantly decreasing.

- Nominal speed of the pump applied in the characteristic curves.

- Fluid density, piping diameters at the pressure measurement points, friction loss factors between the measurement points and the pump discharge and suction flanges, and vertical distance between the pressure sensors for the head calculation.

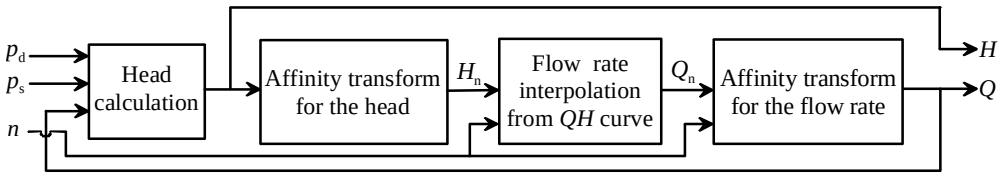

Fig. 3.2: Steps of the QH-curve-based estimation method. The pressure difference and rotational speed of the pump are applied as inputs to the estimator. The estimation method yields values for the pump head and the flow rate that is further applied to determine the velocity head of the pump.

The first step in the QH-based estimation is the calculation of the pump head. It is based on the Bernoulli equation for incompressible fluids, which can be written as follows:

$$H = \frac{p_\mathrm{d} - p_\mathrm{s}}{\rho \cdot g} + \frac{v_\mathrm{d}^2 - v_\mathrm{s}^2}{2g} + \frac{k_\mathrm{f,d} \cdot v_\mathrm{d}^2 + k_\mathrm{f,s} \cdot v_\mathrm{s}^2}{2g} + \left(Z_\mathrm{d} - Z_\mathrm{s}\right), \tag{3.1}$$

where p is the fluid static pressure, v the flow velocity, k_f the friction loss factor between the measurement point and the corresponding pump flange, and Z the vertical distance of the pressure sensor from the reference plane (Sulzer, 1998). The subscripts $_\mathrm{d}$ and $_\mathrm{s}$ denote the discharge and the suction side of the pump, respectively.

In the ideal case, p_d and p_s should be measured at the discharge and suction flanges of the pump. However, in practice there has to be a certain distance between the flanges and measurement points to ensure that the pressure measurement is not disturbed by the pump. In addition, there can be valves and other process system components causing flow losses between the pump flange and the pressure measurement point. These factors can be taken account with the friction loss factor k_f that is affected by the pipe length, pipe inner diameter and dimensionless coefficient called the Darcy friction factor (see e.g. Nesbitt, 2006).

If the piping diameters are different at the discharge and suction measurement points, it will affect the flow velocity, which is taken into account in (3.1). The flow velocity can be calculated, if the cross-sectional area A of the piping and the pump flow rate are known:

$$v = \frac{Q}{A} = \frac{4 \cdot Q}{\pi \cdot d^2}, \tag{3.2}$$

where d is the pipe inner diameter in the case of a rounded pipe. Consequently, the pump head can be written as:

$$H = \frac{p_\mathrm{d} - p_\mathrm{s}}{\rho \cdot g} + \frac{8}{\pi^2 \cdot g} \cdot \left(\frac{1 + k_\mathrm{f,d}}{d_\mathrm{d}^4} - \frac{1 - k_\mathrm{f,s}}{d_\mathrm{s}^4} \right) \cdot Q^2 + \left(Z_\mathrm{d} - Z_\mathrm{s}\right), \tag{3.3}$$

where the pipe diameters and the sensor distances can be regarded as constant parameters. Correspondingly, the fluid density value can be regarded in many cases as a constant.

When the pump head has been calculated, the corresponding flow rate can be determined from the pump QH characteristic curve by numerical interpolation. If the pump is operating at a different speed than what the characteristic curves are published for, affinity equations are applied to transform the pump head value into the nominal speed of the pump n_n and then the corresponding flow rate back to the present rotational speed n:

$$H_\mathrm{n} = \left(\frac{n_\mathrm{n}}{n} \right)^2 \cdot H \tag{3.4}$$

$$Q = \left(\frac{n}{n_\mathrm{n}} \right) \cdot Q_\mathrm{n}, \tag{3.5}$$

where the subscript $_\mathrm{n}$ denotes values at the nominal speed of the pump. Alternatively, the pump QH curve can be transformed into the present rotational speed for the flow rate estimation.

When the flow rate has been estimated for the first time, its possible effect on the pump head can be taken into account, see (3.3). In order to ensure the correct estimation of the pump flow rate, operating point estimations should be performed with a time interval that allows the instant detection of the changing flow rate. Depending on the pump operational state and the process system characteristics, the minimum required time interval can vary from hundreds of milliseconds to several seconds. In practice, a notably shorter time interval, such as 10 ms, is applied to instantly detect the changing flow rate (ABB, 2006).

As this estimation method requires external process measurements, it can partially be considered as a measurement-based estimation method, and its use may be limited in existing installations. On the other hand, the measurement of the actual pump head improves the accuracy of the flow rate estimation compared with the methods using only estimates of a frequency converter. In addition, if the pump is equipped also with appropriate temperature sensors, the efficiency of a centrifugal pump could be estimated by applying the thermodynamic method.

3.2.2 *QP*-curve-based estimation method

This method utilises both the pump *QH* and *QP* characteristic curves for determining the operating point location. The estimated speed *n* and shaft power *P* of the pumping system are applied as the inputs of the estimator illustrated in Fig. 3.3. Compared with the *QH*-curve-based method, only internal estimates of a frequency converter are required for the determination of the operating point location. On the other hand, the *QP* characteristic curve has to be constantly increasing or decreasing in order for this estimation method to produce unambiguous results. For this estimation method, the following information is required:

- Pump *QP* and *QH* characteristic curves in the numeric form.
- Nominal speed of the pump applied in the characteristic curves.
- Density of the fluid.
- For the possible calibration of the published *QP* curve, the shaft power consumption value of the pump should be determined against a closed discharge or at other known operating points.

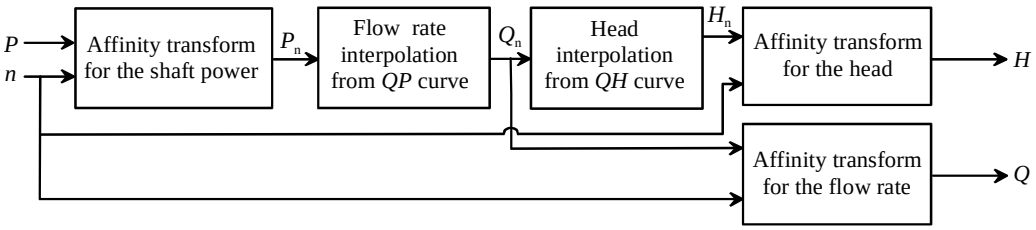

Fig. 3.3: Steps of the *QP*-curve-based estimation method. The shaft power and rotational speed of the pump are applied as inputs to the estimator.

Firstly, the estimated shaft power consumption of the pump is transformed into the nominal speed of the pump with the affinity equation:

$$P_{\mathrm{n}} = \left(\frac{n_{\mathrm{n}}}{n} \right)^3 \cdot P \,. \tag{3.6}$$

Then, the corresponding flow rate value Q_{n} can be determined from the *QP* characteristic curve with numerical interpolation. Consequently, this allows determination of the pump head H_{n} from the *QH* characteristic curve. Finally, these values are transformed into the present rotational speed of the pump with (2.3) and (2.4). Alternatively, affinity transforms could be performed for the pump *QH* and *QP* characteristic curves, resulting in direct interpolation of the present flow rate and head values.

In practice, the actual *QP* curve may differ considerably from the published one affecting the estimation accuracy of the *QP* curve method. For this reason, the published *QP* curve should be calibrated for instance by determining the shaft power consumption against a closed discharge valve or by determining the actual pump *QP* curve with a portable flow rate meter.

3.2.3 System-curve-based estimation method

If the pump and system *QH* curves are known, the pump operating point location can be determined by calculating the intersection point of these curves. Steps of this system-curve-based estimation method are illustrated in Fig. 3.4). In this case, the following information is required:

- Pump *QH* characteristic curve in the numerical form.
- Nominal speed of the pump applied in the characteristic curves.
- Static head H_{st} and the dynamic head coefficient *k* describing the system *QH* curve shape. Alternatively, a set of operating points that describe the system curve shape.

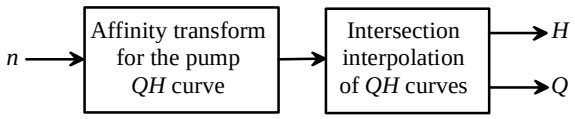

Fig. 3.4: Steps of the system-curve-based estimation method. The pump *QH* characteristic curve is transformed into the present rotational speed. Then, the location of the pump operating point is determined by calculating the intersection of the pump and system *QH* curves.

Firstly, the pump *QH* curve is transformed into the present rotational speed with affinity equations (2.3) and (2.4). Then, it is compared with the system *QH* curve in order to determine the location of the pump operating point. The system curve shape can be obtained from the knowledge of the system static head and a single operating point location of the pump. Alternatively, the system curve shape can be determined by test measurements. However, the system curve shape may alter because of varying process conditions, which decreases the accuracy of the estimation method. Hence, the system-curve-based estimation method is applicable only to applications in which the system curve shape remains constant or its change is known for instance by additional measurements.

3.3 Factors affecting the estimation accuracy of the model-based methods

The previously described methods utilise simple models for the pump operation and are therefore susceptible to the inaccuracy of parameters and input values. In general, estimation accuracy of the model-based methods depends on the operational state of the pump, the accuracy of the parameters describing the characteristics of the pump and the system, the effect of the fluid properties on the pump performance and the accuracy of the operational values used by the models. In addition, the interpolation methods applied to produce the pump characteristic curves from a limited number of data points and to calculate the intersection locations may affect the estimation accuracy, but their impact can be considered small compared with other factors.

3.3.1 Operational state of the pump

In general, the estimation methods may not provide accurate results in an operating region where cavitation or flow recirculation may occur (Hammo, 2005). These hydraulic phenomena have a decreasing effect on the head produced by the pump, and hence they change the shape of the pump *QH* curve (Karassik, 1998). They also cause pressure fluctuations and in the worst case intermittent fluid flow, which is not considered in the estimation methods. On the other hand, near the best efficiency point of the pump, the risk of cavitation and flow recirculation are at minimum. Hence, the estimated location of the pump operating point may also describe the probable accuracy of the estimation method.

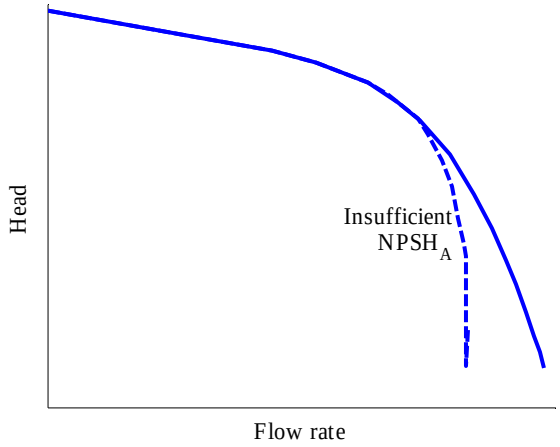

Fig. 3.5: Effect of insufficient $NPSH_A$ and the resulting cavitation on the published pump *QH* characteristic curve. The onset of cavitation restricts the available flow area, and consequently the flow will be lower at a given pump head if cavitation is present.

3.3.2 Pump characteristic curves

The pump characteristic curves provided by the manufacturer are usually measured to match the grade 2 accuracy criteria defined in the ISO 9906 standard (ISO, 1999). It determines the total difference by which the actual operating point of the pump can deviate from the guaranteed values (e.g. from the published pump curve). Annex A of the standard gives the following tolerances for pumps produced in series with selection made from typical performance curves: for the flow rate the allowed tolerance is ±9 %, for the head ±7 %, for the power consumption +9 % and −7 % for the efficiency, respectively. The annex also provides separate tolerances for

pumps with a driver power input less than 10 kW. The grade 1 accuracy criterion of the standard is typically applied for large (0.5–10 MW) pumps, and the allowed tolerances are ±4.5 % for the flow rate, ±3 % for the head and −3 % for the efficiency, respectively. In practice, the pumps may be worn, the actual properties of the impeller and shaft sealing system may differ from the assumed values, or the pumped fluid has different properties than water, which will also decrease the accuracy of the published pump characteristic curves. Hence, identification tests may be needed to determine the actual pump characteristic curves, as they can greatly differ from the assumed ones.

Besides the accuracy of the published characteristic curves, their shape affects the general applicability of model-based methods. If the pump *QH* curve is very flat (i.e., a small $|\mathrm{d}H/\mathrm{d}Q|$) or the pump *QP* curve has a slow rise or a slow decline (i.e., a small $|\mathrm{d}P/\mathrm{d}Q|$), a small error in the measured head or in the estimate for the power consumption causes a notable error in the location of the pump operating point (see Fig. 3.6). In practice, a flat curve shape can totally prevent the usage of model-based methods, if the resulting values are too inaccurate. For this reason, the *QP*-curve-based estimation method is not applicable with all centrifugal pump types. Especially mixed flow pumps (i.e., n_q around 90) can have a flat *QP* curve, or even a *QP* curve with both an increasing and decreasing part, which lead to erroneous estimation results for the pump operating point location, making the *QP*-curve-based estimation method unusable (see Fig. 2.6; Karassik, 1998). Correspondingly, the *QH*-curve-based estimation method cannot reliably work with a centrifugal pump having an unstable operating region in its *QH* characteristic curve. Otherwise, the introduced model-based methods can also be applied with other centrifugal pump types than just with a radial flow centrifugal pump. For instance, the decreasing *QP* curve shape of an axial flow centrifugal pump is as feasible as the increasing *QP* curve of a radial flow centrifugal pump, if just the *QP* curve is steep enough (i.e., $|\mathrm{d}P/\mathrm{d}Q|$ is large enough).

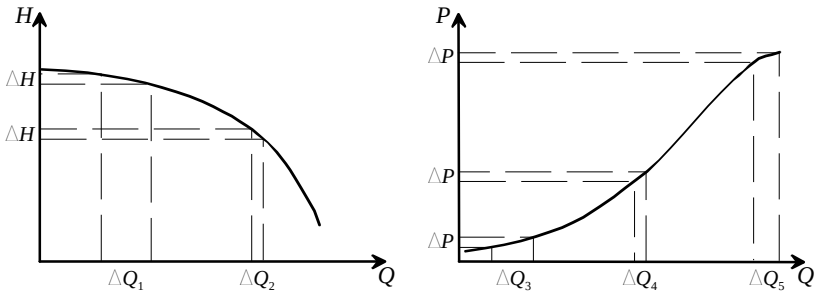

Fig. 3.6: Effect of the pump characteristic curve shape on the estimation accuracy in the case of a radial flow centrifugal pump ($n_q \approx 30$). The *QH* and *QP* curves should be steep enough to ensure sufficient estimation accuracy and the applicability of model-based methods. In this case, ΔQ_2 and ΔQ_4 are notably smaller than ΔQ_1, ΔQ_3 and ΔQ_5 because of the larger $\mathrm{d}H/\mathrm{d}Q$ and $\mathrm{d}P/\mathrm{d}Q$ values at the respective flow rates. In practice, the shape of the pump characteristic curves can prevent the reliable use of model-based methods with certain types of centrifugal pumps.

In practice, it may not be possible to measure the actual characteristic curves of the centrifugal pump. Then, a simple method to correct the inaccuracy of the *QP* curve is to measure the power consumption against a closed discharge valve at various speeds, and then correct the location of the published *QP* curve or the estimated power consumption value of the pump on the basis of these results. Kernan (2007) has introduced such a method, in which a frequency converter is applied to determine the flow rate of a centrifugal pump without external measurements. In the

method, the slope of the power curve is assumed to stay relatively constant although the actual power consumption values may greatly differ from the published ones. In order to improve the estimation accuracy, the actual power consumption is measured against a closed discharge valve at several rotational speeds. Then, the values of the published pump *QP* curve can be corrected or the estimated power consumption of the pump *P* at speed *n* can be corrected with the corresponding shutoff power value. Alternatively, the power consumption can be measured during the normal operation for the correction of the pump *QP* curve shape, if the flow rate is known or it can be measured with a separate device (e.g. a portable flow rate meter). If the pump is already equipped with pressure sensors for the determination of the pump head, also they could be used in the measurement of actual pump characteristic curves.

3.3.3 Fluid properties

Characteristics of the pumped fluid can be described with various parameters such as the density, temperature and viscosity characteristics of the fluid. Characteristic curves of a centrifugal pump are typically given for cold water, which has a constant viscosity. If the fluid properties differ from this, their effect on the pump performance should be determined. Otherwise, the above-described model-based estimation methods may provide inaccurate estimation results. The following fluid properties affect the operation of a centrifugal pump:

- Fluid temperature, which affects the fluid density and the vaporisation pressure of the fluid.
- Boiling and melting point of the fluid that may limit the applicability of the pump in harsh conditions.
- Nature of the fluid viscosity.
- Occurrence of gas in the fluid.
- Amount and nature of the solids in the fluid.

According to (Sulzer, 1998), the **fluid density** ρ does not affect the shape of the pump *QH* characteristics curve, but it has a direct effect on the measured values of pressure and the pump power consumption that can be taken into account by

$$P_{QP} = \left(\frac{\rho_{QP}}{\rho} \right) \cdot P \,, \tag{3.7}$$

where the subscript $_{QP}$ denotes values from the pump *QP* curve. This should be considered in the *QP*-curve-based estimation method. As the fluid density is affected by the **fluid temperature**, it should also be determined.

Boiling and melting point of the fluid may limit the pump usability in harsh conditions. For instance, the impeller may be blocked by the solidified fluid, which may lead to the motor overloading. Correspondingly, fluid vaporisation may lead to the pump cavitation, which can result in an impeller failure.

Viscosity describes the internal friction or “thickness” of the fluid, and is quantified with the dynamic viscosity μ. If the pumped fluid follows Newton’s Law of Viscosity and has a constant

viscosity value, it can be referred to as a Newtonian fluid. The major part of the pumped fluids fall into this category. Some examples of the Newtonian fluids are water, aqueous solutions and oil (Nesbitt, 2006). If the fluid's dynamic viscosity differs from that of water, it affects both the pump *QH* and *QP* characteristic curves, which can be taken into account by the viscosity correction factors that are given in (ISO, 2005).

In the case of non-Newtonian fluids, fluid viscosity does not stay constant, which makes the correction of the pump characteristic curves difficult. However, this can be resolved by the previously-mentioned correction factors, if the viscosity values are known at different operating points and the fluid viscosity has no time dependence. In practice, however, non-constant viscosity can affect the pump characteristic curves so that the estimation results may be severely erroneous. Therefore, the model-based methods are typically considered applicable only to fluids having an expectable behaviour. Some examples of non-Newtonian fluids are paper pulp and different suspensions with high concentrations of small particles such as cement.

The occurrence of gas in the fluid may strongly limit the centrifugal pump performance. If the gas enters a centrifugal pump, it may gather at the impeller hub resulting in the collapse of the fluid flow. As shown in Fig. 3.7, even a 2 % volume content of gas in the pumped fluid can affect the characteristic curves so that the model-based methods may provide inaccurate results or become unusable (Sulzer, 1998). Since the effect of gas on the pump performance cannot be simply described with a mathematical model, their possible effect on the characteristic curves has to be determined with separate test measurements.

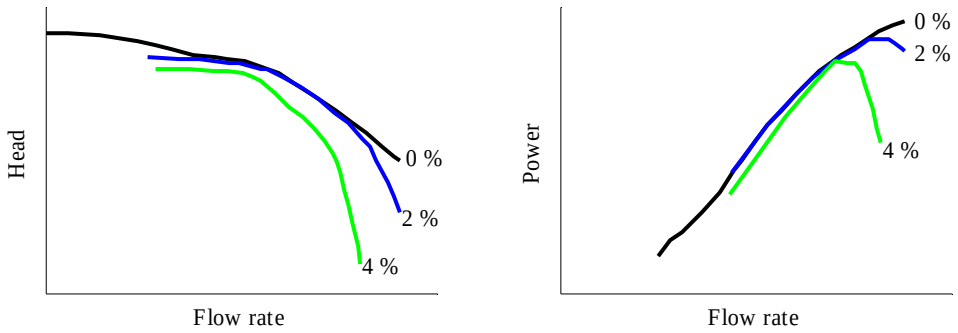

Fig. 3.7: Tested effect of the gas occurrence on the radial flow centrifugal pump characteristic curves (Gülich, 2008). Gas content is quantified as percentage of the gas volume in the fluid. In this case, the 2 % volume content of gas affects the characteristic curves so that the *QH*- and *QP*-curve-based estimation methods cannot provide accurate results.

Amount and nature of solids in the fluid affect the viscosity and density of the fluid, which in turn affect the pump characteristic curves. In addition, solids may seriously affect the wear rate of the pump and hence the pump characteristic curves (Nesbitt, 2006). Solid properties are typically described by the fluid consistency and the characteristics of the particles (size, density, shape etc.). Since the effect of these parameters on the pump characteristic curves is case dependent, the actual characteristic curves should be determined by separate test measurements. Alternatively, the published characteristic curves could be corrected on the basis of the fluid viscosity and density, if these fluid characteristics are known.

3.3.4 Estimates provided by the frequency converter

Model-based methods presented in this chapter use information available from a frequency converter, that is, the estimates of the actual rotational speed and the shaft power of a centrifugal pump. Hence, the accuracy of this data has a direct effect on the performance of model-based methods. Industrial frequency converters are typically controlled by a vector or direct torque control (DTC) method and a mathematical model that estimates the torque and rotational speed of the motor without external measurements (Bose, 2002). The operational state of the motor is then estimated on the basis of the phase currents, the dc link capacitor voltage and the inverter switch states, depending on the applied control method. Since accurate estimates are required for the successful control of the motor operation in certain applications, estimated values can be considered applicable also for diagnosis and control purposes of variable-speed-driven pumps. According to (ABB, 2002), the typical accuracy of a DTC frequency converter is 10 % of the induction motor nominal slip for speed (e.g. 4 rpm for a 1460 rpm motor; 0.3 %) and 2 % for torque. If these values describe the estimation accuracy of a frequency converter, then the converter estimates are comparable even with the required values of instrumentation accuracy in the measurement of an induction motor efficiency: according to (IEC, 2007), the instrumentation accuracy of the torque measurement should be within 0.2 % of the full scale value, and the instrumentation accuracy of the rotational speed should be within 0.1 % of the full scale value.

A specific accuracy for the motor shaft power estimate (i.e., pump power consumption) has not been determined, but by assuming for the sake of simplicity that the speed and shaft torque estimates are independent of each other, the following equation can be formed for the relative error of the shaft power estimate:

$$\left|\frac{\Delta P}{P}\right| \leq \left|\frac{\Delta T}{T}\right| + \left|\frac{\Delta n}{n}\right|. \tag{3.8}$$

By applying (3.8), the resulting shaft power estimation accuracy of the previously mentioned motor is within 2.3 %. However, a centrifugal pump is in many cases driven with a scalar-controlled frequency converter, since it is controlled according to the process measurements and requirements, and there is no need for the sensorless control of the motor. Depending on the converter design, this may significantly decrease the accuracy and amount of the available estimates. For instance, the static speed accuracy of a scalar-controlled frequency converter may be 1–3 % and the accuracy of the torque estimate may be 4 %, respectively (ABB, 2002). Then, the resulting shaft power estimation accuracy is within 5–7 %. Compared with the accuracies given for the DTC method, estimates of a scalar-controlled frequency converter may result in substantially inaccurate results for the pump operating point location. It should also be noted that the actual estimation accuracy of a frequency converter might be even lower because of inaccurate motor model parameters. Hence, a frequency converter that has been designed for the sensorless control of an induction motor could be regarded as a preferred choice for the use of model-based estimation methods.

3.3.5 Numerical methods applied in the operating point estimation

Numerical methods are applied in the model-based estimation methods for the determination of the pump operating point location. Typically, an interpolation or a regression method is needed to determine the characteristic curve values between the known points. Correspondingly, a calculation algorithm is required to determine the intersection of two curves in the system-

curve-based estimation method. If an insufficient number of data points are known from the pump characteristic curves, the applied interpolation and intersection calculation methods may result in erroneous results for the pump operating point location. Typically, a sufficient number of data points can be obtained from the pump characteristic curves, and the effect of applied numerical methods on the estimation accuracy is small compared with other possible factors.

3.3.6 Summary of the factors affecting the estimation accuracy

Each of the previously listed factors may lead to erroneous estimation results for the pump operating point location. However, part of the mentioned factors can be taken into account beforehand (fluid properties, the accuracy of the published characteristic curves, general applicability of the pump characteristic curves to the model-based estimation methods), which allows the compensation of their effects on the estimation results. On the other hand, there are factors, such as the pump operating point location and the shape of the pump characteristic curves, which cannot be affected, and they are always present in the estimation. The object of this section is to summarise the main factors that affect the accuracy of the model-based estimation methods.

All the presented model-based methods are affected by the accuracy of the pump characteristic curves, which can be regarded as the primary[4] reason for possibly incorrect estimation results. As introduced in previous sections, the accuracy of characteristic curves has allowed tolerances, and the actual characteristic curves can also be affected by the fluid properties, the condition of the pump, cavitation and other adverse events. If it is not possible to determine the actual pump characteristic curves, the allowed tolerances may lead to estimation results for the head and the flow rate that differ from the actual operating point location. An example of the allowed tolerances for the characteristic curves of a Sulzer APP22-80 pump is shown in Fig. 3.8. In practice, the actual characteristic curves may be located anywhere between the allowed tolerances, even if the pump had just been manufactured. For this reason, pump-specific characteristic curves should be available from the manufacturer for new pumps besides the generic curve prints.

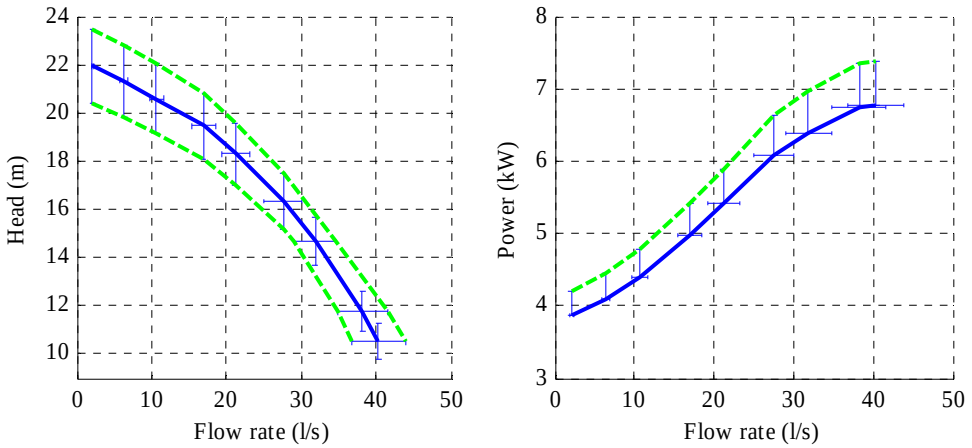

Fig. 3.8: Effect of allowed tolerances (ISO 9906, grade 2 for pumps produced in series) on the characteristic curves of a Sulzer APP-22 80 centrifugal pump. Compared with the published characteristic curves indicated by a blue line, the actual curves may be located between the allowed tolerances (green dashed lines).

[4] For the system-curve-based method it is evident that the accuracy of the system *QH* curve has a main effect with the pump *QH* curve on the resulting operating point locations.

Besides the accuracy of the characteristic curves, their shape may cause erroneous estimation results as shown in Fig. 3.6. As said, the pump *QH* and *QP* curves should be constantly decreasing or increasing, so there would be unambiguous estimation results for the pump operating point location. This limitation may exclude the use of *QP*-curve-based estimation method especially with mixed flow centrifugal pumps (i.e., $n_q \approx 80$), which typically have a flat *QP* curve. In the case of radial flow centrifugal pumps (e.g. $n_q \approx 30$), d*P*/d*Q* of the pump *QP* curve may be lower in the edges of the characteristic curve than near the pump BEP, meaning that the estimation accuracy of the *QP* curve method is at its best when the operating point location is near the best efficiency point.

Correspondingly, the *QH*-curve-based estimation method cannot reliably work with a centrifugal pump having an unstable operating or a totally flat region in their *QH* characteristic curve. This maybe an issue with very low ($n_q \approx 10$) specific speed and high specific speed (i.e., axial flow) centrifugal pumps (ANSI/HI, 1997; Karassik, 1998). In the case of a radial flow centrifugal pump ($n_q \approx 30$), d*H*/d*Q* is often at lowest near the zero flow rate resulting in a possibly lower estimation accuracy in this operating region.

In addition to the characteristic curves, also the estimated rotational speed and the shaft power have an effect on the accuracy of estimation results. In practice, the shaft power estimate is more inaccurate (2.3 %) than the rotational speed estimate (0.3 %), and it can lead to erroneous results especially in the operating region of the *QP* curve with a low d*P*/d*Q* value.

In the case of the *QH*-curve-based estimation method, the accuracy of the head measurement can affect the accuracy of the resulting operating points. However, the practically attainable accuracy of the head measurement (e.g. 1.5 %) can be regarded better than the allowed tolerance for the pump head (±7 %, ISO 9906, grade 2) in the *QH* characteristic curve (Sulzer, 1998). Related to this, also erroneous parameters for the piping diameters may affect the resulting values, but their effect can be considered a secondary problem compared with the erroneous characteristic curves.

3.4 Laboratory tests

Laboratory tests were conducted to analyse the applicability of the above-described estimation methods, when a radial flow centrifugal pump is driven in different operating points, and the pumped fluid is water. Consequently, the methods were tested with the previously-introduced laboratory pumping system comprising an ABB ACS 800 frequency converter that applies the DTC method, an ABB 11 kW induction motor and a Sulzer APP 22-80 centrifugal pump with a 255 mm impeller (Q_{BEP} = 28 l/s, H_{BEP} = 16 m, n_n = 1450 rpm, see Appendix A for other details). The pumping system is attached to a process system, which consists of two water tanks and venturi tubes, piping and control valves as shown in Fig. 2.16. The shape of the system curve can be modified with control valves.

The pumping system is equipped with a Dataflex 22/100 torque and speed measurement shaft (1 Nm accuracy published for torque) that was used in the measurements. The head produced by the pump was measured with two absolute pressure sensors across the pump according to (3.1), and the flow rate was determined by a pressure difference measurement across the venturi tube (see Appendix B for further details). The flow rate was also used to determine the velocity head of the Sulzer pump in the accuracy determination of the published characteristic curves. The pressure difference sensor was calibrated before the measurements. The accuracy of the venturi system has been previously verified with an ISOIL electromagnetic flow meter to be within 2

l/s over the entire pump operating region. Operation of the frequency converter was monitored with an ABB DriveDebug software.

3.4.1 Accuracy of the pump characteristic curves

Firstly, the accuracy of the published pump characteristic curves was determined with a measurement sequence, in which the pump rotational speed was held at 1450 rpm, and the pump head, flow rate and shaft power consumption were measured at nine different operating points. Also the frequency converter's pre-filtered estimates for the rotational speed, shaft torque and shaft power consumption (firmware parameters 1.02, 1.05 and 1.06, respectively) were stored at each operating point. The temperature of the pumped water was about 20 °C during the measurements.

The obtained characteristic curves are shown with the published characteristic curves in Fig. 3.9. Since there are no published characteristic curves available for the 255 mm impeller, they were calculated from the 250 mm diameter characteristic curve with the respective scaling equations (2.7)–(2.9). In addition, the pump head and shaft power consumption for the 42 l/s flow rate were extrapolated into the published characteristic curves in order to improve the estimation accuracy at high flow rates.

The resulting figure shows a notable difference between the published and measured power consumption of the pump, which exceeds the allowed tolerance set by the ISO 9906 grade 2 standard. Most likely, the difference is caused by mechanical losses in the bearings and seals, as the pump *QH* curve is very accurate and shows no signs of pump deterioration. One can see that in this case the use of the published *QP* curve would produce erroneous estimates for the pump operating point location. It should also be noted that this difference can occur as well with other centrifugal pump types than just with radial flow centrifugal pumps. One can also see that the d*P*/d*Q* is lower at the edges of the pump characteristic curve than near the pump BEP, which presumably affects the estimation accuracy of the *QP*-curve-based estimation method.

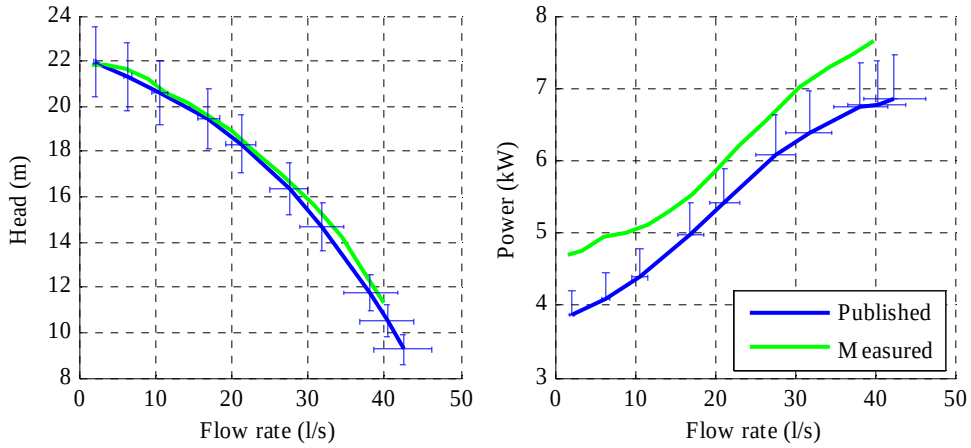

Fig. 3.9: Published and measured characteristic curves of the laboratory pumping system. Allowed tolerances set by the ISO 9906 grade 2 standard are presented for the published characteristic curves. There is a notable difference between the published and measured power consumption of the centrifugal pump, which has an effect on the estimation accuracy of the *QP*-curve-based estimation method.

Since in the existing installations it may not be possible to determine the actual characteristic curves of the pump, an alternative method should be applied to ensure the accuracy of the characteristic curves. As previously discussed, the accuracy of the *QP* curve could possibly be improved by determining the difference of the published and the actual shaft power consumption at zero flow rate, and by correcting the published *QP* curve location with this value. In this case, the correction was performed on the basis of the frequency converter's estimate for the shaft power consumption at a zero flow rate, as this method does not require the actual pump flow rate information. The resulting *QP* curve is shown in Fig. 3.10. Alternatively, accuracy of the pump *QP* curve could be checked for instance by utilising an external ultrasonic flow rate measurement device to check the actual flow rate of the pump.

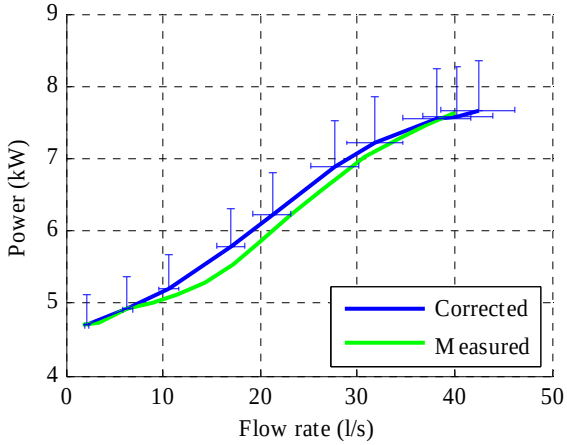

Fig. 3.10: Corrected and measured *QP* curve of the laboratory pump. The allowed tolerances set by the ISO 9906 grade 2 standard are also presented for the corrected curve. The correction of the published *QP* curve has significantly decreased the difference between the published and measured curves, and thus the corrected curve was utilised with the *QP*-curve-based estimation method.

3.4.2 Test results of the *QH*- and *QP*-curve-based estimation methods

In order to test the accuracy of the *QH*- and *QP*-curve-based estimation methods in the case of a radial flow centrifugal pump, test measurements were conducted with five different system curve shapes that were generated with control valves: the valves were adjusted so that the flow rates were approximately 50, 70, 100, 120 and 140 percent of Q_{BEP} 28 l/s at 1450 rpm. With these valve settings, the pump was driven at rotational speeds ranging from 1080 rpm to 1560 rpm. The head and flow rate produced by the pump, the rotational speed and shaft torque of the motor, and the frequency converter estimates for the rotational speed and shaft power consumption (firmware parameters 1.02 and 1.06) were measured in each operating point. Operating point locations were then estimated by applying the presented model-based methods. In the case of the *QH*-curve-based estimation method, magnitude of the velocity head was determined from the initial estimation of the flow rate. After this, the flow rate estimate was determined using the sum of measured head and velocity head (i.e., the head estimate).

The results for the measuring sequence with the 100 % relative flow rate are shown in Fig. 3.11. Separately determined efficiency curves of the pump have also been shown in the figure. In this case, the pump was operating very close to its BEP and in the steep region of the pump *QP* curve, allowing the model-based methods to provide correct results for the pump operating point location: with the *QP*-curve-based method, the estimation error of the flow rate is within

2.0 l/s (7 % of Q_{BEP}), and the estimation error of the head is within 0.5 m (3 % of H_{BEP}) compared with the measured values. For the *QH*-curve-based estimation method, the estimation error of the flow rate is within 0.9 l/s (3 % of Q_{BEP}), which can be regarded as an applicable accuracy even for control purposes.

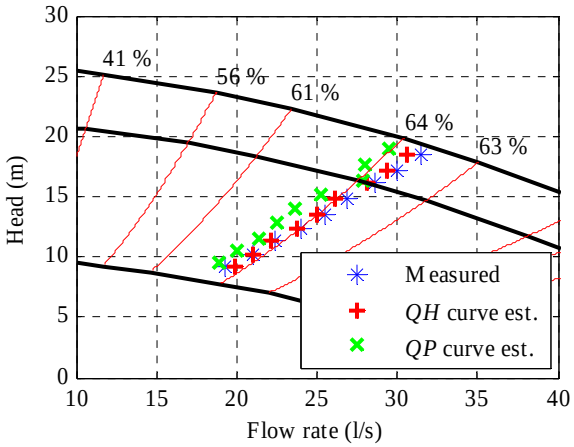

Fig. 3.11: Test results for the *QH*- and *QP*-curve-based estimation methods in the case of a 100 % relative flow rate (i.e., 100 % of Q_{BEP}). The estimation error of the flow rate is within 0.9 l/s (3 % of Q_{BEP}) for the *QH* curve method and within 2.0 l/s (7 % of Q_{BEP}) for the *QP* curve method, respectively. *QH* curves of the pump are drawn for the rotational speeds of 1000 rpm, 1450 rpm and 1600 rpm, respectively.

As discussed in Chapter 2, Hydraulic Institute's guideline advises to use the pump in its preferred operating region, at the flow rates between 70 % and 120 % of the Q_{BEP}. Test results for these two relative flow rate values are shown in Fig. 3.12. In either case, the both estimation methods show that the pump is not operating as near its BEP as in the case of the 100 % relative flow rate. However, there is a systematic difference between the measured and *QP*-curve-estimated operating points, which is most likely caused by the difference between the corrected and measured *QP* curve of the pump. In the case of 70 % relative flow rate, the estimation error of the flow rate is within 3.3 l/s (12 % of Q_{BEP}), and the estimation error of the head is within 1.1 m (7 % of H_{BEP}) compared with the measured values. For the *QH*-curve-based estimation method, the estimation error of the flow rate is within 1.4 l/s (5 % of Q_{BEP}). In the case of 120 % relative flow rate, the estimation error of the *QP*-curve-based method is within 3.0 l/s (11 % of Q_{BEP}) for the flow rate and within 1.1 m (7 % of H_{BEP}) for the head, respectively. The estimation error of the *QH*-curve-based method is again notably smaller, within 0.6 l/s (2 % of Q_{BEP}) for the flow rate.

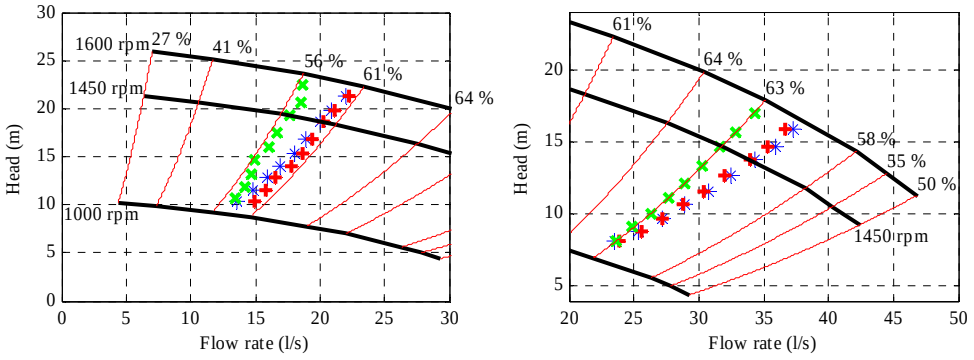

(a) (b)

Fig. 3.12: Test results for the *QH*- and *QP*-curve-based estimation methods, when the relative flow rate is (a) 70 % and (b) 120 % of the Q_{BEP}. The symbols applied are consistent with Fig. 3.11.

When the laboratory pump is driven away from the vicinity of the BEP, it may be prone to events that can alter the actual pump characteristic curves. In addition, the d*P*/d*Q* value of the laboratory pump *QP* curve gets lower at very low and large relative flow rates, which decreases the accuracy of the *QP*-based estimation method. In Fig. 3.13, the test results for the measurement sequence with a 140 % relative flow rate are illustrated. In this case, the operating points are located in the far-right region of the published characteristic curves, where the d*P*/d*Q* of the published *QP* curve is at its minimum. For this reason, the *QP*-curve-based estimation method cannot provide as accurate results for the pump operating point location as in the recommendable operating region of the pump. At the rotational speeds of 1080–1260 rpm, the estimated flow rate values are negative, which is the reason why they are not visible in the figure. At the rotational speeds of 1320–1560 rpm, the estimation error of the flow rate is within 5.3 l/s (19 % of Q_{BEP}), and the corresponding error of the head is within 2.1 m (13% of H_{BEP}), respectively. On the other hand, the *QH*-curve-based estimation method performs well also in this case, since there was neither cavitation nor other adverse phenomena that would have affected the pump performance in this measurement sequence. For the *QH*-curve-based estimation method, the estimation error of the flow rate is within 0.7 l/s (3 % of Q_{BEP}).

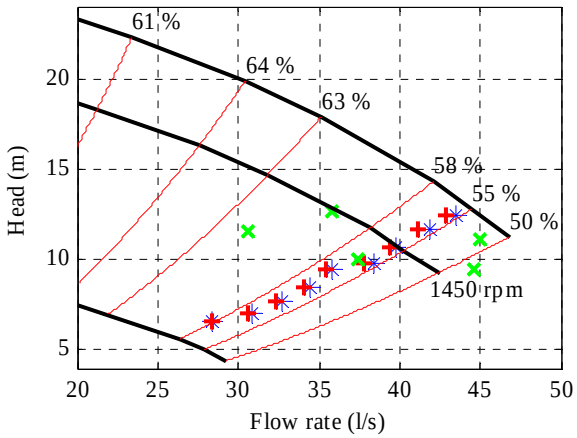

Fig. 3.13: Test results for the *QH*- and *QP*-curve-based estimation methods, when the relative flow rate is 140 %. The symbols applied are consistent with Fig. 3.11.

The estimation methods were also tested with the 50 % relative flow rate, which describes a system with an oversized radial flow centrifugal pump. In this case, the operating points are in the allowable operating region of the pump, and the shape of the *QP* curve is steeper than at the 140 % flow rate. The test results are shown in Fig. 3.14. Compared with the 140 % relative flow rate, the estimates provided by the *QP*-curve-based method are now more accurate. However, at rotational speeds over 1450 rpm, there is a notable difference between the measured and estimated operating points. For this reason, the estimation error of the flow rate is within 3.5 l/s (12 % of Q_{BEP}), and the estimation error of the head is within 0.9 m (5 % of H_{BEP}) for the *QP*-curve-based estimation method. The estimation error of the *QH*-curve based method is within 2.0 l/s (7 % of Q_{BEP}), which is most likely caused by the effect of the flat *QH* curve shape on the estimation accuracy.

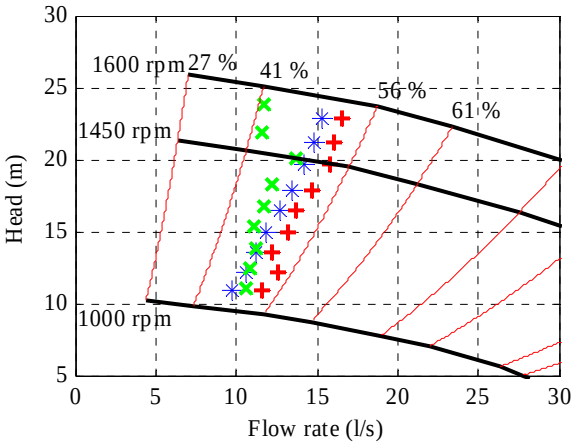

Fig. 3.14: Test results for the *QH*- and *QP*-curve-based estimation methods, when the relative flow rate is 50 %. The symbols applied are consistent with Fig. 3.11.

For the comparison of the *QH*- and *QP*-curve-based estimation methods, test results are gathered in Table 3.1. Based on the test results, both the *QH*- and *QP*-curve-based estimation method are applicable to the laboratory pumping system, if the available pump characteristic curves are accurate enough to describe the pump operation, and the flow estimation accuracy of 2–19 % of Q_{BEP} is acceptable. For the laboratory pumping system, the estimation accuracy of the *QH* and *QP* curve methods can be considered sufficient for the diagnosis purposes, as the methods provide correct information on the operating point location, that is, when it is in the recommendable operating region of the pump. According to the test results, methods are able to inform the user when the actual operating point location of the laboratory pump is outside the recommendable operating region, and the pump operates with a lower efficiency. In practice, however, this cannot be expected with all centrifugal pumps, as the mixed flow centrifugal pumps can have a flat *QP* curve near the pump BEP. The actual characteristic curves of the pump may also be more inaccurate than with the laboratory pumping system, leading presumably to a lower estimation accuracy. It should also be noted that the *QH*- and *QP*-curve-based methods may provide erroneous results, if the pump is actually operating in the region where cavitation or other events may affect the pump characteristic curves. Consequently, the shown test results most likely hold true only for other pumping systems having a radial flow centrifugal pump ($n_q \approx 30$), water as the pumped fluid, good characteristics against the occurrence of cavitation and an option to determine the accuracy of the pump *QP* curve.

According to the test results for the laboratory pumping system, the *QH*-curve-based estimation method could be considered accurate enough for the control purposes of a radial flow centrifugal pump, if this is allowed by the accuracy of the pump characteristic curves. This can also be the situation with other centrifugal pump types and industrial pumping systems, if the actual pump *QH* curve is known, there are no unstable operating regions and curves are not affected by the mechanical wear of the pump or fluid characteristics. On the other hand, the *QP*-curve-based estimation method cannot be recommended for applications where strict estimation accuracy is required or the pump is typically operating at the flat parts of published characteristic curves (i.e., a small $|dP/dQ|$): in such a case, estimated operating points can be clearly unrealistic, or they may lead to false analysis results concerning the pump operational state. Thus, the use of *QP*-curve-based estimation method is limited to pumping systems, where the *QP* curve shape allows the use estimation method for unambiguous results (i.e., radial flow and axial flow centrifugal pumps), and the accuracy of the pump *QP* curve could be checked somehow. In addition, limitations could be added to the model-based methods, so they would not produce unrealistic results for the pump operating point location.

Table 3.1: Relative estimation errors of the *QH*- and *QP*-curve-based estimation methods compared with the measured values at different relative flow rates at the rotational speeds of 1080–1560 rpm. At the relative flow rate of 140 % and at the rotational speeds of 1080–1260 rpm, the estimated flow rates provided by the *QP*-curve-based method have been negative and hence inapplicable.

	***QH* curve method**		***QP* curve method**	
Relative flow rate	$\lvert\Delta Q/Q_{BEP}\rvert$	$\lvert\Delta H/H_{BEP}\rvert$	$\lvert\Delta Q/Q_{BEP}\rvert$	$\lvert\Delta H/H_{BEP}\rvert$
50 %	7 %	–	12 %	5 %
70 %	5 %	–	12 %	7 %
100 %	3 %	–	7 %	3 %
120 %	2 %	–	11 %	7 %
140 %	3 %	–	19 % (at 1320–1560 rpm)	13 % (at 1320–1560 rpm)

3.4.3 Test results of the system-curve-based estimation method

The system-curve-based estimation method was tested with the measurement data introduced in the previous chapter. The system curve parameters were calculated for each measurement sequence based on the expected operating point location and the amount of the estimated static head at 1450 rpm. Since the system conditions stayed relatively constant during the measurement sequence, the system-curve-based estimation should provide correct estimates for the pump operating point location.

Firstly, the system-curve-based method was tested with the 100 % relative flow rate sequence of measurements. The test results are shown in Fig. 3.15. In this case, the estimation error of the flow rate is within 1.0 l/s (4 % of Q_{BEP}), and the estimation error of the head is within 0.2 m (1 % of H_{BEP}), respectively. The difference between the measured and estimated operating points is mainly caused by the inaccuracy of the system curve parameters.

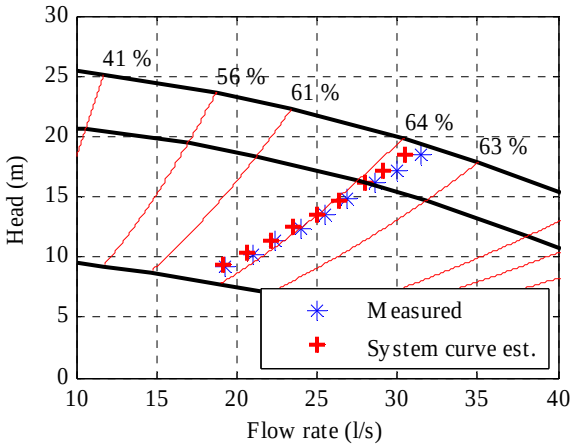

Fig. 3.15: Test results for the system-curve-based estimation methods in the case of a 100 % relative flow rate (i.e., 100 % of Q_{BEP}). The *QH* curves of the pump are drawn for the rotational speeds of 1000 rpm, 1450 rpm and 1600 rpm, respectively.

In Fig. 3.16, test results are shown for the 70 % and 120 % relative flow rates. Also in this case the estimation results provided by the system-curve-based method are comparable with the *QH*-curve-based method. In either case, the estimation error of the flow rate is within 0.9 l/s (3 % Q_{BEP}), and the estimation error of the head is within 0.3 m (2 % of H_{BEP}) compared with the measured values. In this case also, the accuracy of the estimation methods could be improved with more accurate system curve parameters.

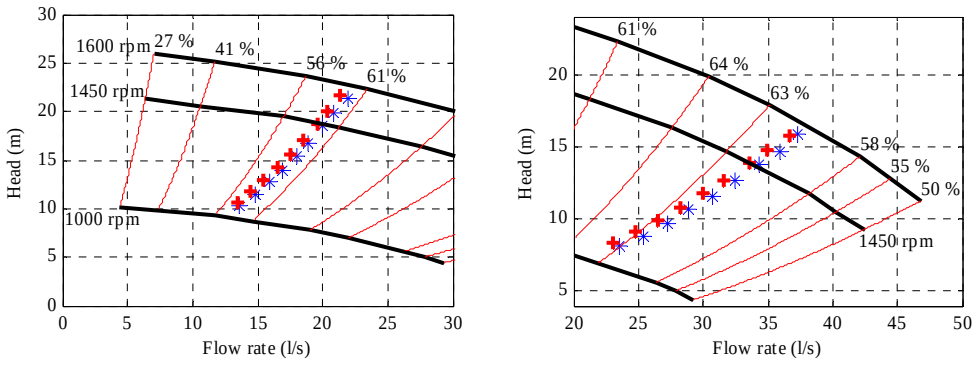

Fig. 3.16: Test results for the system-curve-based estimation methods, when the relative flow rate is (a) 70 % and (b) 120 % of the Q_{BEP}. The symbols applied in the figure are consistent with Fig. 3.15.

In the case of 140 % relative flow rate, the estimation accuracy of the *QP*-curve-based method was affected by the small d*P*/d*Q* value of the *QP* curve. For the system-curve-based method, operation in the far-right region of the pump *QH* curve should not pose a problem, since there were no signs of cavitation that would have affected the pump performance. The test results are shown in Fig. 3.17. In this case, the estimation error of the flow rate is within 1.3 l/s (5 % of Q_{BEP}), and the estimation error of the head is within 0.4 m (2 % of H_{BEP}), respectively. Compared with Fig. 3.13, the estimation error of the system curve method is somewhat larger than the error of the *QH*-curve-based estimation method, but otherwise the system-curve-based estimation method provides correct information on the pump operating point location.

However, also in this case the estimation accuracy could be improved by using more accurate values for the determination of the system curve parameters. If the measured operating point location and the measured amount of static head were applied to determine the system curve shape, the estimation error of the flow rate would be within 0.7 l/s (2 % of Q_{BEP}), and the estimation error of the head would be within 0.3 m (2 % of H_{BEP}), respectively.

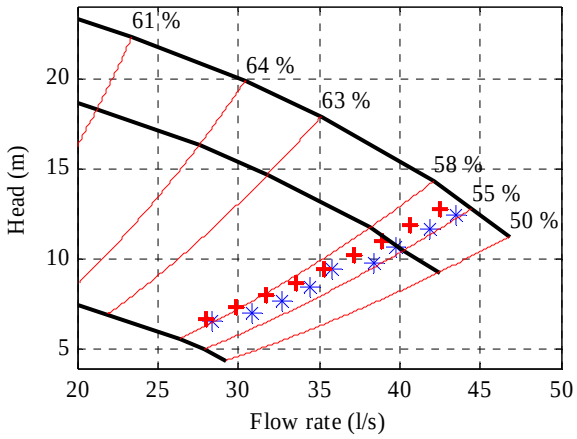

Fig. 3.17: Test results for the system-curve-based estimation method, when the relative flow rate is 140 %. The symbols applied here are consistent with Fig. 3.15.

The system-curve-based estimation method was also tested with the 50 % relative flow rate, and the results are shown in Fig. 3.18. In this case, good accuracy of the pump and system *QH* curves has resulted in accurate estimation results. The estimation error of the flow rate is within 0.3 l/s (1 % of Q_{BEP}) and the estimation error of the head is within 0.3 m (2 % of H_{BEP}), respectively.

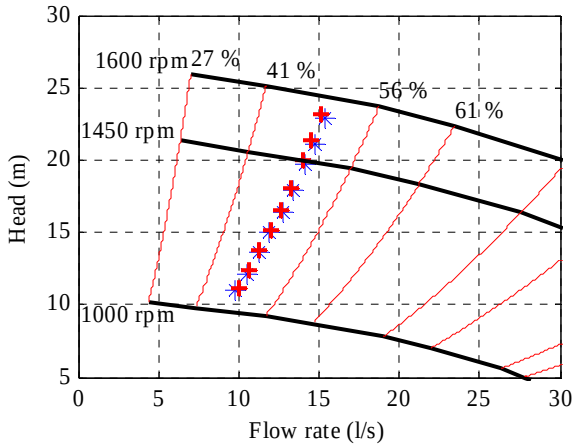

Fig. 3.18: Test results for the system-curve-based estimation methods, when the relative flow rate is 50 %. The symbols applied are consistent with Fig. 3.15.

The test results are gathered in Table 3.2. They show the applicability of the system-curve-based estimation method with the laboratory pumping system, where the pump and system *QH*

curves are accurate, water or a corresponding Newtonian fluid is pumped, and the process conditions can remain constant during the estimation. If these criteria can be met, the system-curve-based estimation method could also be utilised for diagnosis purposes of other pumping systems and centrifugal pump types, if there is no possibility for unstable operation of the pump. The method might also be applicable for control purposes of a pumping system, if the system curve is not affected by valves or other process devices, or the changes in the system characteristics could be taken into account.

In practice, the applicability of this method may however be very limited, as the system characteristics generally change during the pump operation and this change may remain unknown without additional measurements. For this reason, the results shown in Table 3.2 cannot be applied as a general example of the feasibility and accuracy of the system curve method. Therefore, this method can be recommended only for applications where the pump and system characteristics are accurately known or known to remain constant.

Table 3.2: Relative estimation errors of the system-curve-based estimation method compared with the measured values at different relative flow rates at the rotational speeds of 1080–1560 rpm. Compared with the results shown in Table 3.1, the resulting accuracy of the system curve method is comparable with the *QH*-curve-based estimation method.

	System curve method	
Relative flow rate	$\lvert\Delta Q/Q_{BEP}\rvert$	$\lvert\Delta H/H_{BEP}\rvert$
50 %	1 %	2 %
70 %	3 %	2 %
100 %	4 %	1 %
120 %	3 %	2 %
140 %	5 %	2 %

3.5 Pilot tests with the *QP*-curve-based estimation method

Besides laboratory tests, the *QP*-curve-based estimation method has been applied to determine typical operating point locations of two pumping system in a paper mill. The operation of a primary water pump and a pulp pump was monitored by a frequency converter and a measurement computer for the time period of six months. In this section, estimation results are introduced as an example of how model-based estimation can provide additional information for the analysis of the pump operation.

The primary water pumping system consists of an Ahlström P-X80X-1 vertical wet pit (i.e., axial flow) pump, a Strömberg 550 kW induction motor and an ABB ACS 800 frequency converter. The nominal values of the vertical wet pit pump are 1.85 m^3/s for the flow rate, 22 m for the head, 85 % for the efficiency and 740 rpm for the rotational speed, respectively. The water pump transfers cold water from the water station further to the mill, allowing the use of original pump characteristic curves for the analysis. The accuracy of the pump *QH* curve has been previously ensured by a test measurement run, but this has not been carried out for the pump *QP* curve, possibly affecting the estimation accuracy of the *QP*-curve-based method. The rotational speed of the primary water pump is controlled according to the pressure measurement located away from the pump and a typical pressure reference value of 135 kPa. In practice, the reference pressure value and the pump head can differ from each other because of the varying head losses and water consumption before the pressure measurement in the steam power plant.

The pulp pumping system shown in Fig. 3.19 comprises a Sulzer ARP 54-400 centrifugal pump, an ABB 400 kW induction motor and an ABB ACS 600 frequency converter. The nominal operating values of the pulp pump are 675 l/s, 24 m, 85 % and 990 rpm, respectively. The pumped fluid consists of water and wood fibres. However, the fluid consistency is only 1.5 % and it has the same density as water, which enables the use of the original characteristic curves for the analysis also in this case. The pulp pump is located next to the paper machine 3, and it transfers the pulp from a reservoir to the tanks near the paper machine. Also in this case, the rotational speed of the pump is controlled according to the pressure measurement and a typical reference value of 285 kPa. Different from the primary water pump, the location of the pressure measurement is closer to the pump, and there are no valves between the pump and the measurement location.

Fig. 3.19: Pulp pumping system in a paper mill. The pulp pump is located next to the paper machine 3, and it transfers the fluid from a reservoir to the tanks near the paper machine.

For both cases, estimations of the pump operating point locations were carried for a period of six months to ensure inclusion of the most typical operational states for the analysis. The rotational speed and shaft power estimates provided by the frequency converter were fetched and stored every five minutes to a personal computer, which was connected to the frequency converter. For both cases, approximately 50000 estimations were carried out during the measurement period. In both cases, a pre-filtered shaft power estimate (parameter 1.06, -3dB cut-off frequency F_c = 1.6 Hz; ABB, 2009) was used in the estimations. The rotational speed of the primary water pump was determined with the converter parameter 2.17, which is the unfiltered estimate of the motor rotational speed (ABB, 2009). For the pulp pump, a pre-filtered estimate of the rotational speed (parameter 1.02, F_c = 0.3 Hz) was used.

The estimation results for the primary water pumping system were analysed and then divided into two separate time periods based on the pump rotational speed and the resulting operating point locations. The first time period has a duration of one month and the second time period covers the remaining five months. The operating point locations of the first time period are shown in Fig. 3.20, in which the most typical operating point location is indicated by an asterisk. The normal distribution of the operating points (about 68 % of the shown points) around this location is demonstrated with an ellipse. In the first time period, the pump operating point locations varied all over the *QH* curve, and the pump rotational speed was around 655 rpm. The major part of the operating point locations lie at partial flows. Compared with the nominal efficiency of the pump, 85 %, the pump estimated efficiency was typically around 70 %. These results are also a good example of changing system characteristics, which can practically prevent the usage of the system-curve-based estimation method.

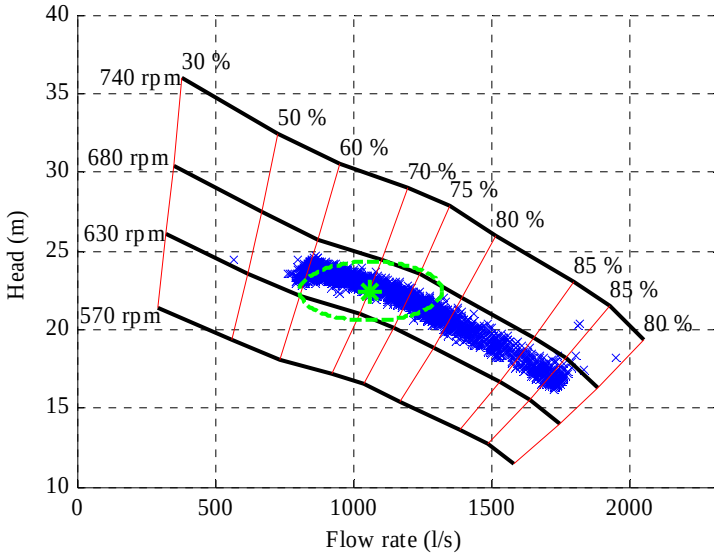

Fig. 3.20: Estimation results of the first time period for the primary water pumping system. Since the pump duty varies greatly depending on the water consumption, the operating points are distributed over the *QH* curve. However, the major part of the operating points are located in the region with a reduced efficiency. It should be noted that the results may have been affected by the possible inaccuracy of the pump *QP* curve.

The operating point locations of the second time period are shown in Fig. 3.21. Over this time period, the pump operating point locations were concentrated at partial flow rates, and the pump rotational speed was mainly around 605 rpm. Occasionally, a larger flow rate has been required from the pump, and the pump rotational speed has increased over 650 rpm. The system characteristics may also have varied as a function of time affecting the resulting operating point locations. Compared with the nominal efficiency of the pump, 85 %, the estimated pump efficiency was typically only 50 %, resulting in a notable efficiency improvement capability. Hence, it has been recommended to the mill personnel that the operation of the pumping system and its energy efficiency should be studied further.

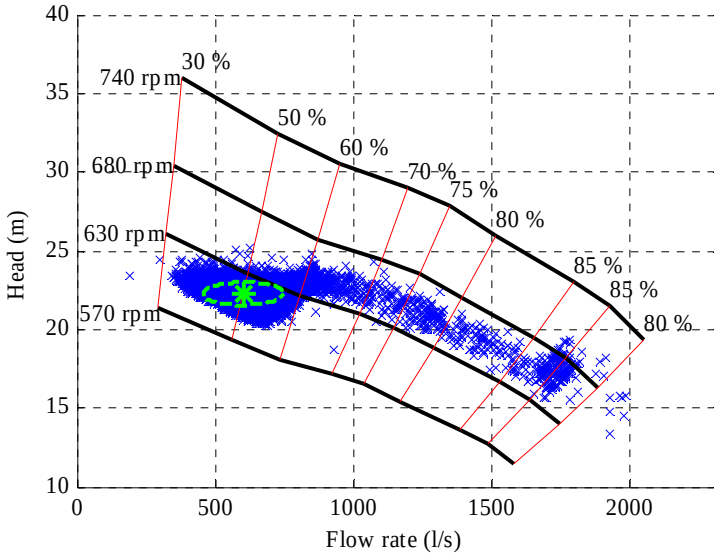

Fig. 3.21: Estimation results of the second time period for the primary water pumping system. In this case, the typical pump efficiency has been only 50 %. It should be noted that the results may have been affected by the possible inaccuracy of the pump *QP* curve.

The estimation results for the pulp pumping system are shown in Fig. 3.22. Its process function is to provide the pulp delivery into tanks, and hence it has a more uniform operating point location distribution than the primary water pump consisting of several fixed-speed pump *QH* curves, which may indicate a constantly changing system static head. Related to this, Fig. 3.23 shows an example of operating points for the time period of two days. Also in this case, the most typical operating point locations are not in the pump's best efficiency point, affecting negatively the total efficiency of the pumping system. Compared with the primary water pumping system, the typical estimated efficiency is however significantly closer to the nominal efficiency of the pump.

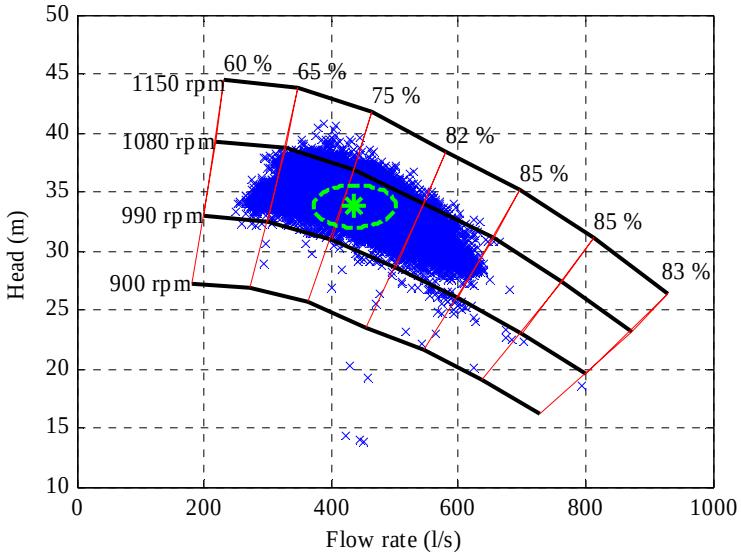

Fig. 3.22: Estimation results for the pulp pumping system. Process variations and normal distribution of the flow rate are considerably smaller compared with the primary water pump. In this case either, the pump is not typically operating in its best efficiency point.

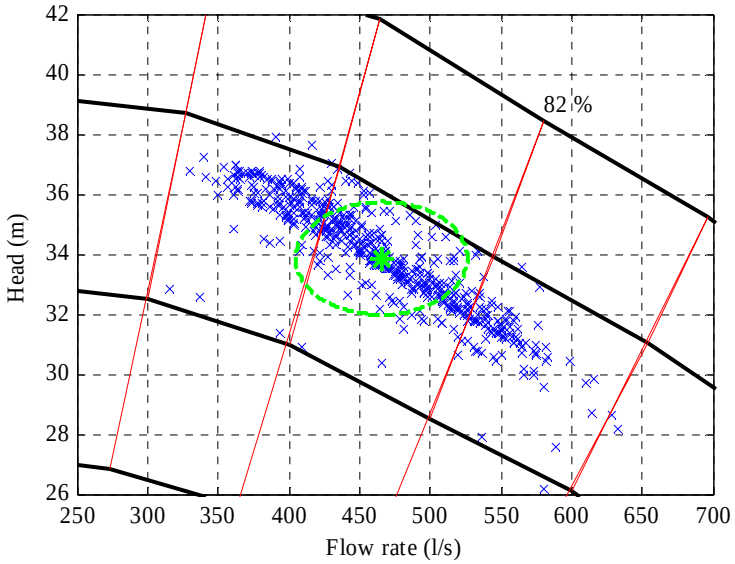

Fig. 3.23: Estimation results for the pulp pumping system from the exemplary time period of two days. Operating point population seems to comprise several fixed-speed *QH* curves, which may indicate a varying system static head.

In addition to the shown operating point group figures, estimation results allow the formation of duration curves for the pump flow rate and other operational values of the pumping system. For

instance, a duration curve can be formed for the pump efficiency to quantify the typical energy efficiency of the pump operation.

3.6 Summary of Chapter 3

In this chapter, methods to determine the operating point location of a centrifugal pump were discussed. The applicable model-based methods that utilise information available from a frequency converter were presented. Factors that may affect the estimation accuracy of the model-based methods were introduced, and also their effects were addressed: in general, it can be concluded that the methods are applicable to diagnostic purposes in the case of Newtonian fluids and with centrifugal pumps in which the characteristic curves allow the estimation of the pump operating point location.

The methods were tested with a radial flow centrifugal pump, and the water was used as the pumped fluid in order to provide results that are generalisable also for other pumping systems. Although the laboratory tests have shown the effect of typical limiting factors on the estimation accuracy, such as the shape and accuracy of the pump and system characteristic curves, the obtained estimation results can be considered valid only for the laboratory pumping system or a corresponding pumping system with a radial flow centrifugal pump. However, the studied methods can be applicable also to other centrifugal pump types (e.g. axial flow centrifugal pumps), if the previously-mentioned factors do not prevent this. As the pump characteristic curves can in practice differ from the published ones for instance as a result of mechanical wear, methods to determine and improve the accuracy of the applied characteristic curves are needed to ensure correct estimation results. Pump manufacturers could also provide more accurate characteristic curves for new pumps besides the generic curve prints. It should also be noted that the practical applicability of the system-curve-based estimation method may be notably poorer compared with the laboratory tests because of the changing system characteristics. Hence, the limited accuracy of the model-based methods should also be taken into account, when the estimation results are analysed. However, model-based methods can provide information that allows the determination of most typical operating point locations of the pump, and formation of the duration curves for the flow rate and other operational values of the pumping system.

4 DETECTION OF CAVITATION AND FLOW RECIRCULATION

Operation of a pumping system in adverse operating conditions or in the avoidable operating region decreases the service life and mechanical reliability of the pump. In addition, adverse operating regions are typically connected with the low efficiency of the pump. Together these factors may increase the life cycle costs of the pumping system. For this reason, methods for detecting the adverse operation of the pump are needed to ensure the efficient use of the pumping system. In particular, methods for detecting the occurrence of cavitation in a centrifugal pump have been widely investigated.

In this chapter, methods to detect cavitation occurrence in a centrifugal pump are discussed. A novel frequency converter-based method to detect the occurrence of cavitation or flow recirculation especially in a radial flow centrifugal pump is proposed. It provides a cost-effective and automatic solution to detect cavitation or flow recirculation in the pump without the need for additional measurements or check-ups. Sensitivity of the proposed method is compared with other published methods for cavitation detection. The method is also evaluated by laboratory measurements for three different centrifugal pumps. In addition, feasibility of the proposed method to detect flow recirculation is discussed.

4.1 Cavitation phenomenon

Cavitation occurs in a centrifugal pump, when the static pressure of the fluid decreases below the vaporisation limit forming cavities in the pumped fluid. The resulting vapour may obstruct the fluid flow resulting in decreased hydraulic efficiency and an intermittently varying flow rate. When the vaporised fluid moves into the region with a higher static pressure, vapour cavities collapse resulting pressure shocks, which cause additional noise and vibration. Ultimately, cavitation may cause removal of material from the impeller and volute casing of the pump, leading to a pump failure.

On the basis of its occurrence location and other characteristics, cavitation occurrence can be classified for instance as an incipient cavitation (i.e., starting cavitation, no effect on the pump head), a damaging cavitation with no effect on the pump head or a fully developed cavitation having a decreasing effect on the pump performance (e.g. 3 % head drop indicated by the $NPSH_R$). It has been shown that the impact of cavitation in a centrifugal pump is often most severe, when there is cavitation occurring although the $NPSH_A$ is over the $NPSH_R$, and the pump head is not yet decreased because of the cavitation (Karassik, 1997; Schiavello, 2009). Thus, there should be a margin over the $NPSH_R$ to ensure that there is no damaging cavitation occurring in the pump. For this reason, NPSH margin values have been proposed for different types of centrifugal pumps, although they can be rather approximate ones. In the case of radial flow centrifugal pumps with a low suction energy level, a margin of 35–50 % has been suggested for the NPSH ratio (Karassik, 1997). However, it is worth noting that these values are as generic as the Hydraulic Institute recommendations for the preferred operating region discussed in Chapter 2.

4.1.1 Known detection methods

Typically, additional measurement sensors are applied to detect the cavitation occurrence in a centrifugal pump. Vibration and suction pressure measurements are widely applied, and they have been studied for instance in (Černetič, 2008; Lahdelma, 2008; Parrondo, 1998). According to experimental tests carried out by (Parrondo, 1998), the development of cavitation (i.e., the

decrease in the $NPSH_A$) should attenuate the magnitude of blade pass frequency (BPF) component and increase the magnitude of low-frequency (0–10 Hz) component of the suction pressure. In addition, with a decreasing $NPSH_A$, the development of cavitation should be visible as an increase and then as a decrease in the magnitude of the rotational speed frequency component of the suction pressure. The results in (Jensen, 2000) and (Kercan, 1979) have also suggested the attenuation of the BPF component of the suction pressure, while the pump is prone to a fully developed, head-decreasing cavitation compared with the no-cavitation situation. According to (Kercan, 1979) and (Perez, 1996), the occurrence of cavitation should also be visible as increasing magnitudes of frequency components (>0 Hz) of the discharge pressure. In any case, the incipient cavitation may already occur in the pump, before it affects the suction or discharge pressure. Thus, the most sensitive method to determine the occurrence of incipient cavitation would be the visual inspection of the flow inside the pump, which typically requires modification of the pump or the installation of an endoscope into the pump.

In the vibration of pump casing, the development of cavitation should be detectable as the increase in the magnitude of the blade pass frequency component (Černetič, 2008; Parrondo, 1998). The development of cavitation should also increase the magnitude of broad-bandwidth vibration that is caused by the collapsing vapour bubbles. However, the frequency range of broad-bandwidth vibration is generally regarded to be a pumping system-specific variable (Karassik, 1998; Parrondo, 1998), why it may have to be determined on the basis of test measurements for the system. It should also be noted that the incipient cavitation may have already developed in the pump, before it affects vibration of the pump.

Also the analysis of rotational speed harmonic components, acoustic emission and audible noise of a centrifugal pump have been reported to be applicable methods to the detection of cavitation occurrence (Al-Hashmi, 2005; Alfayez, 2005; Čudina, 2008). According to (Alfayez, 2005), the occurrence of incipient or damaging cavitation can be seen in the RMS magnitude of the AE signal, which reaches its maximum value, although the NPSH ratio would be sufficient to avoid the head-decreasing cavitation. Also Neill et al. have suggested that the development of damaging cavitation could be detected by acoustic emission measurements before cavitation decreases the pump head (Neill, 1997). As the acoustic emission allows the detection of pressure surges inside the pump, it is generally referred as a more sensitive measurement method for cavitation detection than the measurement of vibration in the pump casing.

Another alternative for the cavitation detection is the analysis of the motor current that is often already measured for control and monitoring purposes. If the vapour obstructs fluid flow and results in uneven running of the pump, it also affects the shaft power requirement and consequently the rotational speed, shaft torque and current consumption of an induction motor. Typically, the occurrence of cavitation can be seen as additional components in the frequency spectrum of the motor current, for instance as several sidebands around the supply and rotational speed components (Perovic, 2001; Hernandez, 2010). Thus, cavitation occurrence can also affect the estimated shaft torque of an induction motor: Wiedenbrug (2002) has reported that a deteriorated and cavitation-prone pump has a notably larger torque ripple (alternating component of steady-state torque) than a healthy one. In his study, the shaft torque was estimated with a separate analyser having voltage and current measurements for all three phases of the motor. Estimation was carried out for a time period of eight seconds (Baker, 2008). The use of electrical measurements in the cavitation detection has also been studied in (Parihara, 2006) with a fixed-speed centrifugal pump. However, these studies contain only case-specific results, and the detection of incipient cavitation (i.e., no effect on the pump performance) has not been specifically considered in them.

Also model-based methods for the detection of cavitation have been presented. They are typically based on the determination of the pump operational state and estimation of the cavitation risk in a centrifugal pump. For instance, Eryurek (2002) and Discenzo (2003) have introduced methods in which the cavitation risk is estimated by comparing the available and required NPSH of a centrifugal pump. The measured flow rate and head of the pump may also be compared with the estimated values in order to detect the occurrence of cavitation (Kallesoe, 2005).

In practice, all these methods have drawbacks, which affect their usability in the existing installations. Firstly, the installation of additional measurement sensors is often costly and time-consuming, and for this reason only the production-critical pumps may be equipped with additional sensors. As the phase current of an induction motor may already be measured for monitoring purposes, a current-based analysis can offer an ability to detect cavitation without additional sensors. However, current-based detection of cavitation has only been applied to directly fed induction motors (i.e., no frequency converter), and it may not be applicable with variable-speed-driven pumps because of harmonic distortion in the current waveform caused by the frequency converter. There is no information available concerning the applicability of current-based analysis methods to the detection of incipient cavitation.

If the pumping system is equipped with a frequency converter, it can be applied in the monitoring of the pump operational state without external measurement sensors as discussed in Chapter 3. Consequently, the detection of pump operational states with and without cavitation occurrence (i.e., normal operational state) can be assumed to be possible with a frequency converter by monitoring torque and rotational speed estimates of a centrifugal pump. Compared with the previously-introduced methods, this can provide a cost-effective and automatic approach to detect the harmful operation of a pumping system, as additional sensors or separate check-ups are not required for the pumping system.

4.2 Proposed method to detect cavitation occurrence by a frequency converter

On the basis of the known effects and detection methods of cavitation, it is assumed that the occurrence of cavitation can be detected by a frequency converter, if it affects the motor operation. The proposed detection method is based on the following hypotheses concerning especially radial flow centrifugal pumps:

- The occurrence of cavitation in a centrifugal pump results in vapour that may obstruct the fluid flow especially in the case of a fully developed cavitation. This leads to an intermittent flow rate, which increases time-domain variation in the pump power consumption.

- Variation of the pump power consumption in the time domain can be detected by a frequency converter by monitoring estimates for the rotational speed and shaft torque (n and T, respectively). While the pump is operating in the steady state (i.e., reference value of the rotational speed and process characteristics stay constant), increased time-domain variation of the rotational speed or shaft torque estimate compared with their variation in a normal state is a feature of cavitation occurrence in a centrifugal pump.

- Depending on the pumping system and the applied control method of a frequency converter, the occurrence of cavitation can affect both the rotational speed and shaft torque estimates, or either one of them.

- Depending on the pump and process characteristics, rotational speed and shaft torque estimates should be monitored for several seconds in order to detect intermittent operation of a centrifugal pump.

- Time-domain variation of the rotational speed and shaft torque estimates can be quantified by calculating the root mean square (RMS) value for the alternating component of the estimates. These are later referred to as n_{RMS} and T_{RMS}, respectively.

If these hypotheses are correct, the occurrence of cavitation in a centrifugal pump can be detected by determining the normal n_{RMS} and T_{RMS} of a centrifugal pump while the pump is known to run normally, and by comparing the present n_{RMS} and T_{RMS} with the normal values. If n_{RMS} or T_{RMS} is notably larger than the normal value, the user could be warned about the increased risk of cavitation damage.

At a general level, the proposed method for cavitation detection can be divided into the determination of the normal n_{RMS} and T_{RMS} (later referred to as $n_{RMS,N}$ and $T_{RMS,N}$, respectively), continuous calculation of the present n_{RMS} and T_{RMS} and comparison of the present RMS values with the normal ones. The flow diagram of the proposed detection method is shown in Fig. 4.1.

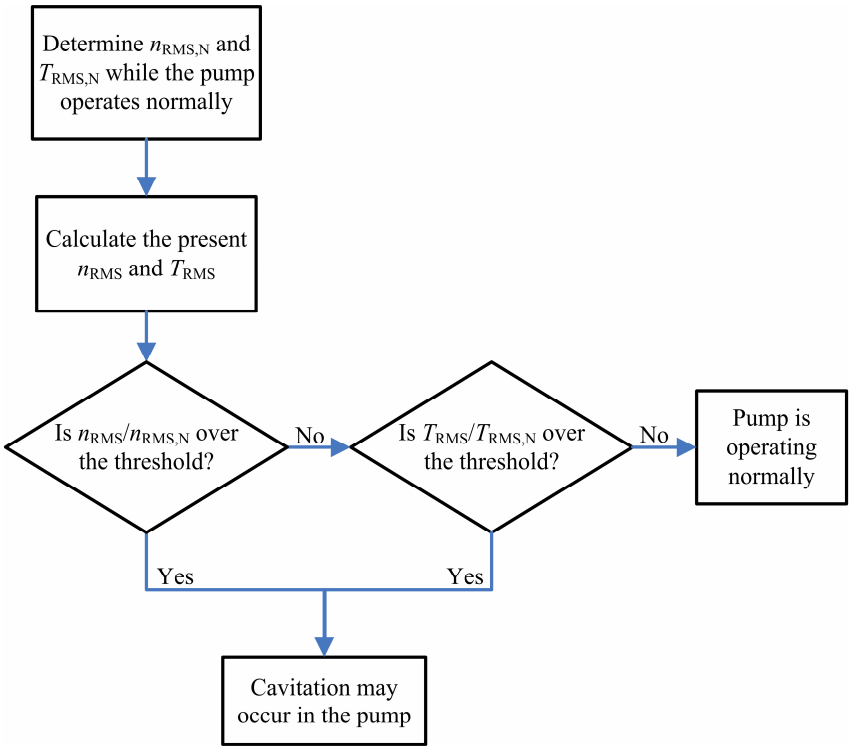

Fig. 4.1: Flow diagram of the proposed method to detect cavitation occurrence in a centrifugal pump.

The proposed method requires information on the $n_{RMS,N}$ and $T_{RMS,N}$. Otherwise, the detection of excessive RMS magnitude in the alternating component of the shaft torque or rotational speed estimate is not possible. $n_{RMS,N}$ and $T_{RMS,N}$ can be automatically determined, when the pump is known to run without cavitation occurrence or alternatively with a separate identification run. When the estimates of a sufficient time period have been stored, $n_{RMS,N}$ and $T_{RMS,N}$ can be

calculated for the detection system. For instance, calculation can be carried out with the following equations for a discrete-time estimate $x(n)$:

$$x_{\mathrm{DC}}(n) = \frac{1}{M}\sum_{k=0}^{M-1} x(n-k) \tag{4.1}$$

$$x_{\mathrm{AC}}(n) = x(n) - x_{\mathrm{DC}}(n) \tag{4.2}$$

$$x_{\mathrm{RMS}}(n) = \sqrt{\frac{1}{M}\sum_{k=0}^{M-1} x_{\mathrm{AC}}^2(n-k)}\ , \tag{4.3}$$

where n and k are discrete-time indices, M is the number of samples applied in the calculation, and the subscripts $_{\mathrm{DC}}$ and $_{\mathrm{AC}}$ denote the direct (i.e., the mean value) and alternating component of the estimate.

During the operation of the pumping system, n_{RMS} and T_{RMS} are continuously calculated for the rotational speed and the shaft torque. If the calculated values are notably higher than the expected $n_{\mathrm{RMS,N}}$ and $T_{\mathrm{RMS,N}}$, it is considered as a symptom of cavitation occurrence in a radial flow centrifugal pump. In practice, the threshold values of the $n_{\mathrm{RMS}}/n_{\mathrm{RMS,N}}$ and $T_{\mathrm{RMS}}/T_{\mathrm{RMS,N}}$ ratios are case-specific, and they may have to be defined by trial and error. However, it can be assumed that at least a doubled time-domain variation of the rotational speed or shaft torque estimate ($n_{\mathrm{RMS}}/n_{\mathrm{RMS,N}} > 2$ or $T_{\mathrm{RMS}}/T_{\mathrm{RMS,N}} > 2$, respectively) is caused by the cavitation occurrence or by some other adverse event in the pump-motor combination (mechanical failure, jammed impeller, etc.). In order to avoid false alarms, a time criterion could also be added to the monitoring of n_{RMS} and T_{RMS}.

The presented hypotheses and applicability of the proposed method were evaluated with laboratory measurements, which are discussed in the following sections. If the hypotheses can be verified, the occurrence of cavitation can be detected by a frequency converter in the case of pumping systems sharing the corresponding characteristics with the laboratory system, such as a radial flow centrifugal pump, water as the pumped fluid and a feasible frequency converter to monitor the pump operation.

4.3 Laboratory measurement setup

The effect of cavitation occurrence on the radial flow centrifugal pump operation was tested with the previously presented Sulzer pumping system, which is equipped with a Dataflex 22/100 speed and torque measurement shaft (0–1 kHz frequency range for the torque measurement) and an ABB ACS 800 frequency converter. The shaft torque was stored with a 5 kHz sampling frequency utilising a National Instruments (NI) PCI-6032E data acquisition card.

The internal estimates of the rotational speed (firmware parameter 2.17) and the shaft torque (firmware parameter 161.07) were stored with the ABB DriveDebug software. According to the converter manuals, these estimates should be unfiltered (ABB, 2000; ABB, 2009). For this reason, 1 kHz sampling frequency was applied for the estimates, as it was the maximum frequency allowed by the software. However, it should also be noted that these estimates may also contain aliased signals because of their unfiltered nature (see Orkisz, 2009). Also the pre-filtered estimates of the rotational speed (parameter 1.02, -3dB cut-off frequency $F_c = 0.3$ Hz) and the shaft torque (parameter 1.05, $F_c = 1.6$ Hz) were stored with the software. The duration

of each measurement was five seconds to ensure the inclusion of low-frequency content (< 1 Hz) in the stored signals.

The operating point location (p_d, p_s and Δp corresponding the flow rate) and rotational speed of the pump were determined with two absolute pressure sensors, a pressure difference sensor across the venturi tube and the Dataflex measurement shaft, which were connected to a Fluke Hydra 2620A data acquisition unit. In addition, a part of the pressure measurements were directly stored to the measurement computer by applying the NI data acquisition card with a 5 kHz sampling frequency.

The temperature of the pumped water was determined with a four-wire PT-100 temperature sensor installed into the suction water tank. During the measurements, temperature of the pumped water was around 20 °C.

Vibration and acoustic emission (AE) of the pump was monitored with separate measurements in order to detect the occurrence of cavitation. A SKF CMSS786A acceleration sensor and the NI data acquisition card were used to measure radial vibration of the Sulzer pump. An acceleration sensor was installed to the location of the pump bearings. Measurements were carried out with a 20 kHz sampling frequency for a time-period of five seconds. Activity of the acoustic emission in the pump was measured from the pump volute casing with a Holroyd MHC-SetPoint measurement unit, which provides a dB value describing the average magnitude of the continuous AE signal around the frequency range of 100 kHz. The measurement setup is shown in Fig. 4.2.

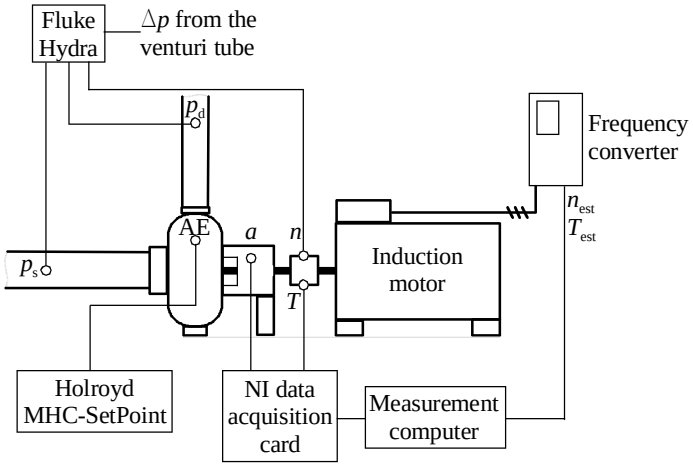

Fig. 4.2: Measurement setup applied to evaluate the sensitivity of different measurements for the detection of cavitation occurrence.

Since the Sulzer pump has a NPSH requirement of 1–3 metres at 1450 rpm (see Fig. A.2 in Appendix A) and a positive suction head, cavitation does not occur in the laboratory pump without additional actions. In this study, the available pump NPSH was regulated by throttling the suction-side flow with a control valve, since it was not possible to create a vacuum into the suction water tank. This may have affected the measurement results, so several measurement sequences were carried out to evaluate the applicability of a frequency converter to the detection of cavitation occurrence.

4.4 Applicability of different measurements to the detection of cavitation occurrence

Common NPSH tests were first conducted for the Sulzer pump to determine the stage of cavitation that can be detected with additional measurements compared with the proposed method. In the common NPSH test, the rotational speed and flow rate of the pump are held constant, and $NPSH_A$ of the pump is gradually decreased by lowering the suction pressure p_s, until the pump head begins to decrease. At least three measurement sequences per operating point location were carried out at the 100 % and 70 % relative flow rates and at the rotational speed of 1500 rpm. In each measurement sequence, the operating point location, shaft torque, rotational speed, radial vibration, acoustic emission and estimates of the frequency converter were measured and stored for each setting of the suction-side control valve. Each measurement was performed, when the pumping system was operating in the steady state with a constant reference for the rotational speed of the pumping system. $NPSH_A$ values were calculated for each measurement on the basis of the measured water temperature (i.e., the related vapour pressure p_v), pump flow rate (i.e., suction-side flow velocity v_s) and fluid static pressure p_s at the pump suction:

$$\mathrm{NPSH_A} = \frac{p_s - p_v}{\rho \cdot g} + \frac{v_s^2}{2g} . \tag{4.4}$$

As previously discussed, the occurrence of cavitation should be visible in the measurements conducted for the pumping system. Below, the known features of cavitation occurrence in the case of different measurements are summarised:

Head produced by the pump begins to decrease with a decreasing $NPSH_A$, when the rotational speed and flow rate are held constant. However, incipient cavitation occurs already in the pump before there is a decrease in the pump head, and therefore the head measurement is not a sensitive method for the detection of cavitation occurrence. The $NPSH_A$ value causing a 3 % decrease in the pump head is referred to as the required NPSH of the pump, and it is commonly applied as the reference point of the fully developed, head-decreasing cavitation. In the head versus $NPSH_A$ curve, there is also a case-specific value of $NPSH_A$ with which the head rapidly collapses because of the fully developed cavitation. According to (Karassik, 1998; Schiavello, 2009), the point of maximum cavitation erosion often occurs when the $NPSH_A$ is between the point of cavitation inception and the point of 3 % head decrease. For this reason, the 3 % decrease in the head does not directly indicate the required NPSH to avoid the occurrence of damaging cavitation in the pump.

Suction pressure of the pump can be affected by the cavitation before there is a decrease in the pump head (Kercan, 1979). According to experimental tests carried out by (Parrondo, 1998), the development of cavitation (i.e., the decrease in the $NPSH_A$) should attenuate the magnitude of blade pass frequency (BPF) component and increase the magnitude of the low-frequency (0–10 Hz) component of the suction pressure. In addition, with a decreasing $NPSH_A$, the development of cavitation should be visible as an increase and then as a decrease in the magnitude of the rotational speed frequency component of the suction pressure. The results in (Jensen, 2000) and (Kercan, 1979) have also suggested the attenuation of the BPF component of the suction pressure, while the pump is prone to a fully developed, head-decreasing cavitation compared with the no-cavitation situation. In any case, the incipient cavitation may already occur in the pump before it affects the suction pressure.

Discharge pressure of the pump should also be more sensitive to the occurrence of cavitation than the head produced by the pump. According to (Kercan, 1979) and (Perez, 1996), the occurrence of cavitation should be detectable as increasing magnitudes of the frequency components (> 0 Hz) of the discharge pressure.

Acoustic emission of the pump can indicate the severity of cavitation, and therefore it can also detect the occurrence of damaging cavitation. According to (Alfayez, 2005), the occurrence of incipient or damaging cavitation can be seen in the RMS component of the AE signal, which attains its maximum value, although the NPSH ratio would be sufficient to avoid the head-decreasing cavitation. Also Neill et al. have suggested that the development of damaging cavitation could be detected by acoustic emission measurements before the decrease in the pump head (Neill, 1997).

Vibration of the pump casing is also affected by the occurrence of cavitation in the pump: the development of cavitation should be detectable as an increase in the magnitude of the blade pass frequency component (Černetič, 2008; Parrondo, 1998). The development of cavitation should also increase the magnitude of broad-bandwidth vibration that is caused by the collapsing vapour bubbles. However, the frequency range of broad-bandwidth vibration is affected by the pumping system setup (Karassik, 1998; Parrondo, 1998), and hence, it may have to be determined on the basis of test measurements for the system. In addition, the sensitivity of vibration measurement is not regarded as good as the sensitivity of acoustic emission measurements for the detection of incipient or damaging cavitation (Al-Sulti, 2005).

4.4.1 Measurement results at the best efficiency point of the Sulzer pump

Three measurement sequences were conducted at the BEP of the Sulzer pump. The measured points cover the $NPSH_A$ range from 1.7 to 9.9 metres. With lower $NPSH_A$, also the pump flow rate begins to rapidly decrease with the pump head. A $NPSH_A$ above 10.2 metres would have required modification of the pumping system, which was not possible during the measurements. For this reason, measurements have not been carried out with larger suction heads, although this may have excluded the range of incipient cavitation occurrence from the measured values. The obtained measurement results are analysed below.

Pump head as a function of $NPSH_A$ is illustrated in Fig. 4.3 for each measurement sequence. The measured head starts to gradually decrease when the $NPSH_A$ decreases below 6.1 metres. It can be assumed that this head decrease is caused by the development of the cavitation phenomenon inside the pump. The value of 3 % head decrease was calculated on the basis of the mean of the head values in measurements with a fully opened suction-side control valve. It is illustrated with a dashed horizontal line in Fig. 4.3. On the basis of the measured head values, the 3 % decrease in the head is caused at the $NPSH_A$ of 2.3 metres for this flow rate. In the following figures, this is applied as the base value for the $NPSH_R$ in this operating point location to show the measurement results as a function of $NPSH_A/NPSH_R$ ratio (later simply referred to as the NPSH ratio). Thus, the previously mentioned decrease in the head starts to occur when the NPSH ratio goes below 2.65 (i.e., below 6.1 metres divided by 2.3 metres). This is clarified by showing the measured pump head as a function of NPSH ratio in Fig. 4.4.

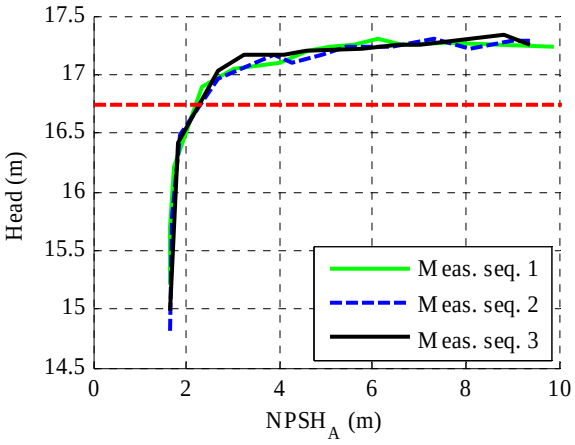

Fig. 4.3: Pump head as a function of pump $NPSH_A$. The pump head starts to decrease when the $NPSH_A$ goes below 6.1 metres. The 3 % head decrease criterion is indicated in the figure by a horizontal dashed line. The resulting $NPSH_R$ for this operating point is 2.3 metres.

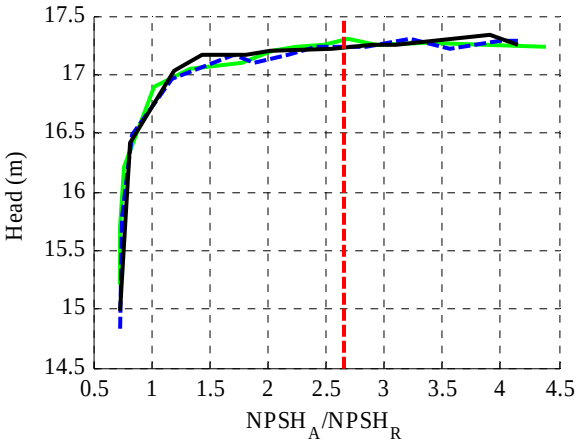

Fig. 4.4: Pump head values given in Fig. 4.3 as a function of NPSH ratio. The pump head starts to decrease when the NPSH ratio goes below 2.65, which is indicated in the figure by a vertical dashed line. Separate measurement sequences are indicated as in Fig. 4.3.

Suction pressure. As previously summarised, the development of cavitation may be visible in the magnitudes of certain frequency components of the measured suction pressure. Power values were calculated for the measured suction pressure at the frequencies 0–2 Hz, 25 Hz and 100 Hz from the Welch power spectral density (PSD) data for each measurement. These frequencies were selected for analysis on the basis of frequency-domain spectrograms formed for the measurement data. To make results comparable with each other, values have been scaled with the value from the measurement case with a fully opened suction-side valve.

The resulting magnitudes are illustrated using decibels in Fig. 4.5. At the 0–2 Hz frequency range, the resulting magnitudes have two distinct peak points at the NPSH ratios of 1.2–1.35 and 2–2.2. In both cases, the pump head has already decreased from the normal state value

because of the cavitation occurrence. The increase of magnitudes starts when the NPSH ratio goes below 3.4, which could be a possible NPSH ratio for the occurrence of incipient or damaging cavitation.

At the rotational speed frequency (25 Hz), the maximum magnitude is reached when the NPSH ratio is approximately 0.8–1.2, below which the magnitudes attenuate, as suggested in (Parrondo, 1998). However, magnitudes of separate measurement sequences differ clearly from each other at this frequency, why this frequency component cannot be regarded very reliable cavitation indicator for this pumping system and measurement setup.

In the blade pass frequency component (at 100 Hz), measurement sequence 1 has a gradual increase in the magnitude with a decreasing NPSH ratio when the ratio goes below 3. This could be caused by the incipient or damaging cavitation, but it can not be seen in other measurement sequences. In addition, all measurement sequences have a local decrease in the magnitude of the BPF component when the NPSH ratio goes below 0.83. Otherwise magnitude differences of separate measurement sequences are notable, why this frequency component does not seem applicable to the detection of incipient or damaging cavitation according to these measurements.

Compared with the head measurements shown in Fig. 4.3, magnitudes at the 0–2 Hz frequency range suggest that the incipient or damaging cavitation could occur, when the NPSH ratio is for instance 3. Otherwise these results do not provide further information concerning the occurrence of incipient cavitation in the pump, as the maximum magnitudes are attained when the pump head is already lowered as a result of the decreased NPSH ratio.

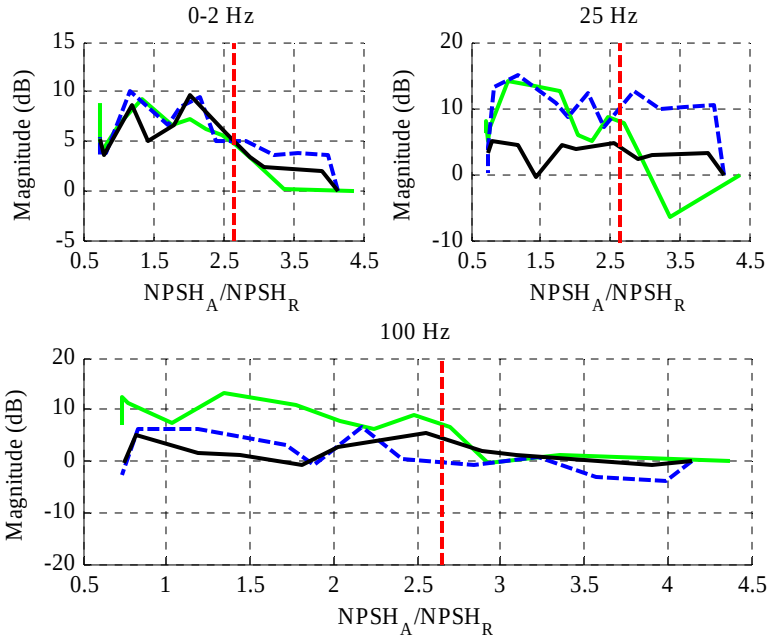

Fig. 4.5: Magnitude of the measured suction pressure in the frequency ranges of 0–2 Hz, 25 Hz and 100 Hz as a function of NPSH ratio. In each figure, the NPSH ratio below which the pump head begins to decrease is shown by a dashed vertical red line. Separate measurement sequences are indicated as in Fig. 4.3. In general, maximum magnitudes are attained when the pump is already prone to a head-decreasing cavitation (i.e., NPSH ratio is below 2.65). At the 0–2 Hz frequency range, the increase of magnitudes begins, when the NPSH ratio goes below 3.4.

Discharge pressure. A similar analysis was conducted for the measured discharge pressure. On the basis of frequency-domain spectrograms, power values were calculated in the 0–5 Hz frequency range from the Welch PSD data for each measurement. The resulting magnitudes are illustrated in Fig. 4.6. As expected, the magnitude of the 0–5 Hz component gradually increases with a decreasing NPSH ratio. There is a local maximum in the magnitudes when the NPSH ratio is approximately 2.7–3.1, before the decrease in the pump head. This may indicate an occurrence of incipient or damaging cavitation in the pump, as it is in the NPSH ratio range between the cavitation inception and the point of 3 % decrease in the pump head. The magnitude of the 0–5 Hz frequency component is at highest when a fully developed, head-decreasing cavitation occurs in the pump. In general, these results seem to indicate more clearly the NPSH ratios related to the occurrence and development of cavitation than the measured suction pressure.

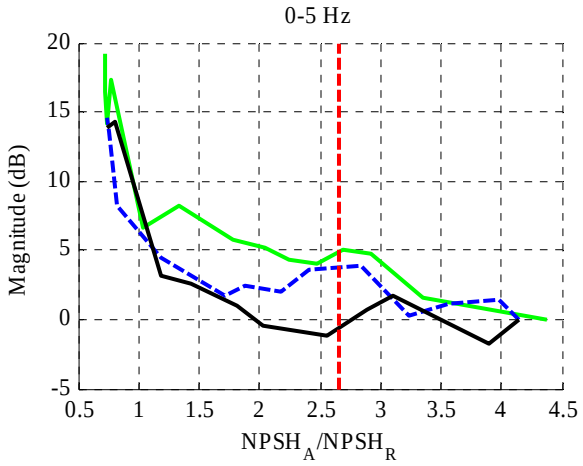

Fig. 4.6: Magnitude of the measured discharge pressure in the frequency range of 0–5 Hz as a function of NPSH ratio. In the figure, the NPSH ratio below which the pump head begins to decrease is shown by a dashed vertical line. Separate measurement sequences are indicated as in Fig. 4.3. The magnitude of the discharge pressure in the 0–5 Hz frequency range increases with a decreasing NPSH ratio. There is a local maximum in the magnitudes when the NPSH ratio is approximately 2.7–3.1.

Acoustic emission. The results of acoustic emission measurements with the Holroyd MHC-SetPoint unit are illustrated in Fig. 4.7. The AE values reach their maximum when the NPSH ratio is approximately 2.7–2.9, before the decrease in the head. Compared with the suction pressure measurements, these results more clearly indicate the location in which the decrease in the pump head starts and damaging cavitation may occur in the pump. It is also worth noting that increased noise was heard from the pump, when the NPSH ratio was approximately 2.7, but otherwise the decrease in the NPSH ratio did not generate, for instance, rattling noise that is commonly caused by the cavitation occurrence.

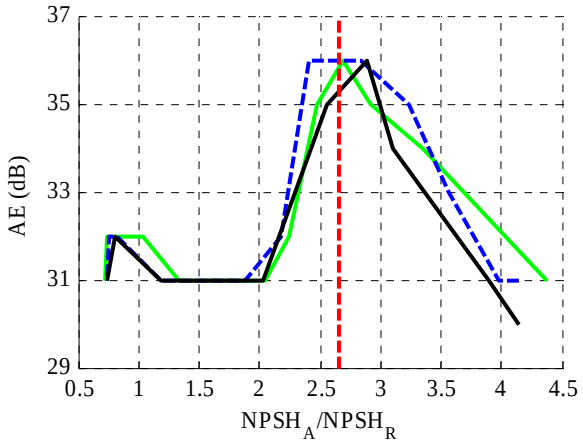

Fig. 4.7: Measured acoustic emission as a function of $NPSH_A/NPSH_R$ ratio. Separate measurement sequences are indicated correspondingly as in Fig. 4.3. The measured AE values reach their maximum when the NPSH ratio is around 2.8. Below this NPSH ratio, also the pump head starts to decrease with the decreasing $NPSH_A$.

Vibration measurements were analysed with a similar procedure. Tests performed by Parrondo have suggested that the blade pass frequency component should increase when a cavitation occurs in the pump (Parrondo, 1998). The development of cavitation should also be detectable as an increase in the broad-bandwidth vibration magnitude caused by the collapses of vapour bubbles. However, the frequency range of this phenomenon is case specific, so it has to be determined on the basis of the measurement results. For this case, the magnitude of radial acceleration at the blade pass frequency of 100 Hz and at the frequency range of 250–750 Hz was chosen for the features of cavitation occurrence. The spectral power values of these frequency components in each case were determined from the respective power spectral densities, and they have been scaled with the values from the measurement case having a totally opened suction-side valve. The resulting magnitudes are shown in Fig. 4.8. The decrease in the NPSH ratio magnifies both properties, which attain their maximum value when the NPSH ratio is approximately one or less. In both cases, the increase in the magnitudes begins when the pump head already decreases because of the cavitation occurrence, as the NPSH ratio is below 2.65. As suggested by the previous studies, this shows that also vibration of a centrifugal pump reacts to the occurrence of cavitation, but the acoustic emission measurements seem to be a more sensitive detection method of the incipient or damaging cavitation in the pump.

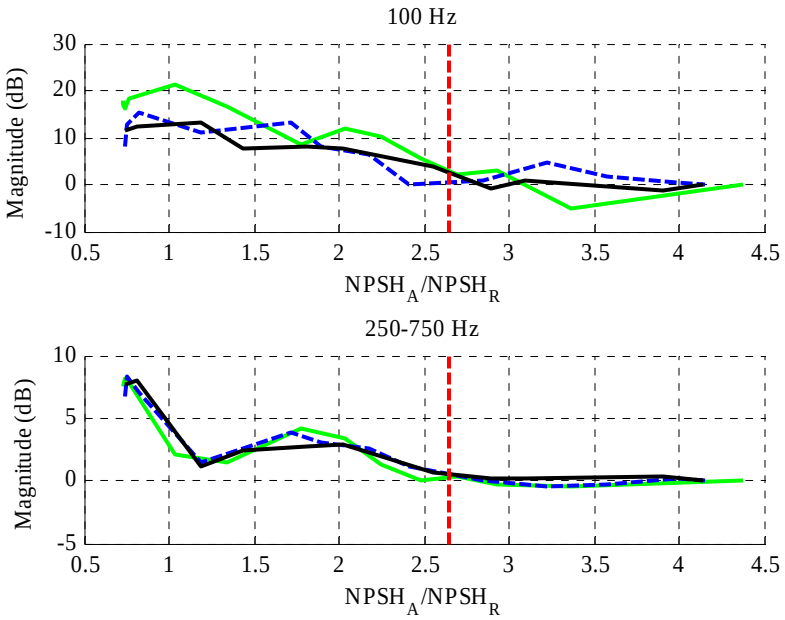

Fig. 4.8: Magnitude of the measured radial vibration in the frequency ranges of 100 Hz and 250–750 Hz as a function of NPSH ratio. In each figure, the NPSH ratio with which the pump head begins to decrease is shown by a dashed red line. Separate measurement sequences are indicated correspondingly as in Fig. 4.3. A decrease in the NPSH ratio so that the pump head starts to decrease has an increasing effect on the magnitude of vibration in both frequency ranges.

Measured shaft torque. According to the presented hypothesis, the occurrence of cavitation should also be visible as an alternating signal component of the rotational speed or shaft torque estimate. A frequency-domain analysis by the Welch method for the power spectral density estimation was first performed for the shaft torque measurements to determine applicable frequency ranges for the cavitation detection in the case of the Sulzer pumping system. The obtained spectrogram for the measured shaft torque in the first measurement sequence is

illustrated in Fig. 4.9. It shows how the decrease in the NPSH ratio below 1.78 intensifies the magnitude of shaft torque at the pump blade pass frequency (100 Hz). At the rotational speed frequency (25 Hz), the decrease in the NPSH ratio attenuates the shaft torque magnitude. In addition, there is a magnified low-frequency component (0–5 Hz) in the spectrogram when the NPSH ratio is below 0.74, and the pump head has already been collapsed because of the cavitation occurrence. It can be assumed that these components could be applied as the properties to detect cavitation occurrence, if they are also visible in the spectrograms of the frequency converter estimates for the shaft torque and rotational speed. These results also point out that the occurrence of incipient or damaging cavitation at the NPSH ratio around 2.8 does not have a distinctive effect on the measured shaft torque of the pump. The energy of the shaft torque signal is also concentrated around the 84 Hz frequency regardless of the NPSH ratio, which might be caused by the mechanical interaction of the pumping system and the measurement shaft. Correspondingly, there is a shaft torque component at the first harmonic of the rotational speed (i.e., at 50 Hz), but the magnitude of this component is not clearly affected by the change in the NPSH ratio.

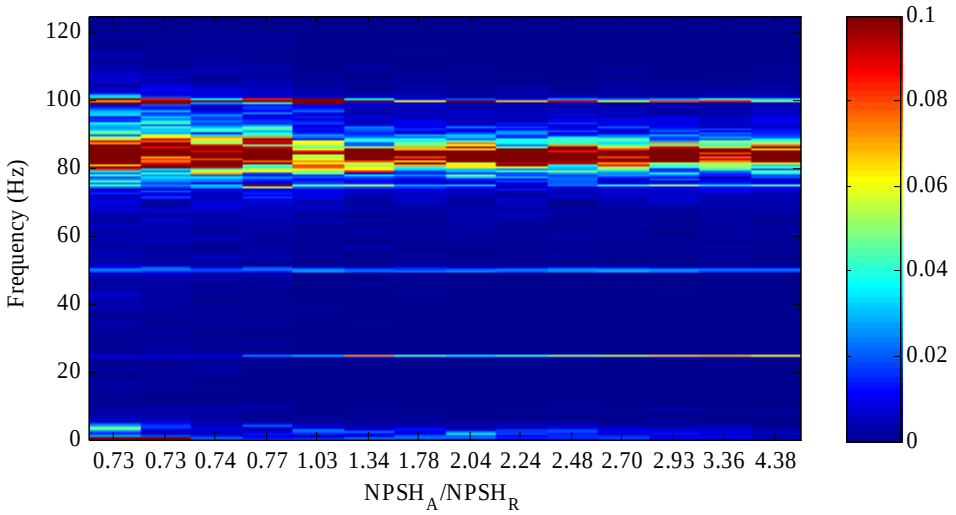

Fig. 4.9: Welch power spectral density of the measured shaft torque as a function of NPSH ratio. The most notable components in the frequency spectrum are around 84 Hz, at the blade pass frequency (four times the frequency of rotational speed), at the frequency of rotational speed and in the low-frequency region (0–5 Hz). It should be noted that the visible frequency axis of this spectrogram has been limited to 125 Hz, as there has not been applicable signal content at higher frequencies.

Estimated rotational speed and shaft torque. For comparison, the corresponding frequency-domain analysis was also performed for the unfiltered estimates of the rotational speed and the shaft torque (parameters 2.17 and 161.07, respectively). A spectrogram of the unfiltered shaft torque estimate is illustrated in Fig. 4.10. As with the measured shaft torque, the occurrence of head-decreasing cavitation has increased the magnitude of shaft torque in the low-frequency region (now 0–2 Hz) when the NPSH ratio is below 0.74, and the pump head has already been collapsed because of the cavitation occurrence. Hence, this frequency component seems only applicable to the detection of fully developed cavitation, which might also be visible in the process-related measurement for the pump. Otherwise, the spectrogram consists of wide-band noise and a faintly visible frequency component in the frequency range of 96–98 Hz, which attains its maximum magnitude at the NPSH ratio of 2.24. This frequency component attains

higher magnitudes also at the NPSH ratios of 2.70 and 3.36, why it could possibly be applicable to the detection of incipient or damaging cavitation.

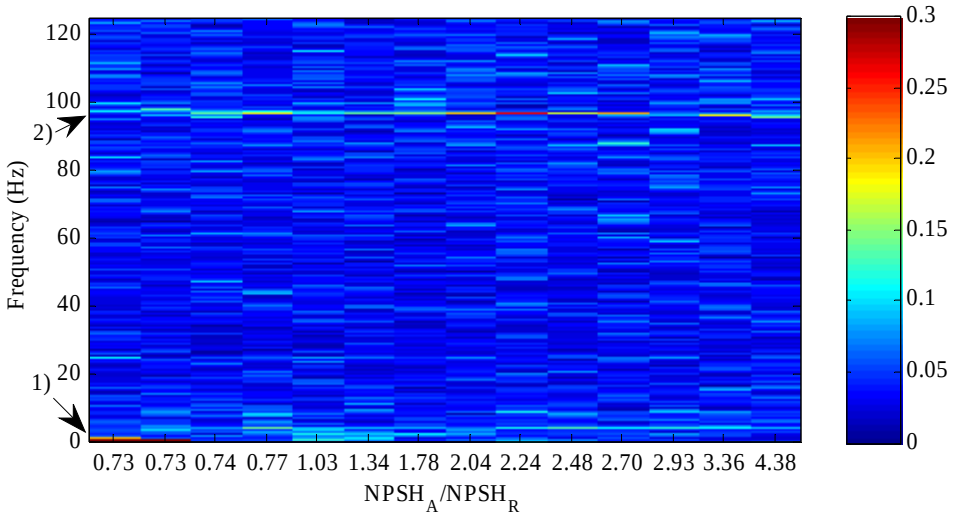

Fig. 4.10: Welch power spectral density of the estimated shaft torque as a function of NPSH ratio. The most notable component is in the low-frequency region (0–2 Hz) when the pump head has already been collapsed because of the cavitation (arrow no. 1). There is also a faintly visible component in the frequency range of 96–98 Hz (arrow no. 2), which attains its maximum magnitude at the NPSH ratio of 2.24. Otherwise, the spectrogram has no components that could be used in the detection of cavitation occurrence. It should be noted that the visible frequency axis of this spectrogram has been limited to 125 Hz, as there has not been applicable signal content at higher frequencies.

A spectrogram for the unfiltered rotational speed estimate is illustrated in Fig. 4.11. Also in this case the occurrence of cavitation is most visible in the low-frequency region when the pump NPSH ratio is below 0.74, and the pump head has significantly decreased because of the cavitation occurrence. Correspondingly, there is a visible component in the frequency range of 96–98 Hz, which attains its maximum magnitude at the NPSH ratio of 2.04 and is possibly increased by the cavitation occurrence at the NPSH ratios of 2.48 and 3.36. This spectrogram also contains the first harmonic of the electric output frequency component at 101 Hz and the rotational speed frequency component at 25 Hz, but they do not seem to have a distinctive relationship with the occurrence of the head-decreasing cavitation in the pump.

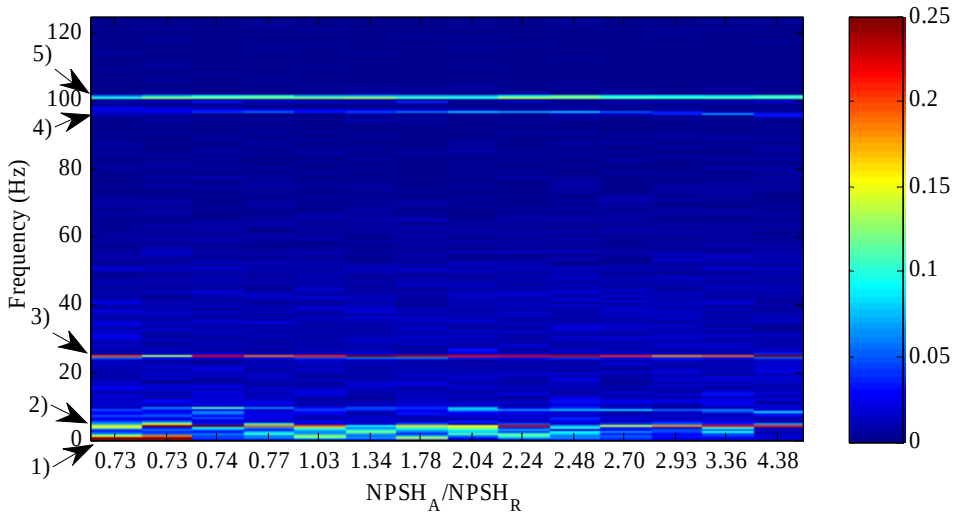

Fig. 4.11: Welch power spectral density of the estimated rotational speed as a function of NPSH ratio. The most notable component is in the low-frequency region (0–2 Hz) when the pump is prone to head-decreasing cavitation (indicated by an arrow no. 1). In addition, there is a component at the frequency of 4 Hz regardless of the NPSH ratio (arrow no. 2). Increased magnitudes in the spectrogram can also be detected at the rotational speed frequency (25 Hz, arrow no. 3), at the frequency range of 96–98 Hz (arrow no. 4) and at the first harmonic of the electric output frequency (101 Hz, arrow no. 5).

Based on these findings, n_{RMS} and T_{RMS} were firstly determined by applying the pre-filtered estimates of the converter (parameter 1.02 for the rotational speed and parameter 1.05 for the shaft torque, respectively), as they are readily filtered for the 0–2 Hz frequency range. As previously, the resulting values were scaled with the RMS value of the measurement case with a fully open suction-side valve. The resulting values are shown in Fig. 4.12 for the rotational speed and in Fig. 4.13 for the shaft torque, respectively.

In the feature defined from rotational speed estimates, that is $n_{RMS}/n_{RMS,N}$, there is a minor increase (from 1 to 1.5) with a decreasing NPSH ratio, until the NPSH ratio is lowered to about 2, and the pump head is lowered as a result of the decrease in the $NPSH_A$. When the NPSH ratio gets below 0.74, there is a notable increase in the $n_{RMS}/n_{RMS,N}$ ratio because of the head-collapsing cavitation occurring in the pump. These findings support the assumption that the development of head-decreasing cavitation increases the time-domain variation of the rotational speed estimate, and thus the occurrence of fully developed cavitation could be detected by a frequency converter at least in the case of this pumping system. However, the results also show that the proposed method may not be very applicable to the detection of incipient or damaging cavitation (e.g. at the NPSH ratio of 2.5), as its effect on the n_{RMS} cannot be considered very significant.

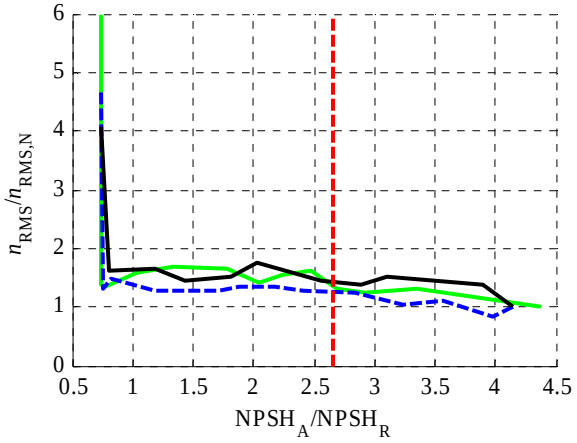

Fig. 4.12: $n_{RMS}/n_{RMS,N}$ ratios of rotational speed estimates as a function of $NPSH_A/NPSH_R$ ratio in the case of pre-filtered estimates. The notations in the figure are consistent with Fig. 4.3. There is an increase in the $n_{RMS}/n_{RMS,N}$ ratios from 1 to 1.5 with a decreasing NPSH ratio, until the NPSH ratio goes below 0.74, and a notable increase can be seen. The maximum $n_{RMS}/n_{RMS,N}$ in the first measurement sequence is 10.4, which is outside the visible $n_{RMS}/n_{RMS,N}$ axis.

In the feature defined from the shaft torque estimates, that is $T_{RMS}/T_{RMS,N}$, a corresponding behaviour can be seen: compared with the initial (i.e. suction-side valve fully open) case, the $T_{RMS}/T_{RMS,N}$ ratio are mainly affected only when the pump head has already clearly decreased because of the low NPSH ratio. As an exception to this, the results of the first measurement sequence are however slightly larger at the NPSH ratios of 1 and 2.3 compared with the other results at the same NPSH ratios, which may just be a statistical error.

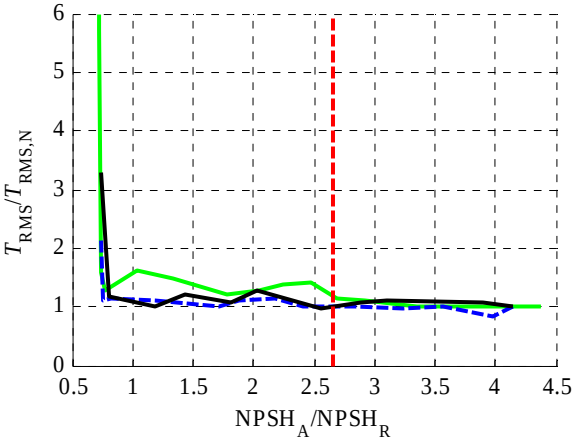

Fig. 4.13: $T_{RMS}/T_{RMS,N}$ ratios of shaft torque estimates as a function of $NPSH_A/NPSH_R$ ratio in the case of pre-filtered estimates. $T_{RMS}/T_{RMS,N}$ ratios attain their maximum when the pump head collapses because of the low NPSH ratio. The maximum $T_{RMS}/T_{RMS,N}$ in the first measurement sequence is 7.4, which is outside the visible $T_{RMS}/T_{RMS,N}$ axis.

In addition, applicability of the 96–98 Hz frequency range to cavitation detection was studied. However, component magnitudes in separate measurement sequences differed clearly from

each other, so there was no distinctive relationship with the occurrence of incipient cavitation and magnitude of the estimate RMS ratios.

As a conclusion, these results showed a better sensitivity of the acoustic emission and discharge pressure measurements for cavitation detection compared with the vibration and suction pressure measurements. These findings are in line with the previous studies. Compared with the additional measurements, the proposed frequency-converter-based detection method seems applicable only to the detection of a fully developed cavitation, which already decreases the pump head. Consequently, in this case, the detection of incipient cavitation does not seem possible with the proposed method.

4.4.2 Measurement results at the 70 % relative flow rate of the Sulzer pump

Similar tests were also conducted at the relative flow rate of 70 % for the Sulzer pump. In all, three measurement sequences were carried out. The measured points cover the $NPSH_A$ range from 1.4 to 9.3 metres. With a lower $NPSH_A$, also the pump flow rate begins to rapidly decrease with the pump head. A $NPSH_A$ clearly above 9.3 metres would have required modification of the pumping system, which was not possible during the measurements. For this reason, measurements have not been carried out with larger suction heads, although this may have excluded the range of incipient cavitation occurrence from the measured values. The obtained measurement results are analysed below.

Pump head as a function of $NPSH_A$ is shown for each measurement sequence in Fig. 4.14. In this operating point location, the measured head starts to gradually decrease when the $NPSH_A$ decreases below 5.8 metres. The value of 3 % head decrease was calculated based on the mean of the head values in the measurements with a fully opened suction-side control valve. This is illustrated with a dashed line in Fig. 4.14. Based on the measured head values, the 3 % decrease in the head is now caused at the $NPSH_A$ of 2.2 metres. This is applied as the base value for the $NPSH_R$ in this operating point location to show the measurement results as a function of NPSH ratio. Thus, the previously mentioned decrease in the head starts to occur when the NPSH ratio goes below 2.64. This is clarified by showing the measured pump head as a function of NPSH ratio in Fig. 4.15.

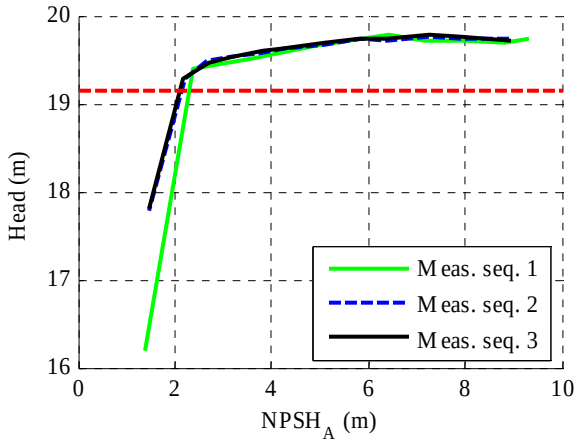

Fig. 4.14: Pump head as a function of pump $NPSH_A$. The pump head starts to decrease when the $NPSH_A$ goes below 5.8 metres. The 3 % head decrease criterion is indicated in the figure by a horizontal dashed line. The resulting $NPSH_R$ for this operating point is 2.2 metres.

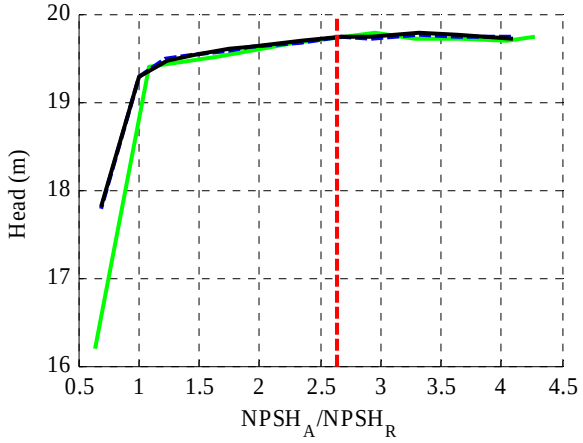

Fig. 4.15: Pump head values given in Fig. 4.14 as a function of NPSH ratio. The pump head starts to decrease when the NPSH ratio goes below 2.64, which is indicated in the figure with a vertical dashed line. Separate measurement sequences are indicated correspondingly as in Fig. 4.14.

Suction pressure. The measured magnitudes of the suction pressure frequency components at 0–2 Hz, 25 Hz and 100 Hz are presented in Fig. 4.16. In the 0–2 Hz frequency range, a gradual increase in the magnitudes can be detected with a decreasing NPSH ratio. The magnitudes reach their maximum when the NPSH ratio is less than 2.3, and the pump head has decreased because of the cavitation occurrence. However, the measurement sequences differ from each other, so there is no distinctive location for the maximum magnitude.

At the rotational speed frequency (25 Hz), a local maximum in the magnitudes can be detected at NPSH ratios of 3–3.6, which could imply the development of damaging cavitation in the pump. However, the magnitudes of separate measurement sequences differ notably from each other, decreasing the applicability of also this frequency component to cavitation detection. Correspondingly, the magnitudes of the BPF component of the suction pressure at 100 Hz do not increase with a decreasing NPSH ratio in this operating point location. Consequently, the effect of the NPSH ratio decrease on the magnitudes of different frequency components is most apparent in the frequency range of 0–2 Hz, although in this case the measurement sequences have differed from each other.

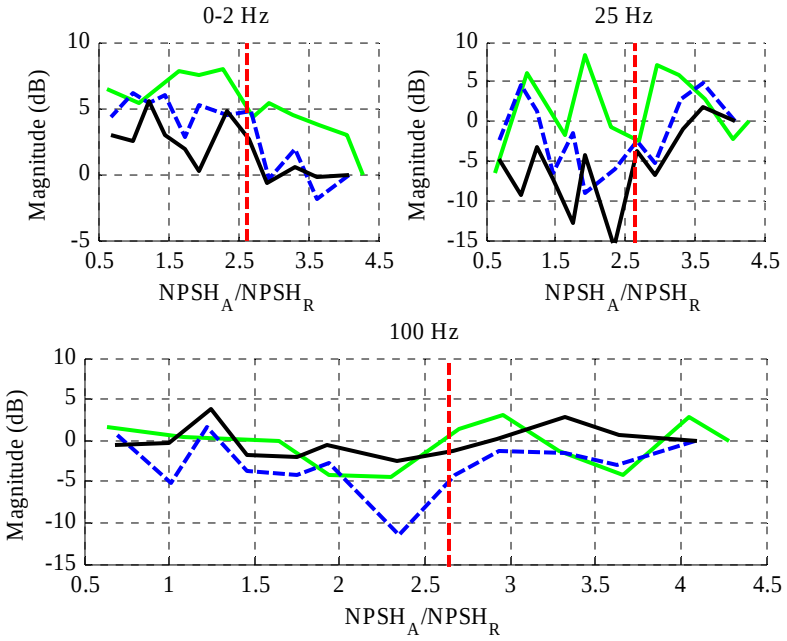

Fig. 4.16: Magnitude of the measured suction pressure in the frequency ranges of 0–2 Hz, 25 Hz and 100 Hz as a function of NPSH ratio. In each figure, the NPSH ratio below which the pump head starts to decrease is shown by a dashed vertical red line. Separate measurement sequences are indicated correspondingly as in Fig. 4.14.

Discharge pressure. A similar analysis was conducted for the measured discharge pressure. Power values were again calculated in the 0–5 Hz frequency range from the Welch PSD data for each measurement. The resulting magnitudes are illustrated in Fig. 4.17. The magnitudes reach their maximum values when the NPSH ratio is 0.6–1.2. In addition, there is a local increase in the magnitudes in the NPSH ratio range of 2.3–2.7, when also the pump head begins to decrease with a decreasing NPSH ratio. Compared with the suction pressure measurements, in this case the discharge pressure reacts more clearly to the occurrence of fully developed, head-decreasing cavitation.

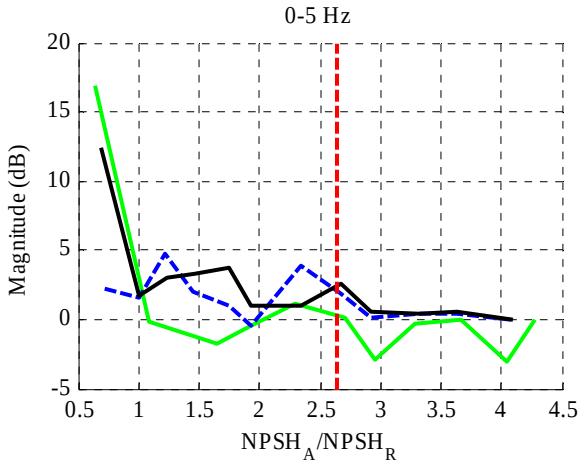

Fig. 4.17: Magnitude of the measured discharge pressure in the frequency range of 0–5 Hz as a function of NPSH ratio. The NPSH ratio below which the pump head begins to decrease is shown by a dashed vertical line. Separate measurement sequences are indicated correspondingly as in Fig. 4.14. There is a local maximum in the magnitudes when the NPSH ratio is around 2.3–2.7.

Acoustic emission. The results of acoustic emission measurements with the Holroyd MHC-SetPoint unit are illustrated in Fig. 4.18. The AE values reach their maximum when the NPSH ratio is approximately 2.7, before the decrease in the head. Compared with the suction and discharge pressure measurements, these results more clearly indicate the location in which the decrease in the pump head starts and a damaging cavitation may occur in the pump.

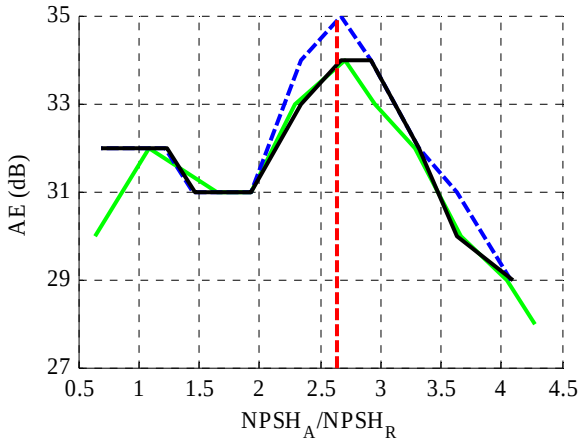

Fig. 4.18: Measured acoustic emission as a function of $NPSH_A/NPSH_R$ ratio. Separate measurement sequences are indicated correspondingly as in Fig. 4.14. In this case, the measured AE values reach their maximum when the NPSH ratio is around 2.7. Below this NPSH ratio, also the pump head begins to decrease with the decreasing $NPSH_A$.

Vibration measurements were also analysed with a similar procedure. The resulting magnitudes are shown in Fig. 4.19. The decrease in the NPSH ratio magnifies both features, which attain their maximum value when the NPSH ratio is approximately one or less. In both cases, the increase in the magnitudes begins when the NPSH ratio is around 2–2.5, and the head already decreases because of the cavitation occurrence. As suggested by previous studies, this

shows that also vibration of a centrifugal pump reacts to the occurrence of cavitation, but the acoustic emission measurements seem to be a more sensitive detection method of the incipient or damaging cavitation in the pump.

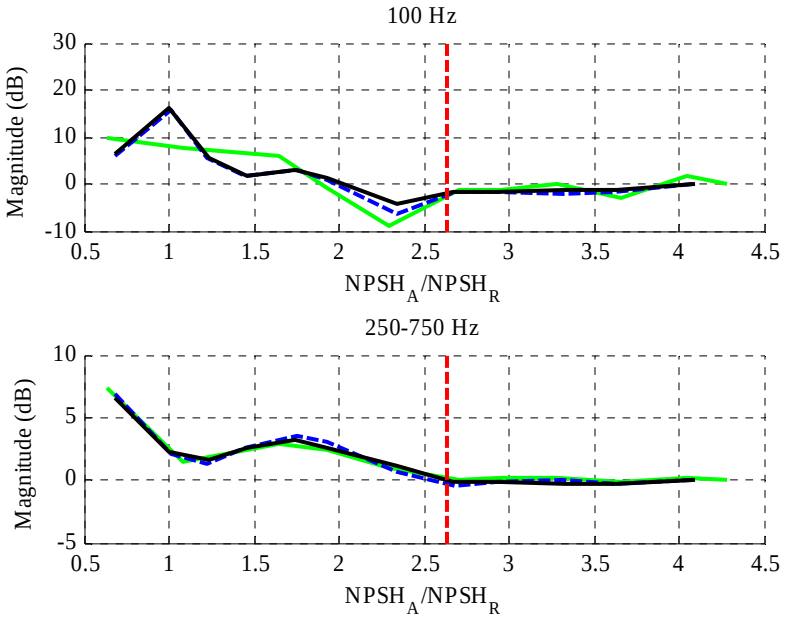

Fig. 4.19: Magnitude of the measured radial vibration in the frequency ranges of 100 Hz and 250–750 Hz as a function of NPSH ratio. In each figure, the NPSH ratio with which the pump head begins to decrease is shown by a dashed red line. Separate measurement sequences are indicated correspondingly as in Fig. 4.14. The decrease in the NPSH ratio so that the pump head begins to decrease has an increasing effect on the magnitude of vibration in both frequency ranges.

Estimated rotational speed and shaft torque. As in the previous section, the occurrence of cavitation should also be visible as an alternating signal component of the rotational speed or the shaft torque estimate. To test this hypothesis, n_{RMS} and T_{RMS} were again determined by applying the pre-filtered estimates of the converter (parameter 1.02 for the rotational speed and parameter 1.05 for the shaft torque, respectively). The resulting values are shown in Fig. 4.20 for the rotational speed and in Fig. 4.21 for the shaft torque, respectively.

In the feature defined from the rotational speed estimates, $n_{RMS}/n_{RMS,N}$, there is a gradual increase with a decreasing NPSH ratio, until the NPSH ratio gets below 0.74, and the collapse of the pump head causes a notable increase in the $n_{RMS}/n_{RMS,N}$ ratio. As previously, these findings support the assumption that only a fully developed cavitation can be detected with this characteristic. In addition, $n_{RMS}/n_{RMS,N}$ ratio is nearly two at NPSH ratios of 1.5 and 1.9, possibly because of the cavitation occurrence, although the head decrease is below 3 percent. Compared with Fig. 4.12, the $n_{RMS}/n_{RMS,N}$ ratio reacts more sensitively to the decrease in the NPSH ratio, although the resulting maximum value of $n_{RMS}/n_{RMS,N}$ is smaller than in the case of Fig. 4.12.

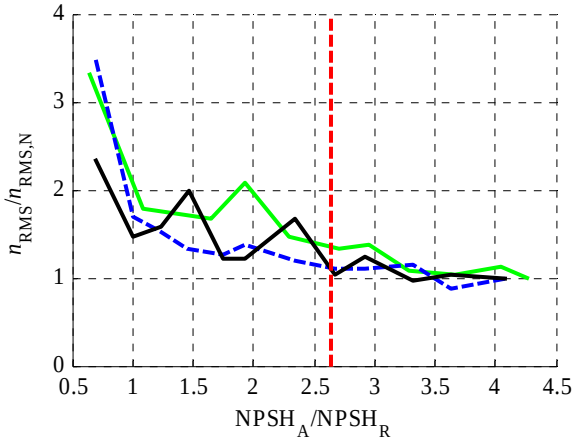

Fig. 4.20: $n_{RMS}/n_{RMS,N}$ ratios of rotational speed estimates as a function of $NPSH_A/NPSH_R$ ratio in the case of pre-filtered estimates. The notations in the figure are consistent with Fig. 4.14. There is a gradual increase in the ratios with a decreasing NPSH ratio.

In the feature defined from the shaft torque estimates, $T_{RMS}/T_{RMS,N}$, a corresponding behaviour can be seen: compared with the initial (i.e. suction-side valve fully open) case, the $T_{RMS}/T_{RMS,N}$ ratios increase with a decreasing NPSH ratio and attain their maximum values when the pump head has already clearly decreased because of the low NPSH ratio.

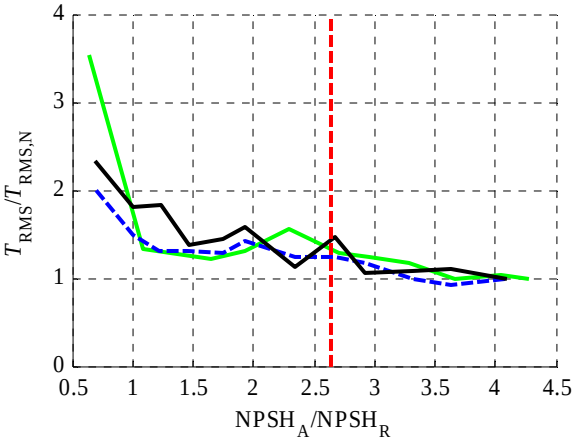

Fig. 4.21: $T_{RMS}/T_{RMS,N}$ ratios of shaft torque estimates as a function of $NPSH_A/NPSH_R$ ratio in the case of pre-filtered estimates. There is a gradual increase in the ratios with a decreasing NPSH ratio.

As a conclusion, also these results have shown the sensitivity of acoustic emission in the detection of cavitation compared with other measurement-based methods. Also in this case, the sensitivity of the proposed frequency-converter-based method seems applicable only to the detection of head-decreasing cavitation. Compared with the results at the BEP of the Sulzer pump, the proposed features have now more sensitively reacted to the decrease in the NPSH ratio. However, the maximum values of the $n_{RMS}/n_{RMS,N}$ and $T_{RMS}/T_{RMS,N}$ ratios are smaller than in the results shown for the BEP of the Sulzer pump shown in Fig. 4.12 and in Fig. 4.13.

4.5 Detection of cavitation occurrence with the proposed method in the case of variable speed operation

As the occurrence of cavitation may be related to the instantaneous rotational speed of the pump, test measurements were also conducted by varying the rotational speed of the Sulzer pump, while the suction-side control valve was held in a constant position. The idea of these test measurements was to simulate a practical case, in which the increase in rotational speed to fulfill the process requirement for the pressure or flow rate leads to the occurrence of fully developed, head-decreasing cavitation.

Cavitating conditions were formed by driving the pump at a 140 % relative flow rate, by throttling the pump suction-side flow, and by increasing the pump rotational speed, until the pump was notably cavitating. Together, these actions significantly decreased the ratio of the available and required NPSH. Compared with the previous NPSH tests, also the rotational speed of the pump affects the measurement results, and the occurrence of cavitation cannot be determined as precisely as in the previous sections. To determine somehow the risk of cavitation, NPSH ratios were again applied to compare measurement results with each other. Since the Sulzer can be regarded as a low suction energy pump because of its 9.1 m/s impeller inlet velocity and SE ratio of 0.4 at 1450 rpm (Karassik, 1997; (2.20)), a NPSH ratio of 1.35 was applied to separate measurement results into two classes.

In the first measurement sequence, the operating point location, shaft torque, rotational speed, radial vibration and estimates of the frequency converter were measured and stored at 12 different rotational speeds ranging from 1320 to 1800 rpm. Each measurement was performed, when the pumping system was operating in the steady state with a constant reference for the rotational speed of the pumping system. $NPSH_A/NPSH_R$ ratios were calculated for each rotational speed based on the measured water temperature, pump flow rate, suction pressure and published NPSH requirement for the Sulzer pump (see (2.6), (4.4) and Fig A.2). The resulting NPSH ratios with the respective flow rates are shown in Fig. 4.22. The previously selected threshold of the NPSH ratio (1.35) is illustrated with a dashed line in the figure, and it was reached at the rotational speed of 1560 rpm. During the measurements, this NPSH ratio was also related to the occurrence of strong cavitation in the pump: operation of the pump at rotational speeds over 1560 rpm caused a significant low-frequency pulsation of the discharge pressure and the measured flow rates did not anymore increase with the increasing rotational speed. Without the suction-side throttling this has not been detected, as the flow rate has been almost a linear function of pump rotational speed in an otherwise similar measurement sequence (see Fig. 4.23).

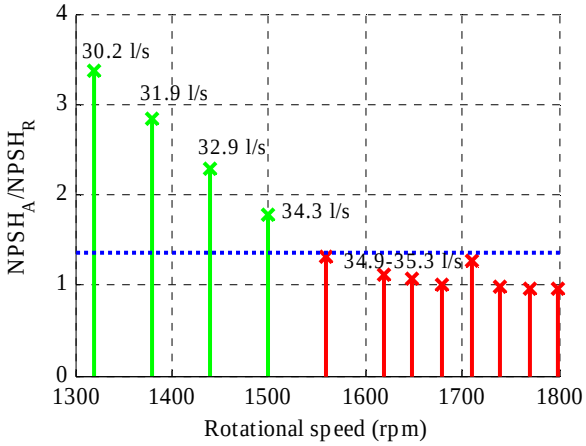

Fig. 4.22: $NPSH_A/NPSH_R$ ratios and pump flow rates as a function of rotational speed when the pump was driven in cavitation-prone operating conditions. At the rotational speeds over 1560 rpm, the pump was in a strongly cavitating condition. This was also detected from the measured flow rate, which did not increase anymore with the rotational speed. At the rotational speeds of 1560–1800 rpm, the measured flow rate was between 34.9 and 35.3 l/s.

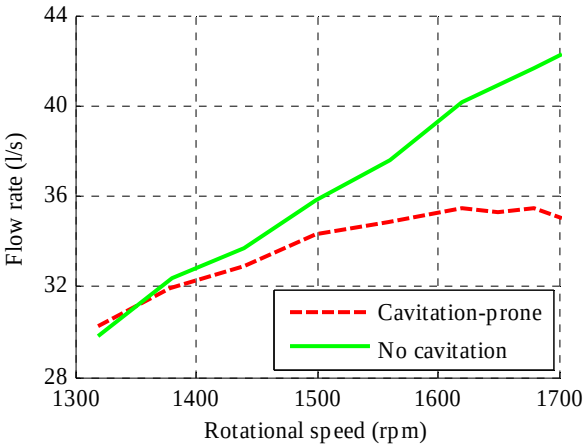

Fig. 4.23: Pump flow rate as a function of rotational speed when the pump was driven with and without the risk of cavitation occurrence.

Besides the flow rate measurements and NPSH ratio calculation from the pressure measurements, the occurrence of cavitation was verified by vibration measurements. Frequency content of the measured radial vibration was determined for each case utilising the Welch method for the power spectral density estimation. The resulting Campbell diagram (i.e., a spectrogram for the Welch PSD of the radial vibration as a function of rotational speed) is illustrated in Fig. 4.24. In this case, there is a notable increase in the wide-bandwidth (400–1600 Hz) vibration when the rotational speed is over 1600 rpm. As the wide-bandwidth vibration is a well-known feature of cavitation in a centrifugal pump (Černetič, 2008; Parrondo, 1998), it verifies the findings of the NPSH ratio determination shown in Fig. 4.22. Besides the wide-bandwidth vibrations, energy of the radial vibration is concentrated around the 810 Hz

frequency, which is most likely a process-related resonance frequency, since it is not affected by the rotational speed. Also the blade pass frequency of the pump (88–120 Hz) is visible in the spectrogram.

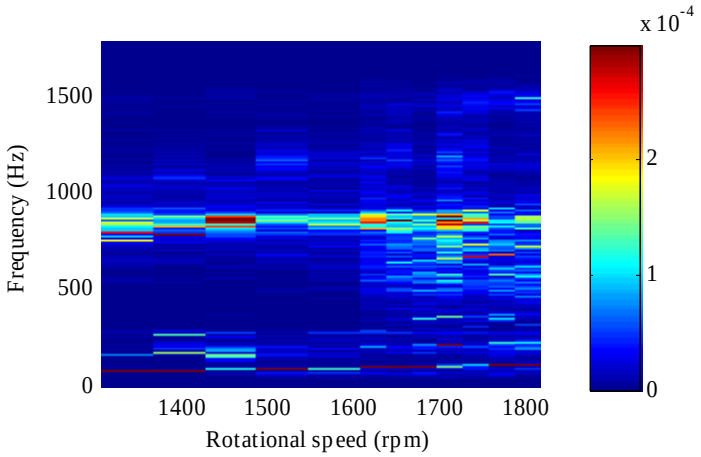

Fig. 4.24: Welch power spectral density of the radial vibration as a function of rotational speed. Wide-bandwidth (400–1600 Hz) variation of the vibration gets stronger at rotational speeds over 1600 rpm. This is a typical feature of cavitation (Černetič, 2008; Parrondo, 1998), and it verifies the occurrence of cavitation in the pump at rotational speeds over 1600 rpm.

According to the presented hypothesis, the occurrence of cavitation should be visible as the time-domain variation of the rotational speed or shaft torque. Again, a frequency-domain analysis by the Welch method for the power spectral density estimation was performed for the shaft torque measurements to determine applicable frequency range to the cavitation detection in the case of the laboratory pumping system. The obtained Campbell diagram is illustrated in Fig. 4.25. It shows how the occurrence of cavitation increases the magnitude of the low-frequency component (0–5 Hz) of the shaft torque, when the rotational speed is over 1600 rpm. In addition, the occurrence of cavitation increases the magnitude of the frequency component at the frequency region 44–60 Hz, which is double the rotational speed frequency. The energy of the shaft torque signal is also concentrated around the 84 Hz frequency, when the pump is prone to cavitation. However, this is most likely caused by the mechanical interaction of the pumping system and the measurement shaft, since the frequency of this component is not affected by the rotational speed, and it is also present at lower rotational speeds and in Fig. 4.9. Other notable components in the frequency spectrum are located at the rotational speed (22–30 Hz) and blade pass frequencies (88–120 Hz), but these components are apparent also without the occurrence of cavitation.

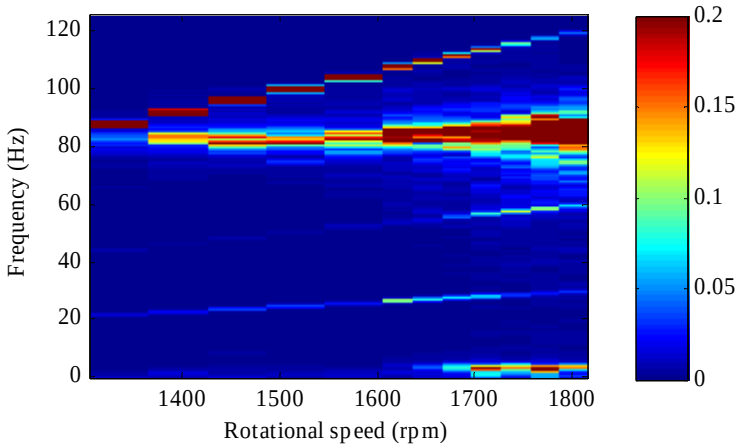

Fig. 4.25: Welch power spectral density of the measured shaft torque as a function of rotational speed. The most notable components in the frequency spectrum are around 84 Hz, at the frequency of rotational speed, at the blade pass frequency (four times the frequency of rotational speed) and in the low-frequency region (0–5 Hz). It should be noted that the visible frequency axis of this spectrogram has been limited to 125 Hz, as there has not been applicable signal content at higher frequencies.

The corresponding frequency-domain analysis was also performed for the unfiltered estimates of the rotational speed and the shaft torque. A Campbell diagram for the unfiltered shaft torque estimate is illustrated in Fig. 4.26. As with the measured shaft torque, the occurrence of cavitation has increased the magnitude of the low-frequency component of the estimated shaft torque (now 0–10 Hz), when the rotational speed is over 1750 rpm. Otherwise, the spectrogram consists of wide-band noise and aliased components of the electric output frequency. Consequently, there are no distinct components that could be applied in the detection of cavitation occurrence.

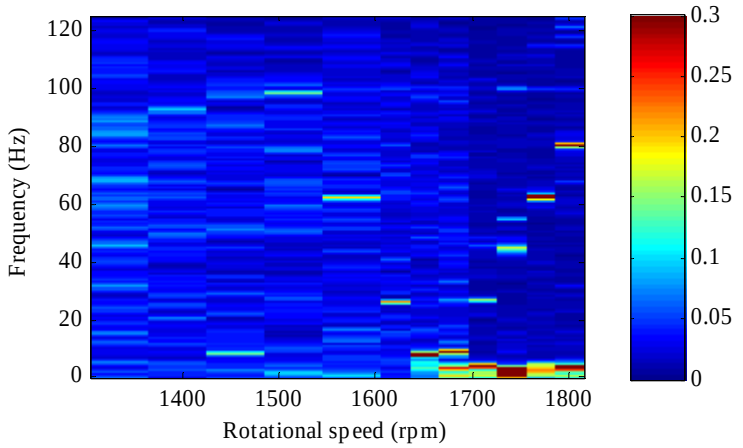

Fig. 4.26: Welch power spectral density of the estimated shaft torque as a function of rotational speed. The most notable component is in the low-frequency region (0–10 Hz) when the pump is prone to cavitation. Otherwise, the spectrogram has no components that could be used in the detection of cavitation occurrence. It should be noted that the visible frequency axis of this spectrogram has been limited to 125 Hz, as there has not been applicable signal content at higher frequencies.

A Campbell diagram for the unfiltered rotational speed estimate is illustrated in Fig. 4.27. Also in this case the occurrence of cavitation is visible in the low-frequency region, when the rotational speed is over 1600 rpm. However, there are no other components that could be applied in the detection of cavitation occurrence for this pumping system. For instance, the first harmonic of the electric output frequency around 88–120 Hz is not distinctively affected by the cavitation occurrence. Thus, it seems again possible to detect cavitation only by monitoring the low-frequency content (now 0–10 Hz) of the rotational speed and the shaft torque estimates. This also means that the detection of cavitation should be possible with the filtered estimates of the rotational speed and the shaft torque.

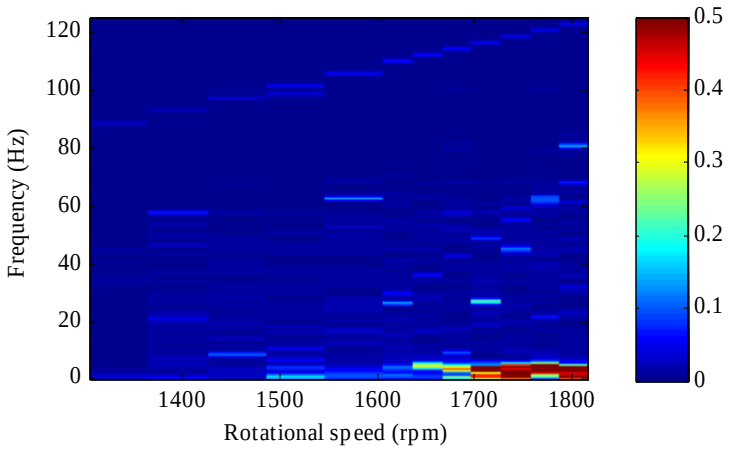

Fig. 4.27: Welch power spectral density of the estimated rotational speed as a function of rotational speed. The most notable component is again in the low-frequency region (0–5 Hz) when the pump is prone to cavitation. Also the blade pass frequency of the pump is visible in the spectrogram. In order to improve the readability of the figure, the visible frequency axis of this spectrogram has been limited to 125 Hz, as there has not been applicable signal content at higher frequencies.

To test this assumption, unfiltered estimates were firstly low-pass filtered and decimated into the frequency ranges of 0–10 Hz for the rotational speed and 0–5 Hz for the shaft torque, respectively. Then, n_{RMS} and T_{RMS} were determined at each rotational speed. Normal values of the speed and torque time-domain variation ($n_{RMS,N}$ and $T_{RMS,N}$, respectively) were calculated by determining the mean of n_{RMS} and T_{RMS} values, which had a sufficient NPSH ratio to avoid the occurrence of strong cavitation ($NPSH_A/NPSH_R > 1.35$).

The resulting data points are illustrated in Fig. 4.28. Figure shows that especially n_{RMS} values rise, when the NPSH ratio decreases near 0.95. Hence, the rotational speed estimate seems in this case to be a feasible variable to determine the occurrence of fully developed cavitation. There is also an increase in the $T_{RMS}/T_{RMS,N}$ ratio, when the NPSH ratio gets near 1. However, the shaft torque variation does not have now such a clear correlation that would allow its reliable use in the detection of cavitation occurrence with the laboratory pumping system. In general though, these results support again the assumption that the occurrence of a fully developed cavitation is related to the larger time-domain variation of the estimates. However, they also show the case-specific nature of the feasible threshold values for the $n_{RMS}/n_{RMS,N}$ and $T_{RMS}/T_{RMS,N}$, respectively: on the basis of NPSH ratios, the pump could be prone to cavitation occurrence without a significant increase in the calculated ratios. In the case of this pumping system, the threshold values could be 2 for the $n_{RMS}/n_{RMS,N}$ and 1.5 for the $T_{RMS}/T_{RMS,N}$, since

then there would not be erroneous results for the data points, where head-decreasing cavitation should not occur.

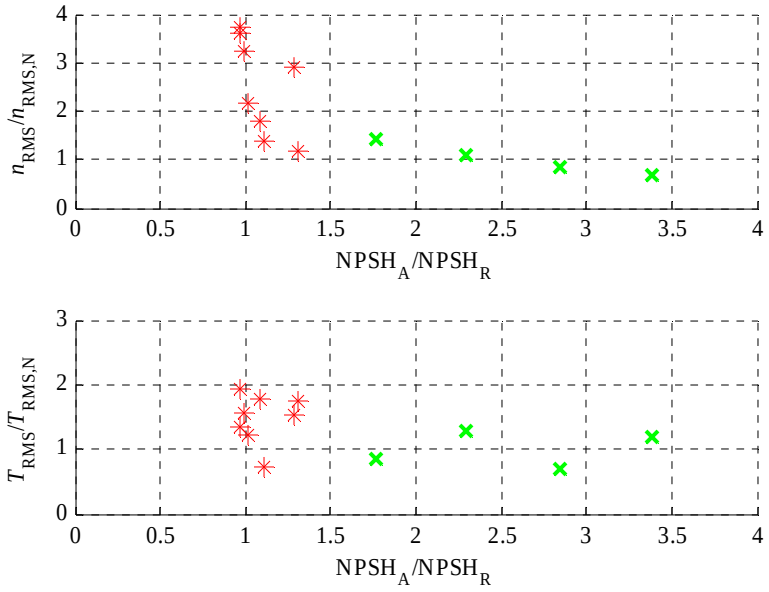

Fig. 4.28: $n_{RMS}/n_{RMS,N}$ and $T_{RMS}/T_{RMS,N}$ ratios as a function of $NPSH_A/NPSH_R$ ratio in the case of unfiltered estimates (parameters 2.17 and 161.07, respectively) that have been low-pass filtered to the frequency range of 0–5…10 Hz. Data points with a NPSH ratio over 1.35 are illustrated by green crosses. Red stars indicate the data points with a smaller NPSH ratio. Compared with the normal operating conditions, cavitation occurrence can increase the n_{RMS} and T_{RMS}.

Correspondingly, also the applicability of pre-filtered estimates to the rotational speed and shaft torque was evaluated. The resulting data points are illustrated in Fig. 4.29. Figure shows that both RMS values rise, when the NPSH ratio decreases below 1.35, indicating that the proposed method might detect the development of cavitation. However, the most significant increase in relative values can be seen at lower values of the NPSH ratio, in the range of 0.97–1.07, where a fully developed cavitation already occurs. This supports the assumption that the proposed method may not be feasible for the detection of incipient cavitation at least with this pumping system. For some reason, the variation of shaft torque estimates has a clearer correlation with the NPSH ratio than in the case of Fig. 4.28. This may be related to the internal filtering of the estimates, meaning that the obtained results may be frequency converter specific. In this case though, it seems that the pre-filtered estimates could be as feasible for the cavitation detection as the originally unfiltered signals. It should also be noted that the previously suggested threshold values for the $n_{RMS}/n_{RMS,N}$ and $T_{RMS}/T_{RMS,N}$ seem to result in the same conclusions for the cavitation occurrence as in the previous case.

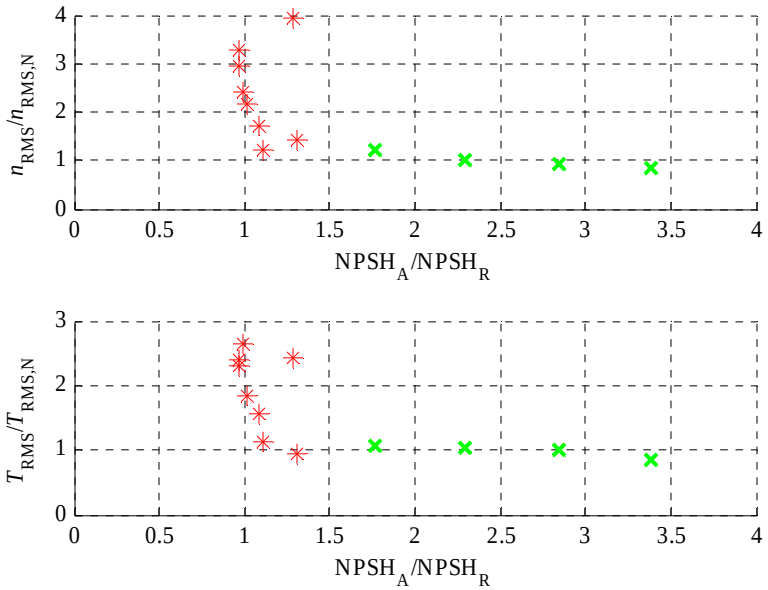

Fig. 4.29: $n_{RMS}/n_{RMS,N}$ and $T_{RMS}/T_{RMS,N}$ ratios as a function of $NPSH_A/NPSH_R$ ratio in the case of pre-filtered estimates (parameters 1.02 and 1.05, respectively). Compared with the normal operating conditions, cavitation occurrence can notably increase the n_{RMS} and T_{RMS}. Data points with a NPSH ratio over 1.35 are illustrated by green crosses. Red stars indicate the data points with a smaller NPSH ratio.

The previously shown estimated values of the shaft torque were also verified by torque measurements, which showed similar characteristics when the pump was prone to cavitation: in Fig. 4.30, results are presented from an evaluation where the original shaft torque measurement data was low-pass filtered to the 0–10 Hz frequency range, and RMS values for the shaft torque variation (referred to as T_{MEAS}) were calculated for each case. Correspondingly, normal value for the shaft torque variation ($T_{MEAS,N}$) was determined by calculating the mean of T_{MEAS} values, which have a sufficient NPSH ratio to avoid head-decreasing cavitation. As seen in the figure, the occurrence of cavitation has increased the time-domain variation of the measured shaft torque. Also the measurements for the rotational speed showed a higher amount of time-domain variation, when the pump was strongly cavitating.

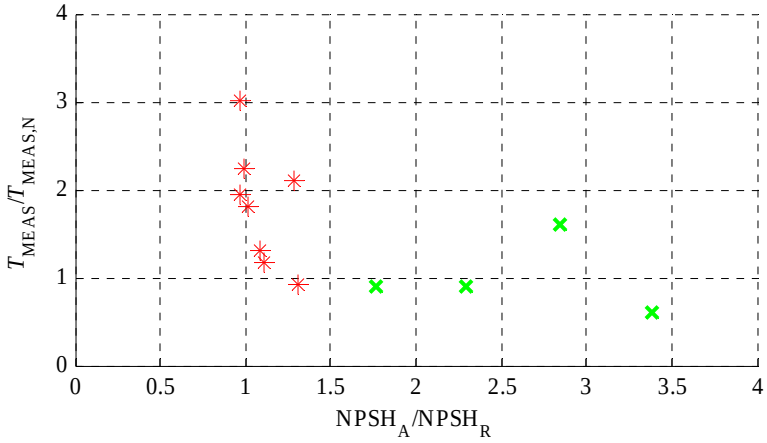

Fig. 4.30: $T_{MEAS}/T_{MEAS,N}$ ratio as a function of $NPSH_A/NPSH_R$ ratio. Compared with the normal operating conditions, cavitation occurrence can notably increase the T_{MEAS}.

Although these results hold true only for this laboratory pumping system, a similar behaviour could be expected also with other corresponding pumping systems having a radial flow centrifugal pump ($n_q \approx 30$), a similar frequency converter and water as the pumped fluid. However, the results may have been affected by the suction-side throttling, decreasing the general applicability of these test results. Also the suggested threshold values for the $n_{RMS}/n_{RMS,N}$ and $T_{RMS}/T_{RMS,N}$ might be case-specific, and therefore they should not be considered as universally applicable limit values.

It should also be noted that these estimates have been stored during a constant rotational speed reference value and constant process characteristics. Thus, the test results could be different in practical installations, where the process characteristics may vary during the pump operation.

Since the test results may be different with another radial flow centrifugal pump, and they can also be affected by the frequency converter, tests have also been conducted with two other pumps and with a frequency converter applying the vector control method, which is discussed in the following section.

4.5.1 Effect of the frequency converter on the measurement results

The results show that the occurrence of cavitation can be detected by a frequency converter, if cavitation phenomenon causes uneven running of a centrifugal pump (i.e., variation in the power consumption of the pump) at least in the case of the Sulzer pumping system. Since these results may be pumping system specific, a similar measurement sequence was carried out with an ABB ACS 550 frequency converter driving the Sulzer pump. Compared with the DTC method applied by the ACS 800 frequency converter, ACS 550 applies the vector control method that is more commonly used in the industrial frequency converters. Compared with the ACS 800, only pre-filtered estimates are available for the rotational speed and shaft torque. In addition, the rotational speed estimate of an induction motor is given with a resolution of 1 rpm compared with the 0.1 rpm resolution of the ACS 800 converter, which decreases the applicability of this estimate to the detection of cavitation occurrence. However, estimated torque values are given with a similar resolution in both cases (0.1 % of the nominal torque value).

The resulting $n_{RMS}/n_{RMS,N}$ and $T_{RMS}/T_{RMS,N}$ ratios are shown in Fig. 4.31 as a function of NPSH ratio. As expected, the $n_{RMS}/n_{RMS,N}$ ratio does not have a clear correlation with the occurrence of cavitation in a centrifugal pump owing to the insufficient resolution of the rotational speed estimate. Consequently, a smaller threshold value for the $n_{RMS}/n_{RMS,N}$ should be selected compared with the Sulzer pumping system having the ACS 800 converter. However, the $n_{RMS}/n_{RMS,N}$ ratio gets higher, when the NPSH ratio is about 0.75. In addition, the $T_{RMS}/T_{RMS,N}$ ratio seems to increase, when the pump is prone to cavitation. In addition, the suggested threshold value of 1.5 would be feasible in this case, since then there would not be erroneous results for the data points, where the cavitation should not occur. In general, the shown results support again the presented hypothesis that cavitation occurrence can be detected by a frequency converter, if it clearly affects the motor operation.

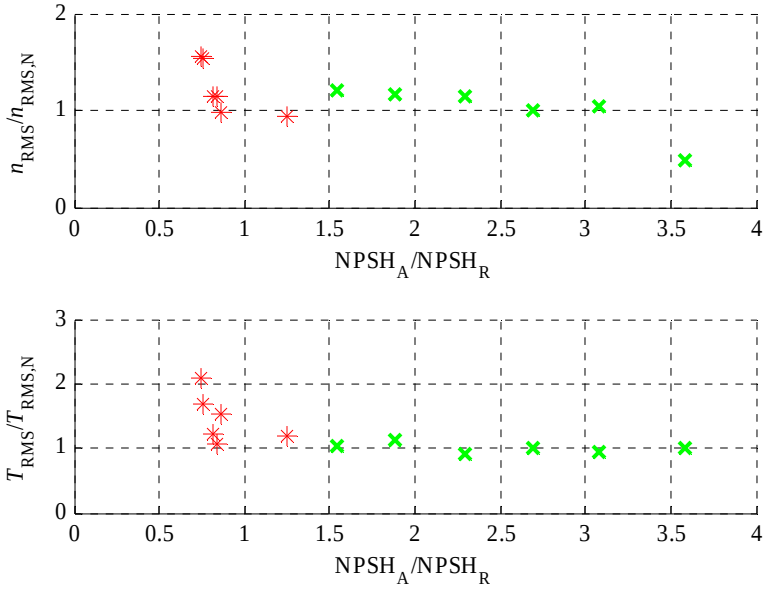

Fig. 4.31: $n_{RMS}/n_{RMS,N}$ and $T_{RMS}/T_{RMS,N}$ ratios as a function of NPSH ratio, when the pump was driven with an ABB ACS 550 frequency converter. Compared with Fig. 4.29, the occurrence of cavitation is distinctively visible only in the $T_{RMS}/T_{RMS,N}$ ratios.

The increase in the shaft torque variation was verified by analysing the shaft torque measurements. The frequency content of the measured shaft torque was determined by utilising the Welch method for the power spectral density estimation. The resulting Campbell diagram is illustrated in Fig. 4.32. Also in this case, the occurrence of cavitation increases the magnitude of the low-frequency component (0–5 Hz) of the torque. Correspondingly, the energy of the shaft torque signal is also concentrated around the 84 Hz frequency, when the pump is prone to cavitation. However, there are also differences compared with Fig. 4.25. In this case, the first rotational speed harmonic is much stronger than with a DTC frequency converter. There is also a trace of the second rotational speed harmonic component, as well as a clear, rotational speed independent line at 100 Hz.

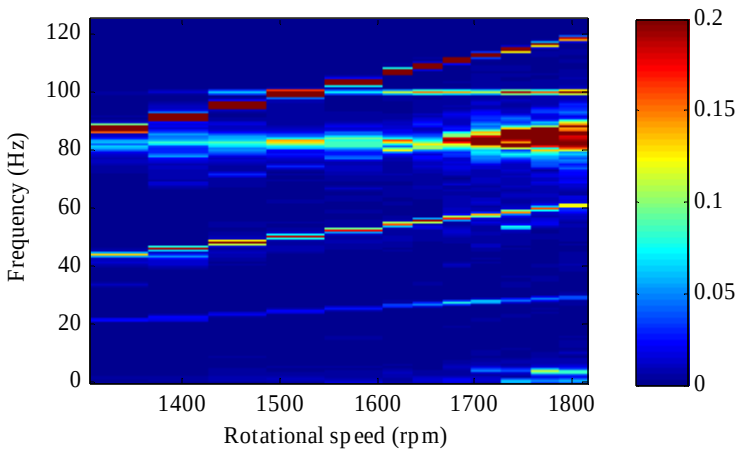

Fig. 4.32: Welch power spectral density of the measured shaft torque as a function of rotational speed, when the pump was driven with an ABB ACS 550 frequency converter. Also in this case, the occurrence of cavitation increases the low-frequency variation (0–5 Hz) in the shaft torque.

4.5.2 Measurement results with different pumps

The effect of cavitation occurrence on the estimated rotational speed and shaft torque was also tested with two other pumps in the laboratory in order to have more general results. For the laboratory measurements, the pumping systems were installed in the same water tank system as the Sulzer pump. Since different pumps have their own operational characteristics and $NPSH_R$ curves, these tests allow more generalised conclusions concerning the use of a frequency converter in the detection of cavitation occurrence, although the specific speeds and BEP values of these pumps are relatively close to each other.

Serlachius pumping system. Firstly, tests were conducted with a pumping system consisting of a Serlachius DC-80/260 radial flow centrifugal pump, a four-pole 15 kW Strömberg induction motor and an ABB ACS 800 frequency converter (see Fig. 4.33 and Appendix A). The operating point location of the pump was monitored with the pressure measurements for the pump head and flow rate. The mean values of the rotational speed and shaft torque were determined with an HBM torque measurement transducer on the motor shaft. The estimates provided by the frequency converter were stored with the ABB DriveDebug software similarly as with the Sulzer pumping system. Compared with the Sulzer pump, the required NPSH of the Serlachius is notably higher, 2–7 metres at 1425 rpm (see Fig. A.3). This allows the occurrence of cavitation in the laboratory without additional suction-side throttling, which may have affected the test results of the Sulzer pumping system.

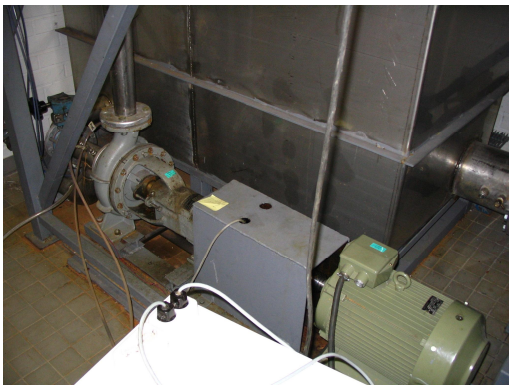

Fig. 4.33: Serlachius pumping system. It consists of a Serlachius DC-80/260 centrifugal pump and a Strömberg induction motor. The rotational speed of the pumping system was controlled with an ABB ACS 800 frequency converter.

Five measurement sequences were carried out with the Serlachius pumping system. Each measurement sequence had a specific system curve shape: the valves were adjusted so that the flow rates were approximately 50, 70, 100, 120 and 150 % of 22 l/s at 1425 rpm that is the Q_{BEP} of the Serlachius pump. With these valve settings, the pump was driven at rotational speeds ranging from 1050 rpm to 1800 rpm. At each rotational speed, pressure measurements for the pump operating point location were carried out, and estimates for the rotational speed and shaft torque were read from the frequency converter.

Values of n_{RMS} and T_{RMS} were calculated for each measurement from the pre-filtered estimates of the rotational speed and shaft torque, as they have been feasible in the case of the Sulzer pump. Normal values $n_{RMS,N}$ and $T_{RMS,N}$ were determined by calculating the mean of n_{RMS} and T_{RMS} values, which have a sufficient NPSH ratio to avoid the occurrence of 3 % head-decreasing cavitation: as the suction energy and impeller inlet velocity values of the Serlachius and Sulzer pump are almost the same, the corresponding NPSH criterion of 1.35 was applied for this pumping system. The resulting $n_{RMS}/n_{RMS,N}$ ratios are shown in Fig. 4.34 as a function of NPSH ratio. Respectively, $T_{RMS}/T_{RMS,N}$ ratios are shown in Fig. 4.35. These figures clearly show the impact of fully developed cavitation occurrence on the $n_{RMS}/n_{RMS,N}$ and $T_{RMS}/T_{RMS,N}$ ratios. They also support the assumption that feasible threshold values for $n_{RMS}/n_{RMS,N}$ and $T_{RMS}/T_{RMS,N}$ are case-specific, which is why a further study for the determination of these threshold values should be carried out. The occurrence of cavitation in the measurement sequence with a 150 % flow rate was also noticed during the measurements from the rattling noise of the pump and varying measurement values of the rotational speed and shaft torque, which is captured by $n_{RMS}/n_{RMS,N}$ and $T_{RMS}/T_{RMS,N}$.

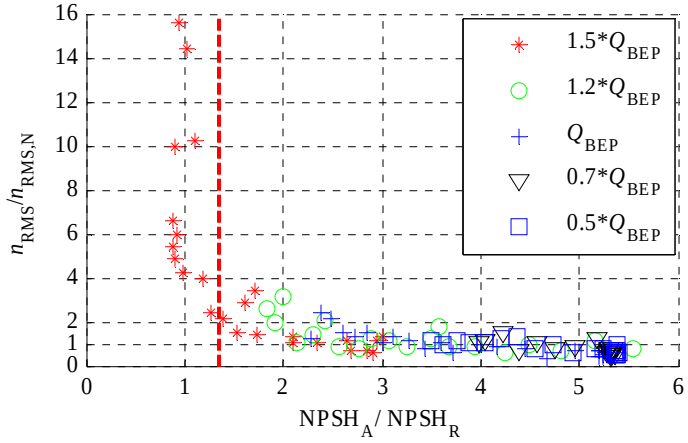

Fig. 4.34: $n_{RMS}/n_{RMS,N}$ ratios as a function of $NPSH_A/NPSH_R$ ratio for the Serlachius pumping system. The chosen NPSH ratio of 1.35 for the result classification is shown by a dashed vertical line. In this case, the occurrence of cavitation has a strong impact on the relative values.

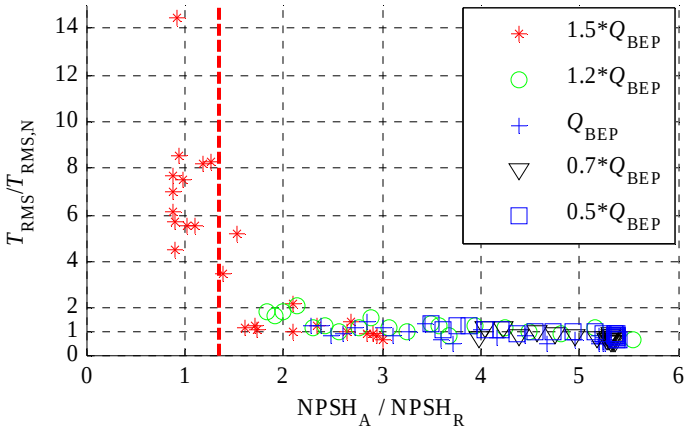

Fig. 4.35: $T_{RMS}/T_{RMS,N}$ ratios as a function of $NPSH_A/NPSH_R$ ratio for the Serlachius pumping system. The chosen NPSH ratio of 1.35 for the result classification is shown by a dashed vertical line.

As a more detailed example of the results obtained for the Serlachius pumping system, $n_{RMS}/n_{RMS,N}$ and $T_{RMS}/T_{RMS,N}$ ratios are given in Fig. 4.36 for the rotational speed of 1500 rpm. The NPSH ratios for each measurement are also given in the figure. The figure shows that the RMS ratios are clearly higher when the NPSH ratio is 1.18.

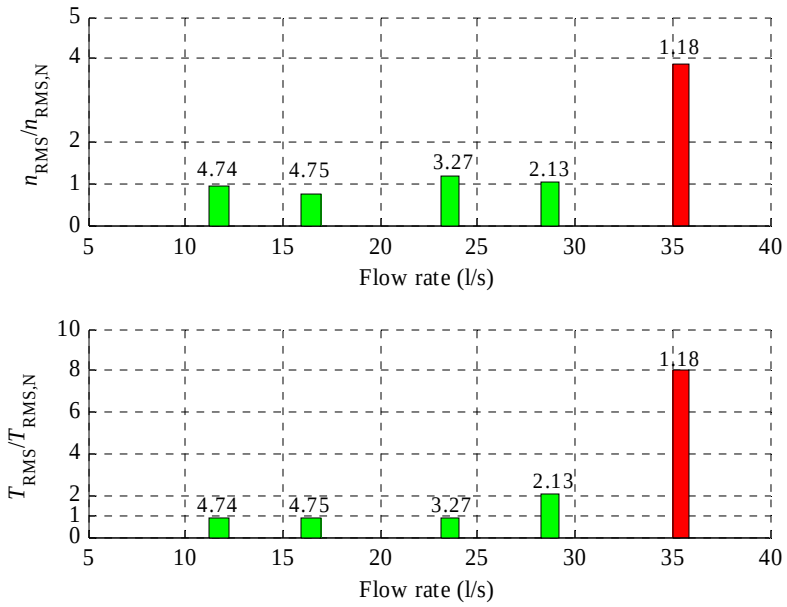

Fig. 4.36: $n_{RMS}/n_{RMS,N}$ and $T_{RMS}/T_{RMS,N}$ ratios as a function of flow rate at the rotational speed of 1500 rpm. NPSH ratio of the Serlachius pump is also given for each measurement.

Grundfos pumping system. Another sequence of test measurements was carried out with a pumping system consisting of a Grundfos LP 100-125/130 mixed flow centrifugal pump, a two-pole 5.5 kW Grundfos induction motor and an ABB ACS 800 frequency converter (see Fig. 4.37 and Appendix A). This pumping system was tested to have results also with a different type of centrifugal pump, and consequently to analyse, if the proposed method could be also feasible with other pump type than just with the radial flow centrifugal pumps.

The operating point location of the pump was monitored with the pressure measurements for the pump head and flow rate. Also this pump has a larger NPSH requirement than the Sulzer pump, 2–9 metres at 2900 rpm. In addition, this pump has higher n_q and n_{ss} than the Sulzer pump because of its mixed flow impeller. For this reason, a larger margin of $NPSH_A$ may be required to avoid the occurrence of cavitation.

Fig. 4.37: Grundfos pumping system. It consists of a Grundfos LP 100-125/130 centrifugal pump and a Grundfos induction motor. The rotational speed of the pumping system was controlled with an ABB ACS 800 frequency converter.

Five measurement sequences were carried out with the Grundfos pumping system. Each measurement sequence had a specific system curve shape: the valves were adjusted so that the flow rates were approximately 50, 70, 100, 120 and 155 % of 24 l/s at 3000 rpm (Q_{BEP} of the Grundfos pump). With these valve settings, the pump was driven at rotational speeds ranging from 2100 rpm to 3180 rpm. At each rotational speed, pressure measurements for the pump operating point location were carried out, and estimates for the rotational speed and shaft torque were read from the frequency converter. Correspondingly, normal values $n_{RMS,N}$ and $T_{RMS,N}$ were again determined by calculating the mean of n_{RMS} and T_{RMS} values, which have a sufficient NPSH ratio to avoid cavitation ($NPSH_A/NPSH_R$ ratio of 2 was selected because of the larger suction specific speed compared with other pumps).

The resulting $n_{RMS}/n_{RMS,N}$ ratios are illustrated in Fig. 4.38 as a function of NPSH ratio. Correspondingly, $T_{RMS}/T_{RMS,N}$ ratios are shown in Fig. 4.39. In this case, the occurrence of cavitation has a clearer effect on the shaft torque than on the rotational speed. A measurement sequence with the 120 % relative flow rate has a notably high $n_{RMS}/n_{RMS,N}$, although the pump was otherwise operating without signs of cavitation during the measurement. This may be caused by the design of this pump, possibly by incipient cavitation occurring at NPSH ratios of 2.5–3, or by some other pump or process-related issue. Otherwise, also in this case the occurrence of head-decreasing cavitation has generally an increasing effect on the $n_{RMS}/n_{RMS,N}$ and $T_{RMS}/T_{RMS,N}$ ratios, when the pump is prone to a fully developed cavitation having an effect on the pump performance.

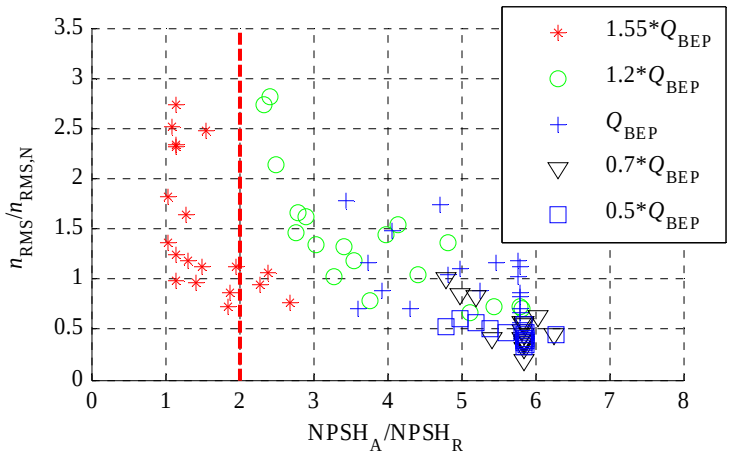

Fig. 4.38: $n_{RMS}/n_{RMS,N}$ ratios as a function of $NPSH_A/NPSH_R$ ratio for the Grundfos pumping system. The chosen NPSH ratio of 2 for the result classification is shown by a dashed vertical line. According to $n_{RMS}/n_{RMS,N}$ ratios cavitation may already occur with higher NPSH ratios.

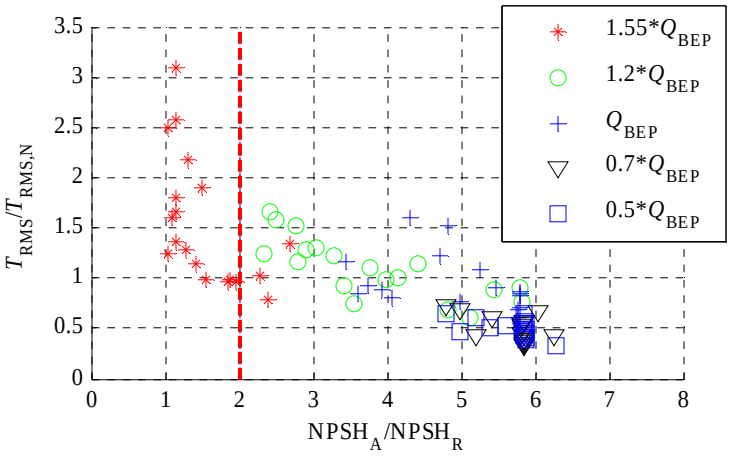

Fig. 4.39: $T_{RMS}/T_{RMS,N}$ ratios as a function of $NPSH_A/NPSH_R$ ratio for the Grundfos pumping system. The chosen NPSH ratio of 2 for the result classification is shown by a dashed vertical line.

As a more detailed example of the results obtained for the Grundfos pumping system, $n_{RMS}/n_{RMS,N}$ and $T_{RMS}/T_{RMS,N}$ ratios are given in Fig. 4.40 for the rotational speed of 3000 rpm. The NPSH ratios for each measurement are also given in the figure. The figure shows that the RMS ratios are at highest when the NPSH ratio is 1.09. At this rotational speed, however, the difference in $T_{RMS}/T_{RMS,N}$ ratios is small between the NPSH ratios of 1.09 and 2.78, which could indicate that the pump may be cavitating also at NPSH ratios over 2. However, this was not detected during the measurements.

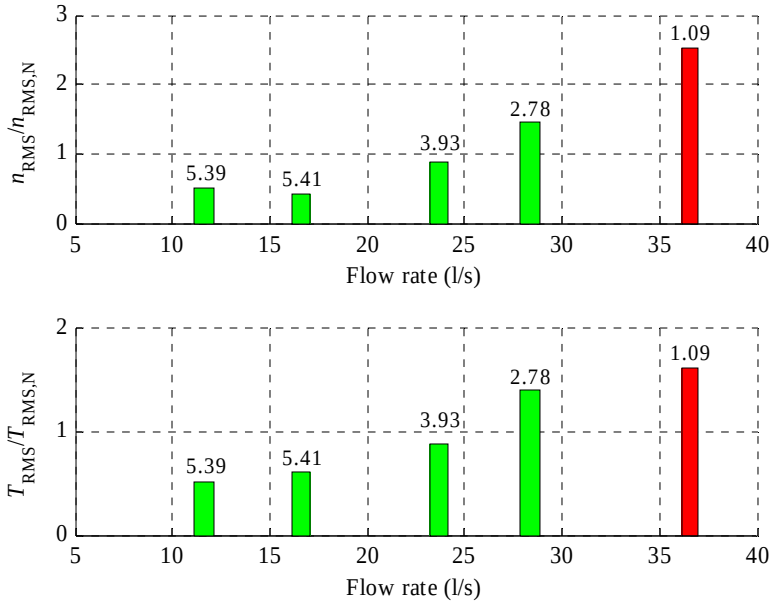

Fig. 4.40: $n_{RMS}/n_{RMS,N}$ and $T_{RMS}/T_{RMS,N}$ ratios as a function of flow rate at the rotational speed of 3000 rpm. NPSH ratio of the Grundfos pump is also given for each measurement.

4.6 Detection of flow recirculation

Besides the inadequate NPSH ratio, cavitation may occur in a centrifugal pump because of the internal flow recirculation of the fluid. Recirculation can result in vortices, where the local pressure of the fluid is decreased below the vaporisation limit, resulting in cavitation. Flow recirculation may occur if the pump is driven at a partial flow rate. Typically, flow recirculation occurs in the operating region where the pump is already operating with a notably decreased efficiency. Hence, the detection of occurring flow recirculation provides an opportunity to avoid inefficient use of a centrifugal pump.

Since it seems possible to detect NPSH-related occurrence of a fully developed cavitation by a frequency converter, and flow recirculation may cause cavitation phenomenon in a centrifugal pump, the presented method may also be applicable to the detection of flow recirculation. In order to test the frequency converter's applicability to detect flow recirculation especially in the case of radial flow centrifugal pumps, measurements were carried out with the Sulzer pumping system.

For the evaluation, a measurement sequence was performed at a 1450 rpm rotational speed by changing the operating point location with a control valve on the discharge side. With this method, the operating point location, shaft torque, rotational speed, radial vibration, acoustic emission and estimates of the frequency converter were measured and stored at 14 different flow rates ranging from 0 to 143 % of the Sulzer Q_{BEP}. Each measurement was performed when the pump was operating in the steady state. The $NPSH_A/NPSH_R$ ratios were calculated for each operating point on the basis of the measured water temperature, pump flow rate and suction pressure values (see (4.4)). However, the NPSH ratio values have not been calculated for the flow rates below 7.5 l/s (27 % of the Q_{BEP}), since there is no given $NPSH_R$ curve for this operating region. Since the pump manufacturer has given the allowable operating region with

the $NPSH_R$ curve, the pump may be susceptible to the flow recirculation and other harmful phenomena at these partial flow rates. The obtained values for the NPSH ratios are shown in Fig. 4.41, where a limit value of 1.35 has been applied as a threshold for the occurrence of NPSH-related, head-decreasing cavitation.

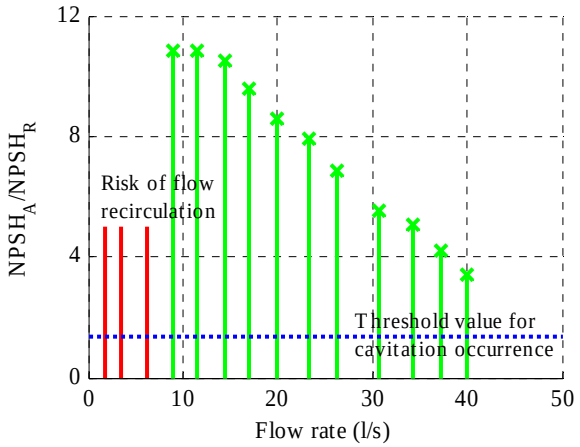

Fig. 4.41: $NPSH_A/NPSH_R$ ratios as a function of flow rate in the measurement sequence with a constant rotational speed. In this measurement sequence, the NPSH ratios are sufficient to avoid the cavitation occurrence. However, the pump may be susceptible to flow recirculation and other harmful events at reduced flow rates.

For comparison, the results of the AE measurements are shown in Fig. 4.42. They support the assumption of flow recirculation occurring in the pump at flow rates below 7.5 l/s, as in this region the highest values are attained for the AE activity. Since the AE values increase with a decreasing flow rate below 23 l/s, an incipient occurrence of flow recirculation is possible also in the flow rate region of 8.9–14.4 l/s, as the AE values are there larger than at the maximum flow rate of 40 l/s.

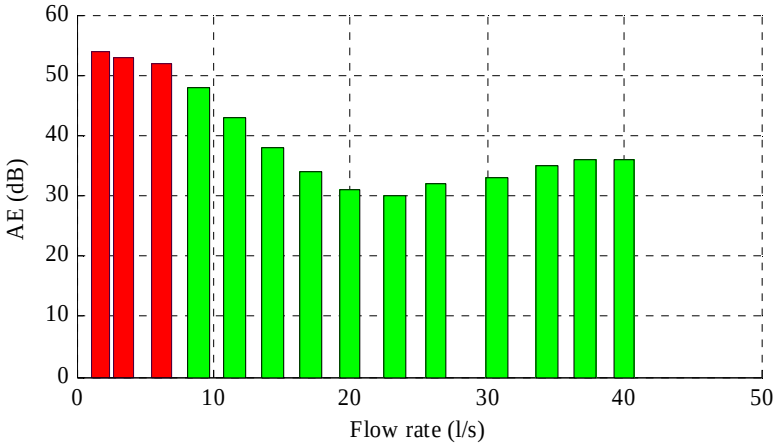

Fig. 4.42: Measured acoustic emission as a function of flow rate. The AE reaches its maximum value when the pump flow rate is at its minimum, and there is an apparent risk of flow recirculation occurrence in the pump.

Pre-filtered estimates of the rotational speed and shaft torque were applied to determine $n_{RMS}/n_{RMS,N}$ and $T_{RMS}/T_{RMS,N}$ as a function of flow rate. Normal values $n_{RMS,N}$ and $T_{RMS,N}$ were calculated from the RMS values of the rotational speed and shaft torque, which have a sufficient flow rate (Q > 7.5 l/s) to avoid the occurrence of flow recirculation. The results are shown in Fig. 4.43 for both estimates. There is a notable increase in the RMS values, when the flow rate is below 10 l/s and the risk of flow recirculation is apparent. This supports the hypothesis that also the flow recirculation of a centrifugal pump can be detected by a frequency converter.

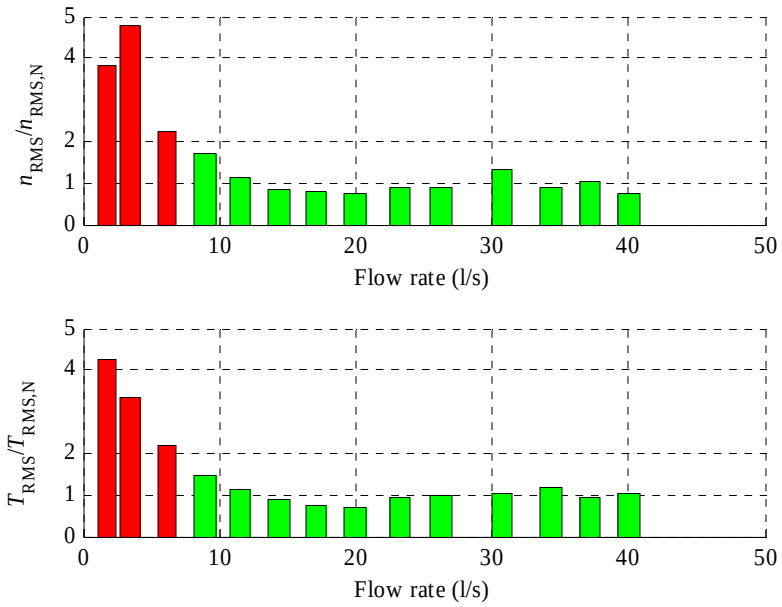

Fig. 4.43: $n_{RMS}/n_{RMS,N}$ and $T_{RMS}/T_{RMS,N}$ ratios as a function of flow rate. The estimated values are highest at partial flow rates, especially below 10 l/s, where the risk of flow recirculation is also more apparent.

The shaft torque measurements were analysed to see if the flow recirculation has similar effects as the NPSH-related cavitation. The frequency content of the measured shaft torque is illustrated in Fig. 4.44. As previously, the energy of the measured shaft torque is concentrated on the frequencies of 84 Hz and 96 Hz, which is the blade passing frequency of the pump. The energy content at these frequencies increases when the pump is operating away from its best efficiency point. In addition, there is a low frequency component (0–10 Hz) in the shaft torque at flow rates below 10 l/s. It can be concluded that the occurrence of flow recirculation has similar effects on the shaft torque as the occurrence of cavitation.

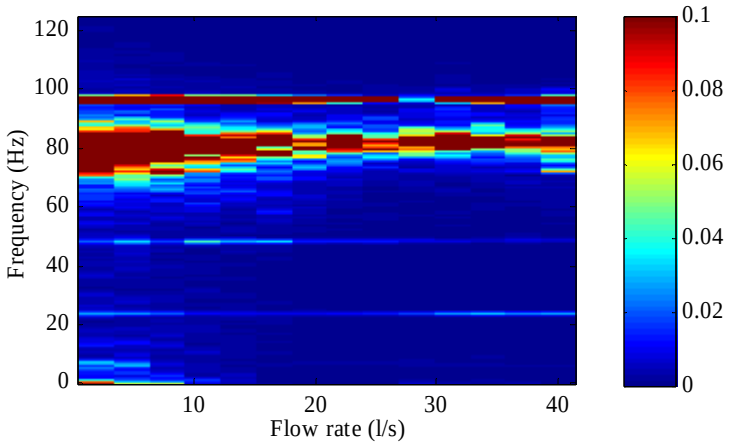

Fig. 4.44: Welch power spectral density of the measured shaft torque as a function of flow rate. The spectral density values are highest at partial flow rates, especially below 10 l/s, where the risk of flow recirculation is apparent. At these flow rates, a low-frequency variation (0–10 Hz) is visible in the shaft torque.

Also the unfiltered estimates for the rotational speed and shaft torque were analysed. As assumed, the occurrence of flow recirculation is visible in the low-frequency region (0–10 Hz) of their spectrograms. In Fig. 4.45, a spectrogram for the unfiltered rotational speed estimate is presented. Besides the low-frequency component (0–10 Hz) that is apparent at flow rates below 10 l/s, the rotational speed and the blade pass frequency component are visible in the spectrogram. However, there is no visible frequency component around 80 Hz as in the spectrogram for the measured shaft torque. Thus, also the occurrence of flow recirculation seems possible to detect by monitoring the low-frequency variation of the rotational speed and the shaft torque at least in the case of the Sulzer laboratory pumping system. Naturally, these results may not hold true for all other pumping systems and for other pump types. However, it can be assumed that the corresponding phenomenon could be visible with similar pumping systems having a radial flow centrifugal pump.

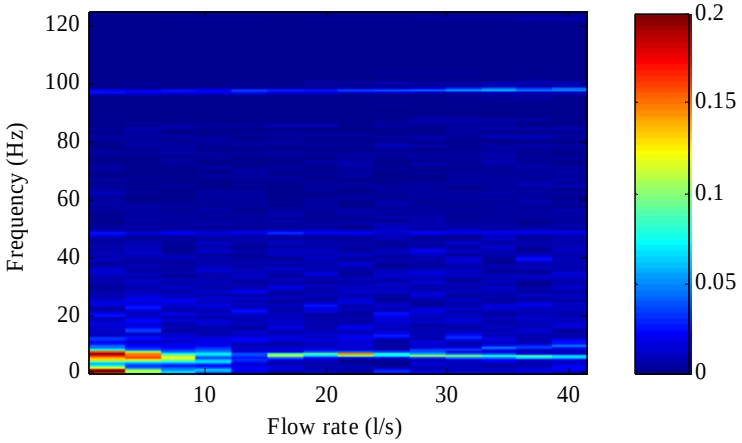

Fig. 4.45: Welch power spectral density of the estimated rotational speed as a function of flow rate. The most notable component is in the low-frequency region (0–10 Hz) when the flow rate is below 10 l/s.

4.7 Summary of Chapter 4

In this chapter, methods to detect cavitation occurrence in a centrifugal pump were discussed. A novel method to detect the occurrence of cavitation or flow recirculation especially in a radial flow centrifugal pump was proposed. It is based on the assumption that the occurrence of cavitation causes additional time-domain variation in the pump power consumption, which is visible in the estimated values of the rotational speed and shaft torque of an induction motor. Sensitivity of the proposed method was compared with known measurement-based methods for cavitation detection. According to these test results, the proposed method is applicable only to the detection of already head-decreasing cavitation. Therefore, the increase in the estimate time-domain variation may take place only as a result of a fully developed cavitation, which already affects the pump performance. Test results also showed the applicability of the acoustic emission measurements to the detection of the cavitation stage that starts to affect the pump head. A qualitative summary of the studied cavitation detection methods together with the proposed method based on their sensitivity is given in Table 4.1.

Table 4.1: Feasibility of different cavitation detection methods according to their sensitivity. The pump head measurement is used as a reference for applicable sensitivity. Sensitivity classes of poor, applicable, good and the best are used in this summary.

Test type	Measurement	Sensitivity	Comments
Constant rotational speed	Pump head	Applicable	Detects performance decreasing cavitation
	Suction pressure	Applicable (0–2 Hz), poor (other freq.)	0–2 Hz range reacts before the decrease of the pump head.
	Discharge pressure	Good (0–5 Hz)	Reacts more clearly to the decrease of the pump head than the suction pressure.
	Acoustic emission	Best	Shows most clearly the possible NPSH ratio for the occurrence of damaging cavitation.
	Vibration	Applicable	Detects performance decreasing cavitation.
	Estimated rotational speed and shaft torque	Poor	Detects only fully developed cavitation.
Increasing rotational speed	Estimated rotational speed and shaft torque	Applicable/Poor	Seems applicable only to the detection head decreasing cavitation.

To obtain generalisable results, the proposed method and the effects of cavitation occurrence were tested with three different pumps and two different frequency converters. The results showed that the occurrence of cavitation can be detected by monitoring the time-domain variation of the rotational speed and shaft torque estimates, if the cavitation phenomenon is developed enough to affect the pump performance on the basis of NPSH ratio. At least in the laboratory, this was detected both with a radial flow and mixed flow centrifugal pump. In together, these results support the assumption that a frequency converter could be applied to the detection of cavitation occurrence especially in a radial flow centrifugal pump, and possibly with other centrifugal pump types. Naturally, the time-domain variation of these estimates can also be caused by other events than just by cavitation, which has not been studied in this thesis. In addition, the proposed method is also applicable to the detection of flow recirculation, which may occur at partial flow rates of the pump.

However, there are still practical issues that should be further studied in order for the proposed method to be feasible in practice. For instance, the selection of suitable threshold values for the

$n_{RMS}/n_{RMS,N}$ and $T_{RMS}/T_{RMS,N}$ should be possible without separate test measurements. Correspondingly, the method was tested in the same process system consisting of two water tanks, so the shown results may be system-specific. In addition, tests were carried out only during the steady-state operation of the pumping system, and thus, the effect of system or rotational speed reference change on the feasibility of the method has not been tested. In practice, the changing process conditions may notably affect the feasibility of the proposed method, as there is then additional and possibly irregular change in the time-domain variation of both estimates. However, the effect of rotational speed change can be taken into account by using the method only when the rotational speed reference value remains constant. Correspondingly, the process changes could be detected by utilising the available information concerning the process. As said, these issues require a further study.

Despite their possible case-specificity, the shown results generally support the assumption that the occurrence of fully developed cavitation (which was visible in the NPSH ratios and additional measurements) can increase the relative variation in the rotational speed and shaft torque estimates, allowing the cavitation detection by a frequency converter. Further studies with different centrifugal pumps, pumping systems and also in different locations should be conducted to have more proof on the practical applicability of the proposed method. As the variation of the motor rotational speed and shaft torque during the pump operation is presumably affected by the pump characteristics, perhaps the variation of these values in different operating conditions could already be studied in the design phase of a centrifugal pump.

It was also shown that the detection of cavitation should be possible regardless of the applied control method in a frequency converter. However, the converter should estimate the motor operation so that small time-domain variation of rotational speed and shaft torque can be monitored. For this reason, frequency converters applying the vector control and DTC methods were used in the laboratory tests.

The method proposed in this chapter was tested only with radial and mixed centrifugal pumps having an inadequate NPSH or an increased risk of flow recirculation. However, it is possible that the proposed method could also be applied more extensively to the condition monitoring of centrifugal pumps, fans and other load machines.

5 SUMMARY AND CONCLUSIONS

This doctoral thesis studies the monitoring of a radial flow centrifugal pump operation utilising the information available from a frequency converter. Variable-speed-driven radial flow centrifugal pumps are widely used in industrial and municipal applications, and often the pump may be driven in adverse operating conditions, which can lead to an increase in the energy and maintenance costs for the pumping system. In the worst case, the failure of a centrifugal pump may lead to the stoppage of production resulting in substantial costs. As a modern frequency converter can estimate the operational state of an induction motor without external measurements, it can also be applied in the determination of the pump operating point location and in the detection of adverse events that may lead to a pump failure. Although the thesis focuses on radial flow end-suction centrifugal pumps, the studied methods can also be applied to other centrifugal pump types, such as mixed flow and axial flow pumps, if allowed by their characteristics.

In the introductory chapter of this thesis, typical issues of industrial pumping systems were outlined. Also the previous research concerning the use of frequency converters in the monitoring purposes was reviewed. In Chapter 2, theory concerning variable-speed-driven pumps was discussed. The use of generic energy-efficiency- and reliability-based criteria in the determination of the recommendable operating region of a VSD centrifugal pump was investigated. It was shown by a case study for the laboratory pumping system how the limits of the recommendable operating region could be determined.

Chapter 3 discussed the model-based estimation of the pump operating point location, which can be performed by a frequency converter. *QH*-, *QP*- and system-curve-based methods were studied in the chapter. Factors affecting the accuracy of the presented methods were reviewed. The applicability of the methods was evaluated by laboratory measurements with a radial flow centrifugal pump. The obtained results showed the applicability of model-based methods to the operating point estimation without additional measurements. Also the applicability of the studied methods with other centrifugal pump types was discussed in the chapter. In addition, estimation results from two pilot installations were introduced in the chapter.

In Chapter 4, a novel method to detect the occurrence of cavitation by a frequency converter was proposed especially in the case of radial flow centrifugal pumps. The method is based on the estimates for the rotational speed and the shaft torque, which are affected by cavitation: the low-frequency time-domain variation of the estimates is larger when cavitation occurs in the pump. Sensitivity of the proposed method was compared with known cavitation methods, and according to the results, the method is applicable only to the detection of fully developed, head-decreasing cavitation. The applicability of the method to the cavitation detection was tested by laboratory measurements for three different pumps. Also the effect of a frequency converter control scheme on the detection of cavitation was discussed. The proposed method was also successfully applied to the detection of flow recirculation in a radial flow centrifugal pump.

5.1 Key results of the work

In the following, the key results of the work are summarised:

- Energy-efficiency- and reliability-based determination of the recommendable operating region for a variable-speed-driven centrifugal pump was studied in Chapter 2. The inapplicability of the existing guidelines to VSD pumps was demonstrated. The

use of an E_s-based criterion in the determination of the recommendable operating region was proposed. Exemplary limits were determined for the laboratory pumping system using the proposed E_s-based approach and indices for the pump reliability.

- Three known model-based estimation methods (i.e., *QH*, *QP* and system curve methods) for the pump operating point location were studied in Chapter 3. Laboratory evaluation of the model-based estimation methods showed that the methods are feasible, if the pump characteristic curves and other required parameters are accurate. In practice, the greatest source of error for the estimation methods in the case of a radial flow centrifugal pump seemed to be the inaccuracy of the published characteristic curves, which should be verified for instance by a closed discharge valve test or by separate test measurements for the pump flow rate and head. Pump manufacturers could also provide more accurate characteristic curves for new pumps besides the generic curve prints. The use of the *QP*-curve-based estimation method for the analysis of pump operation was demonstrated with the results of pilot tests carried out in a paper mill.

- A novel method to detect the occurrence of cavitation or flow recirculation by a frequency converter was proposed in Chapter 4. Its sensitivity compared with known methods for cavitation detection was tested by laboratory measurements. According to the tests, the detection of cavitation by the proposed method is possible when it already affects the pump head: the occurrence of head-decreasing cavitation increased the time-domain variation of the rotational speed and the shaft torque estimates.

- The applicability of the method to cavitation detection was also evaluated by laboratory measurements with three different pumps and with two different frequency converters. In practice, the effect of cavitation occurrence on the estimates for the rotational speed and the shaft torque was affected by the characteristics of the pump and the frequency converter, and thus, the limit values for the occurrence of cavitation may be pumping system specific. Consequently, further studies in different locations are recommended concerning the feasibility of the method.

- According to the test measurements, the proposed method could also be applicable to the detection of flow recirculation in the pump: the time-domain variation in the rotational speed and shaft torque estimates was larger at the partial flow rates, at which the risk of flow recirculation was also apparent.

5.2 Suggestions for future work

The methods studied in this thesis allow the determination of the pump operating location and its feasibility by a frequency converter. In addition, the occurrence of cavitation can be detected by a frequency converter applying the method proposed in Chapter 4 at least with the laboratory pumping systems. The presented methods can be applied separately, but it would be interesting to study the use of these methods as part of an analysis system for the pump operation quality. This kind of a system could be applied to determine the general effectiveness of the pump operation for the user. The system could warn the user if the pump is driven with a poor efficiency or if the pump is prone to cavitation. For instance, linguistic equations and fuzzy logic could be applied to compose the analysis system.

In addition, more studies should be carried out concerning the feasibility of the discussed methods in practice, for instance in industrial locations. Related to this, further research is also

required to determine more accurately the connection of pump reliability and rotational speed. So far, only a few papers have discussed this topic.

This thesis has focused on variable-speed-driven radial flow centrifugal pumps and their monitoring by a frequency converter. The presented methods may also work with other pumps, fans and compressors controlled by a frequency converter. Therefore, future research concerning these devices is expected by the author.

REFERENCES

(ABB, 2000) ABB, *ACA 635 IGBT Supply Sections (ISU)*, ABB, Helsinki, Finland, 2000.

(ABB, 2002) ABB, *Technical Guide No. 1: Direct Torque Control*, ABB, Helsinki, Finland, 2002.

(ABB, 2006) ABB, *Product Notes: Flow Calculation in ABB Industrial Drives*, ABB, Helsinki, Finland, 2006.

(ABB, 2009) ABB, *ACS800 Standard Control Program 7.x*, ABB, Helsinki, Finland, 2009.

(Abrahamsen, 2000) F. Abrahamsen, *Energy Optimal Control of Induction Motor Drives*, Doctoral dissertation, Aalborg University, Institute of Energy Technology, 2000.

(Ahola, 2010) J. Ahola, T. Ahonen and J. Tamminen, "Diagnostics of Electrical Drive Systems," in *Proceedings of the 3rd International Seminar on Maintenance, Condition Monitoring and Diagnostics*, Oulu, Finland, 29–30 September 2010, pp. 109–119.

(Ahonen, 2007) T. Ahonen, J. Ahola, J. Kestilä, R. Tiainen and T. Lindh, "Life Cycle Cost Analysis of Inverter-Driven Pumps," in *Proceedings of the 20th International Congress on Condition Monitoring and Diagnostic Engineering Management (COMADEM 2007)*, Faro, Portugal, 13–15 June 2007, pp. 397–405.

(Ahonen, 2008a) T. Ahonen, R. Tiainen, J. Viholainen, J. Ahola and J. Kestilä, "Pump Operation Monitoring Applying Frequency Converter," in *Proceedings of the 19th International Symposium on Power Electronics, Electrical Drives, Automation and Motion (SPEEDAM 2008)*, Ischia, Italy, 11–13 June 2008, pp. 184–189.

(Ahonen, 2008b) T. Ahonen and J. Ahola, "Method and System for Detecting Cavitation of Pump and Frequency Converter," European patent application, application number 08171028.7-2315, application filed 9 December 2008.

(Ahonen, 2009a) T. Ahonen, J. Ahola, J. Tamminen and J. Kestilä, "Consideration of Recommended Operating Region for Inverter-Driven Pumps," in *Proceedings of the 6th International Conference on Condition Monitoring and Machinery Failure Prevention Technologies (CM and MFPT 2009)*, Dublin, Ireland, 23–25 June 2009, pp. 951–962.

(Ahonen, 2009b) T. Ahonen, J. Tamminen, J. Ahola and J. Kestilä, "Sensorless Pump Operation Estimation," in *Proceedings of the 13th European Conference on Power Electronics and Applications (EPE 2009)*, Barcelona, Spain, 8–10 September 2009, pp. 1–10.

(Ahonen, 2009c) T. Ahonen and J. Ahola, "Method and System for Detecting Cavitation of Pump and Frequency Converter," United States of America patent application, application number 12/628,669, application filed 1 December 2009.

(Ahonen, 2010a) T. Ahonen, J. Tamminen and J. Ahola, "Method in Connection with a Pump Driven with a Frequency Converter and a Frequency Converter," European patent application, application number 10153168.9-1267, application filed 10 February 2010.

(Ahonen, 2010b) T. Ahonen, J. Tamminen, J. Ahola, J. Viholainen, N. Aranto and J. Kestilä, "Estimation of Pump Operational State with Model-Based Methods," *Energy Conversion and Management*, Vol. 51, Iss. 6, June 2010, pp. 1319–1325.

(Ahonen, 2010c) T. Ahonen, J. Tamminen, J. Ahola and J. Kestilä, "Novel Method for Detecting Cavitation in Centrifugal Pump with Frequency Converter," in *Proceedings of the 7th International Conference on Condition Monitoring and Machinery Failure Prevention Technologies (CM and MFPT 2010)*, Stratford-upon-Avon, UK, 22–24 June 2010, pp. 1–13.

(Ahonen, 2011) T. Ahonen, J. Tamminen and J. Ahola, "Method in Connection with a Pump Driven with a Frequency Converter and a Frequency Converter," United States of America patent application, application number 13/024,705, application filed 10 February 2011.

(Alfayez, 2005) L. Alfayez and D. Mba, "Acoustic Emission and Pump Monitoring," in *Proceedings of the 18th International Congress and Exhibition on Condition Monitoring and Diagnostic Engineering Management (COMADEM 2005)*, Cranfield, UK, 31 August–2 September 2005, pp. 165–170.

(Almeida, 2003) A.T. de Almeida, P. Fonseca, H. Falkner and P. Bertoldi, "Market Transformation of Energy-Efficient Technologies in the EU," *Energy Policy*, Vol. 31, Iss. 6, May 2003, pp. 563–575.

(Al-Hashmi, 2005) S.A. Al-Hashmi, F. Gu and A.D. Ball, "Instantaneous Angular Speed Analysis for Cavitation Monitoring in Centrifugal Pump," in *Proceedings of the 18th International Congress and Exhibition on Condition Monitoring and Diagnostic Engineering Management (COMADEM 2005)*, Cranfield, UK, 31 August–2 September 2005, pp. 201–209.

(Al-Sulti, 2005) S. Al-Sulti, B. Samanta K.R. Al-Balushi, M. Al-Zedjali, S.A. Al-Araimi and R.A. Siddiqi, "Comparison of Signal Processing Techniques for Detecting Pump Cavitation Inception," in *Proceedings of the 18th International Congress and Exhibition on Condition Monitoring and Diagnostic Engineering Management (COMADEM 2005)*, Cranfield, UK, 31 August–2 September 2005, pp. 183–193.

(Angers, 2009) P. Angers, "Variable Frequency Drive Testing," in *Proceedings of Motor Efficiency Performance Standards Australia 2009*, Sydney, Australia, 4–5 February 2009.

(ANSI/HI, 1997) ANSI/HI 9.6.3, *Centrifugal and Vertical Pumps for Allowable Operating Region*, 1997.

(ANSI/HI, 1998) ANSI/HI 9.6.1, *Centrifugal and Vertical Pumps – NPSH Margin*, 1998.

(Aranto, 2009) N. Aranto, T. Ahonen and J. Viholainen, "Energy Audits: University Approach with ABB," in *Proceedings of the 6th International Conference on Energy Efficiency in Motor Driven Systems (EEMODS '09)*, Nantes, France, 14–17 September 2009.

(Armstrong, 2010) Armstrong, *Armstrong Extends Sensorless Control Variable Speed Pumps Range up to 55 kW*, available at http://impeller.net/magazine/news_en/doc4927x.asp, accessed on June 2010.

(Baker, 2008) Baker Instrument Company, *EXP3000 User's Manual*, Baker Instrument Company, Fort Collins, Colorado, USA, 2008.

(Barringer, 2003) P. Barringer, "A Life Cycle Cost Summary," in *Proceedings of the International Conference of Maintenance Societies (ICOMS®-2003)*, Perth, Australia, 20–23 May 2003.

(Bartoni, 2008) E. da Costa Bartoni, R.A. de Almeida and A.N.C. Viana, "Optimization of Parallel Variable-Speed-Driven Centrifugal Pumps Operation," *Energy Efficiency*, Vol. 1, No. 3, 2006, pp. 167–173.

(Binder, 2008) A. Binder, "Potentials for Energy Saving with Modern Drive Technology," in *Proceedings of the 19th International Symposium on Power Electronics, Electrical Drives, Automation and Motion (SPEEDAM 2008)*, Ischia, Italy, 11–13 June 2008, pp. 90–95.

(Bloch, 1994) H.P. Bloch and F.K. Geitner, *An Introduction to Machinery Reliability Assessment*, second edition, Gulf Publishing Company, Houston, Texas, USA, 1994.

(Bloch, 2010) H.P. Bloch and A.R. Budris, *Pump User's Handbook: Life Extension*, Fairmont Press, Lilburn, Georgia, USA, 2010.

(Bose, 2002) B.K. Bose, *Modern Power Electronics and AC Drives*, Prentice Hall, Upper Saddle River, New Jersey, USA, 2002.

(Budris, 1997) A.R. Budris and P.A. Mayleben, "The Effects of Entrained Air, NPSH Margin and Suction Piping on Centrifugal Pumps" in *Proceedings of the 15th International Pump Users Symposium*, Houston, Texas, USA, 1997.

(Budris, 2001) A. Budris, E.P. Sabini, R.B. Erickson, "Pump Reliability – Correct Hydraulic Selection Minimizes Unscheduled Maintenance," *PumpLines*, Fall, 2001, pp. 1–3.

(Burt, 2009) C.M. Burt, X. Piao, F. Gaudi, B. Busch and N.F.N. Taufik, "Electric Motor Efficiency under Varying Frequencies and Loads," *Journal of Irrigation and Drainage Engineering*, Iss. 134, 2009, pp. 129–136.

(Carlson, 1999) R. Carlson, "The Correct Method of Calculating Energy Savings to Justify Adjustable Frequency Drives on Pumps," in *Proceedings of the 46th Annual Conference on Petroleum and Chemical Industry*, San Diego, California, USA, 13–15 September 1999, pp. 275–283.

(Cartwright, 2009) S. Cartwright and B. Eaton, "Investigating Energy Savings in Pumps and Pumping System by the Thermodynamic Method," in *Proceedings of Pumps: Maintenance, Design and Reliability Conference 2009*, Brisbane, Australia, 12–14 May 2009.

(Černetič, 2008) J. Černetič, J. Prezelj and M Čudina, "Use of Noise and Vibration Signal for Detection and Monitoring of Cavitation in Kinetic Pumps," in *Proceedings of Acoustics '08 Conference*, Paris, France, 15 June–4 July 2008, pp. 2199–2204.

(Čudina, 2008) M. Čudina and J. Prezelj, "Use of Audible Sound for Safe Operation of Kinetic Pumps," *International Journal of Mechanical Sciences*, Vol. 50, Iss. 9, 2008, pp. 1335–1343.

(D'Alterio, 2003) G.A. D'Alterio, "In Search of Middle Ground," *Chemical Processing*, May, 2003.

(Danfoss, 2009) Danfoss, *VLT*® AQUA Drive FC 200 Operating Instructions, available at http://mcliterature.danfoss.com/WebPublish/downloadPub.do?no=0, accessed on June 2010.

(Discenzo, 2002) F.M. Discenzo, D. Rusnak, L. Hanson, D. Chung and J. Zevchek, "Next Generation Pump Systems Enable New Opportunities for Asset Management and Economic Optimization," in *Proceedings of 2002 TAMU Pump Show Conference*, Texas, Houston, USA, 2002.

(Discenzo, 2003) F.M. Discenzo, D. Chung and J.K. Zevchek, System and Method for Controlling Pump Cavitation and Blockage, US Patent, US 6,663,349 B1.

(DoE, 1998) U.S. Department of Energy, *United States Industrial Motor Systems Market Opportunities Assessment*, U.S. Department of Energy, Washington D.C., USA, 1998.

(Durán, 2006) M.J. Durán, J.L Durán, F. Pérez and J. Férnandez, "Induction-Motor Sensorless Vector Control with Online Parameter Estimation and Overcurrent Protection," *IEEE Transactions on Industrial Electronics*, Vol. 53, No. 1, 2006, pp. 154–161.

(EC, 2009) European Commission, *Commission Regulation (EC) No 640/2009*, 2009.

(Erickson, 2000) R.B. Erickson, E.P. Sabini and A.E. Stavale, "Hydraulic Selection to Minimize the Unscheduled Maintenance Portion of Life Cycle Cost," in *Proceedings of Pump Users International Forum 2000*, Karlsruhe, Germany, 10–12 October 2000.

(Eryurek, 2002) E. Eryurek, Cavitation Detection in a Process Plant, United States of America patent, US 2002/0123856 A1.

(Europump, 1999) Europump and Hydraulic Institute, *Attainable Efficiencies of Volute-Casing Pumps: A Reference Guide*, Elsevier Advanced Technology, Kidlington, Oxford, UK, 1999.

(Europump, 2004) Europump and Hydraulic Institute, *Variable Speed Pumping – A Guide to Successful Applications*, Elsevier, Kidlington, Oxford, UK, 2004.

(Feng, 2004) H.D. Feng, L. Xu, R.P. Xu, L.J. Wu, X.H. Shi, J.D. Yan and T.Y. Wang, "Uncertainty Analysis Using the Thermodynamic Method of Pump Efficiency Testing," in *Proceedings of the Institution of Mechanical Engineers, Part C: Journal of Mechanical Engineering Science*, Iss. 218, 2004, pp. 543–555.

(Ghozzi, 2004) S. Ghozzi, K. Jelassi and X. Roboam, "Energy Optimization of Induction Motor Drives," in *Proceedings of 2004 IEEE International Conference on Industrial Technology (ICIT)*, Hammamet, Tunisia, 8–10 December 2004, pp. 602–610.

(Gülich, 2008) J.F. Gülich, *Centrifugal Pumps*, Springer-Verlag, Berlin, Germany, 2008.

(Hammo, 2005) S. Hammo and J. Viholainen, "Testing the Accuracy of Pump Flow Calculation without Metering," *World Pumps*, Iss. 471, 2005, pp. 36–39.

(Hammo, 2006) S. Hammo and J. Viholainen, "Providing Flow Measurements in Parallel Pumping Systems from Variable Speed Drives," *World Pumps*, Iss. 483, 2006, pp. 30–33.

(Henshaw, 2001) T. Henshaw, "How Much NPSH Does Your Pump Really Require?" *Pumps & Systems*, September, 2001.

(Hernandez, 2010) A. Hernandez-Solis, and F. Carlsson, "Diagnosis of Submersible Centrifugal Pumps: A Motor Current and Power Signature Approaches," *European Power Electronics and Drives Association Journal*, Vol. 20, No. 1, 2010, pp. 58–64.

(HI, 1999) Hydraulic Institute, Europump and U.S. Department of Energy, *Pump Life Cycle Costs: A Guide to LCC Analysis for Pumping Systems*, Elsevier, Kidlington, Oxford, UK, 1999.

(Hovstadius, 2001) G. Hovstadius, "Life-Cycle Strategy for Pumps Improves Cost Structure," *World Pumps*, Iss. 413, 2001, pp. 30–32.

(Hovstadius, 2005) G. Hovstadius, V. Tutterow and S. Bolles, "Getting it Right, Applying a Systems Approach to Variable Speed Pumping," in *Proceedings of the 4th International Conference on Energy Efficiency in Motor Driven Systems (EEMODS '05)*, Heidelberg, Germany, 5–8 September 2005.

(Hovstadius, 2007) G. Hovstadius, "Using KPIs to Monitor and Improve Pump Performance," in *Proceedings of the 5th International Conference on Energy Efficiency in Motor Driven Systems (EEMODS '07)*, Beijing, China, 10–15 June 2007.

(Hydrovar, 2003) Hydrovar Team, *HYDROVAR-sensorless – Technical Information*, available at http://www.lowara.com/lowdata/doc/EN/sensorless-sl-en.pdf, accessed on June 2010.

(IEC, 2007) IEC 60034-2-1: *Rotating Electrical Machines – Part 2-1: Standard Methods for Determining Losses and Efficiency from Tests (Excluding Machines for Traction Vehicles)*, 2007.

(IEC, 2008) IEC 60034-30: *Rotating Electrical Machines – Part 30: Efficiency Classes of Single-Speed, Three-Phase, Cage-Induction Motors*, 2008.

(IEC, 2009a) IEC 60034-31: *Rotating Electrical Machines – Part 31: Guide for the Selection and Application of Energy-Efficient Motors Including Variable-Speed Applications*, 2009.

(IEC, 2009b) IEC 60034-2-3: *Rotating Electrical Machines – Part 2-3: Specific Test Methods for Determining Losses and Efficiency of Converter-Fed AC Motors*, 2009.

(ISO, 1987) ISO 5198:1987, *Centrifugal, Mixed Flow and Axial Pumps – Code for Hydraulic Performance Tests – Precision Class*, 1987.

(ISO, 1999) ISO 9906:1999, *Rotodynamic Pumps – Hydraulic Performance Acceptance tests – Grades 1 and 2*, 1999.

(ISO, 2005) ISO 17766:2005, *Centrifugal Pumps Handling Viscous Liquids – Performance Corrections*, 2005.

(ITT, 2006) ITT, *PS200 v5 Configuration & Operation Guide*, available at http://www.ittmc.com/itemfiles/PS200_v5.01_Configuration_and_Operation_Guide.pdf, accessed on June 2010.

(Jensen, 2000) J. Jensen and K. Dayton, "Detecting Cavitation in Centrifugal Pumps – Experimental Results of the Pump Laboratory," *Orbit*, Second Quarter, 2000, pp. 26–30.

(Karassik, 1998) I.J. Karassik and T. McGuire, *Centrifugal Pumps*, second edition, Chapman & Hall, New York, USA, 1998.

(Kallesoe, 2005) C.S. Kallesoe, *Fault Detection and Isolation in Centrifugal Pumps*, Doctoral dissertation, Aalborg University, Institute of Electrical Systems, 2005.

(Kercan, 1979) V. Kercan and F. Schweiger, "Cavitation Phenomena Detection by Different Methods," in *Proceedings of the 6th Conference on Fluid Machinery*, Budapest, Hungary, 17–22 September 1979, pp. 535–544.

(Kernan, 2007) D.J. Kernan, E.P. Sabini, N.W. Ganzon and A.E. Stavale, Method for Determining Pump Flow without the Use of Traditional Sensors, United States of America patent, US 2007/0212210 A1.

(Klugman, 2007) S. Klugman, M. Karlsson and B. Moshfegh, "A Scandinavian Chemical Wood-Pulp Mill. Part 1. Energy Audits Aiming at Efficiency Measures," *Applied Energy*, Vol. 84, Iss. 3, 2007, pp. 326–339.

(Kneip, 2005) B. Kneip, "Comparison of Variable Speed Drives and Control Valves for Flow Control in Pumping Systems," in *Proceedings of the 4th International Conference on Energy Efficiency in Motor Driven Systems (EEMODS '05)*, Heidelberg, Germany, 5–8 September 2005.

(Lahdelma, 2008) S. Lahdelma and E.K. Juuso, "Vibration Analysis of Cavitation in Kaplan Water Turbines," in *Proceedings of the 17th IFAC World Congress*, Seoul, South Korea, 6–11 July 2008, pp. 13420–13425.

(Ma, 2009) Z. Ma and S. Wang, "Energy Efficient Control of Variable Speed Pumps in Complex Building Central Air-Conditioning Systems," *Energy and Buildings*, Vol. 41, Iss. 2, 2009, pp. 197–205.

(McKinney,2010) R. McKinney, *Conserve Your Energy – The Benefits of Pump System Optimization*, available at http://reliabilityweb.com/index.php/articles/conserve_your_energy_pump_benefits, accessed on December 2010.

(Nash, 1997) J.N. Nash, "Direct Torque Control, Induction Motor Vector Control Without an Encoder," *IEEE Transactions on Industry Applications*, Vol. 33, No. 2, 1997, pp. 333–341.

(Neill, 1997) G.D. Neill, R.B. Reuben, P.M. Sandford, E.R. Brown and J.A. Steel, "Detection of Incipient Cavitation in Pumps Using Acoustic Emission," in *Proceedings of the Institution of Mechanical Engineers, Part E: Journal of Process Mechanical Engineering*, Iss. 211, 1997, pp. 267–277.

(Nesbitt, 2006) B. Nesbitt, *Handbook of Pumps and Pumping*, Elsevier, Jordan Hill, Oxford, UK, 2006.

(Nelik, 2005) L. Nelik, "What Happens When a Pump No Longer Operates at Optimum Conditions? – Part 2: (Quantifiable) Reliability Aspects," *Pumps & Systems*, February, 2005, pp. 54–63.

(Orkisz, 2008a) M. Orkisz, M. Wnek and P. Joerg, "Using Variable Speed Drive Data for Condition Monitoring," in *Proceedings of Euromaintenance 2008 Conference*, Brussels, Belgium, 8–10 April 2008.

(Orkisz, 2008b) M. Orkisz, M. Wnek, K. Krycka and P. Joerg, "Variable Frequency Drive as a Source of Condition Monitoring Data," in *Proceedings of the 19th*

International Symposium on Power Electronics, Electrical Drives, Automation and Motion (SPEEDAM 2008), Ischia, Italy, 11–13 June 2008, pp. 179–184.

(Orkisz, 2009) M. Orkisz, M. Wnek, P. Joerg, K. Ruetten and E. Jellum, "Selected Data Analysis Techniques for Equipment Monitoring Using Drive's Control Signals," in *Proceedings of the 19th International Symposium on Diagnostics for Electric Machines, Power Electronics and Drives (SDEMPED 2009)*, Cargese, France, 31 August–3 September 2009, pp. 1–5.

(Parihara, 2006) P.P. Parihara and A.G. Parlos, "Sensorless Detection of Cavitation in Centrifugal Pumps," in *Proceedings of 2006 ASME International Mechanical Engineering Congress and Exposition (IMECE 2006)*, Chicago, Illinois, USA, 5–10 November 2006, pp. 1–6.

(Parrondo, 1998) J.L. Parrondo, S. Velarde and C. Santolaria, "Development of a Predictive Maintenance System for a Centrifugal Pump," *Journal of Quality in Maintenance Engineering*, Vol. 4, No. 3, 1998, pp. 198–211.

(Perez, 1996) R.X. Perez, R.A. Akins, C.E. Lee and H.F. Taylor, "Fiber-Optic Pressure Sensors Detect Cavitation and Flow Instabilities in Centrifugal Pumps," *World Pumps*, Iss. 359, 1996, pp. 28–33.

(Perovic, 2001) S. Perovic, P.J. Unsworth and E.H. Higham, "Fuzzy Logic System to Detect Pump Faults from Motor Current Spectra," in *Proceedings of 2001 IEEE Industry Applications Conference*, Chicago, Illinois, USA, 30 September–4 October 2001, pp. 274–280.

(PSM, 2008) Pump Systems Matter™ and Hydraulic Institute, *Optimizing Pumping Systems: A Guide for Improved Energy Efficiency, Reliability & Profitability*, Elsevier, New York, USA, 2008.

(Schiavello, 2009) B. Schiavello and F.C. Visser, "Pump Cavitation – Various $NPSH_R$ Criteria, $NPSH_A$ Margins, and Impeller Life Expectancy," in *Proceedings of the 25th International Pump Users Symposium*, Houston, USA, 23–26 February 2009, pp. 1–6.

(Stavale, 2001) A.E. Stavale, J.A. Lorenc and E.P. Sabini, "Development of a Smart Pumping System," in *Proceedings of 2001 TAMU Pump Show Conference*, Houston, Texas, USA, 2001.

(Stavale, 2008) A.E. Stavale, "Reducing Reliability Incidents and Improving Meantime between Repair," in *Proceedings of the 24th International Pump Users Symposium*, Houston, USA, 2008, 21–24 April 2008, pp. 1–10.

(Sulzer, 1998) Sulzer Pumps, Sulzer *Centrifugal Pump Handbook*, second edition, Elsevier, Kidlington, Oxford, UK, 1998.

(Sulzer, 2000) Sulzer Pumps Finland Oy, *AHLSTAR™ Process Pumps, Intended Use*, Sulzer Pumps Finland Oy, Mänttä, Finland, 2000.

(Sulzer, 2006a) Sulzer Pumps Finland Oy, Cross-section figures of centrifugal pumps in the AutoCAD file format, electronic document, 2006.

(Sulzer, 2006b) Sulzer Pumps Finland Oy, *AHLSTAR™ A_P22-80 (125-80-250), Characteristic Curve K13837*, Sulzer Pumps Finland Oy, Mänttä, Finland, 2006.

(Tiainen, 2006) R. Tiainen, V. Särkimäki, J. Ahola and T. Lindh, "Utilization Possibilities of Frequency Converter in Electric Motor Diagnostics," in *Proceedings of the 18th International Symposium on Power Electronics, Electrical Drives, Automation and Motion (SPEEDAM 2006)*, Taormina, Italy, 23–26 May 2006, pp. 24–29.

(Tiainen, 2007) R. Tiainen, V. Särkimäki, J. Ahola, T. Lindh and M. Niemelä, "Current Measurement-Based Detection of Load Torque Changes in a Variable Speed VSI Induction Motor Drive to Support Motor Diagnostics," in *Proceedings of the 12th European Conference on Power Electronics and Applications (EPE 2007)*, Aalborg, Denmark, 2–5 September 2007, pp. 1–10.

(Tiitinen, 1996) P. Tiitinen and M. Surandra, "The Next Generation Motor Control Method, DTC Direct Torque Cotnrol," in *Proceedings of 1996 International Conference on Power Electronics, Drives and Energy Systems for Industrial Growth*, Delhi, India, 8–11 January 1996, pp. 37–43.

(USC, 2007) United States Congress, *Energy Independence and Security Act of 2007*, 2007.

(Vas, 1998) P. Vas, *Sensorless Vector and Direct Torque Control*, Oxford University Press, Oxford, UK, 1998.

(Viholainen, 2009) J. Viholainen, J. Kortelainen, T. Ahonen, N. Aranto and E. Vakkilainen, "Energy Efficiency in Variable Speed Drive (VSD) Controlled Parallel Pumping," in *Proceedings of the 6th International Conference on Energy Efficiency in Motor Driven Systems (EEMODS '09)*, Nantes, France, 14–17 September 2009.

(Wiedenbrug, 2002) E.J. Wiedenbrug, A. Ramme, E. Matheson, A. von Jouanne and A.K. Wallace, "Modern Online Testing of Induction Motors for Predictive Maintenance and Monitoring," *IEEE Transactions on Industry Applications*, Vol. 38, No. 5, 2002, pp. 1466–1472.

APPENDIX A

Laboratory pumping systems

Characteristic curves of the applied pumping systems in the laboratory tests are presented in this Appendix.

Sulzer pumping system consists of a Sulzer APP22-80 centrifugal pump, a four-pole 11 kW ABB induction motor and an ABB ACS 800 frequency converter. Measurements were also carried out by driving the pump and the motor with an ABB ACS 550 frequency converter. The Sulzer pump is equipped with a four-bladed impeller having a diameter of 255 mm. The published characteristic curves of the pump are illustrated in Fig. A.1.

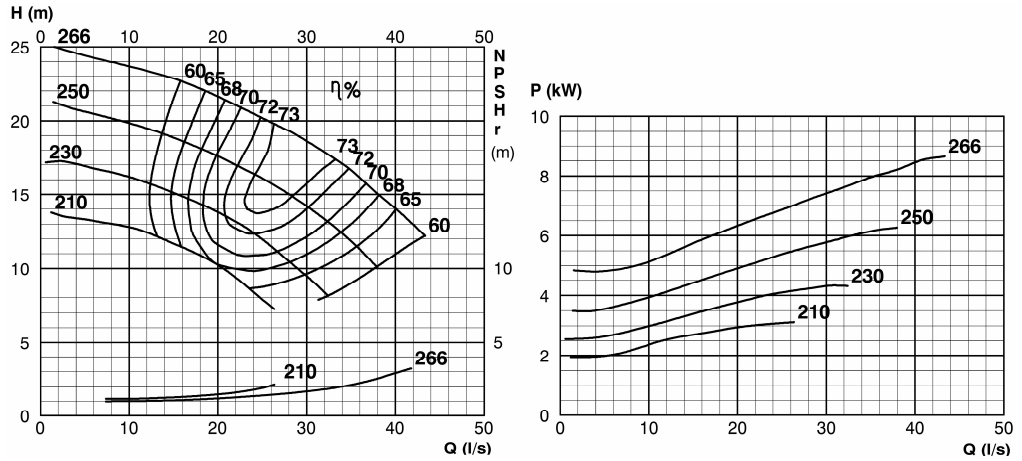

Fig. A.1: Published characteristic curves of a Sulzer APP22-80 centrifugal pump for the rotational speed of 1450 rpm (Sulzer, 2006b). The curves show the pump head, efficiency, $NPSH_R$ and shaft power requirements as a function of flow rate.

Since there are no published curves for the 255 mm impeller diameter in Fig. A.1, they were determined from the curves of the 250 mm impeller by applying Equations (2.7)–(2.9). However, the $NPSH_R$ curve of a 266 mm diameter impeller was directly applied as the $NPSH_R$ curve for the sake of simplicity. The resulting characteristic curves of the Sulzer pump are depicted in Fig. A.2.

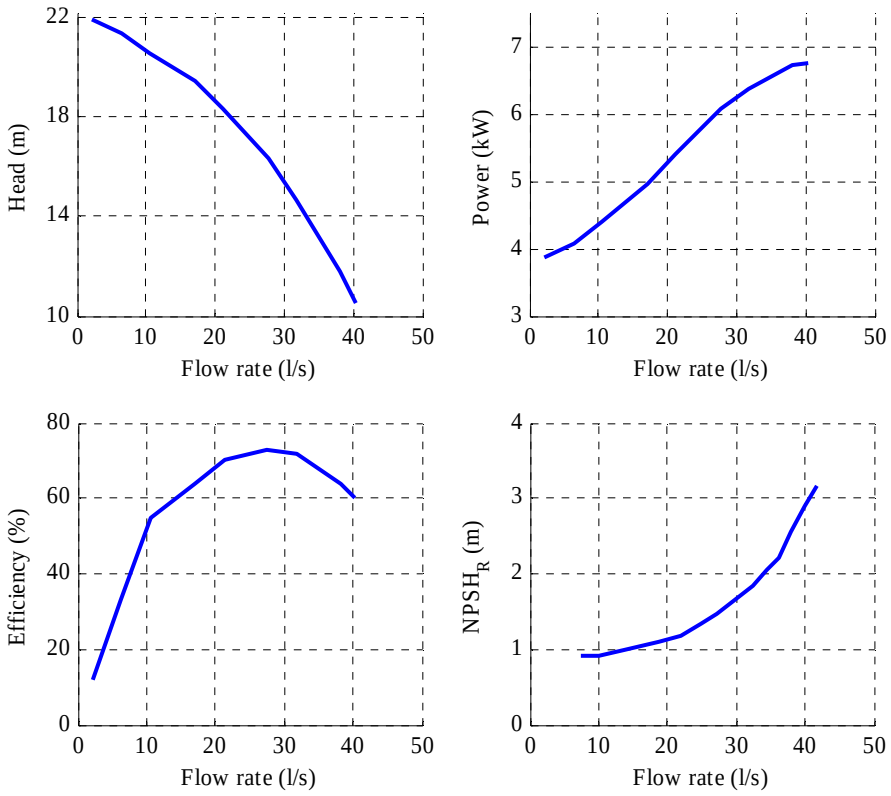

Fig. A.2: Characteristic curves for the 255 mm impeller diameter.

On the basis of the BEP values of the Sulzer pump, the specific speed n_q of the Sulzer pump is

$$n_q = \frac{1450 \cdot \sqrt{0.028}}{16^{0.75}} \approx 30 . \tag{A.1}$$

Suction specific speed n_{ss} of the Sulzer pump:

$$n_{ss} = \frac{1450\sqrt{0.028}}{1.5^{0.75}} \approx 179 . \tag{A.2}$$

Serlachius pumping system comprises a Serlachius DC-80/260 centrifugal pump, a four-pole 15 kW Strömberg induction motor and an ABB ACS 800 frequency converter. The pump is equipped with a five-bladed impeller having a diameter of 259 mm. The published characteristic curves of the pump are illustrated in Fig. A.3 for the rotational speed of 1425 rpm.

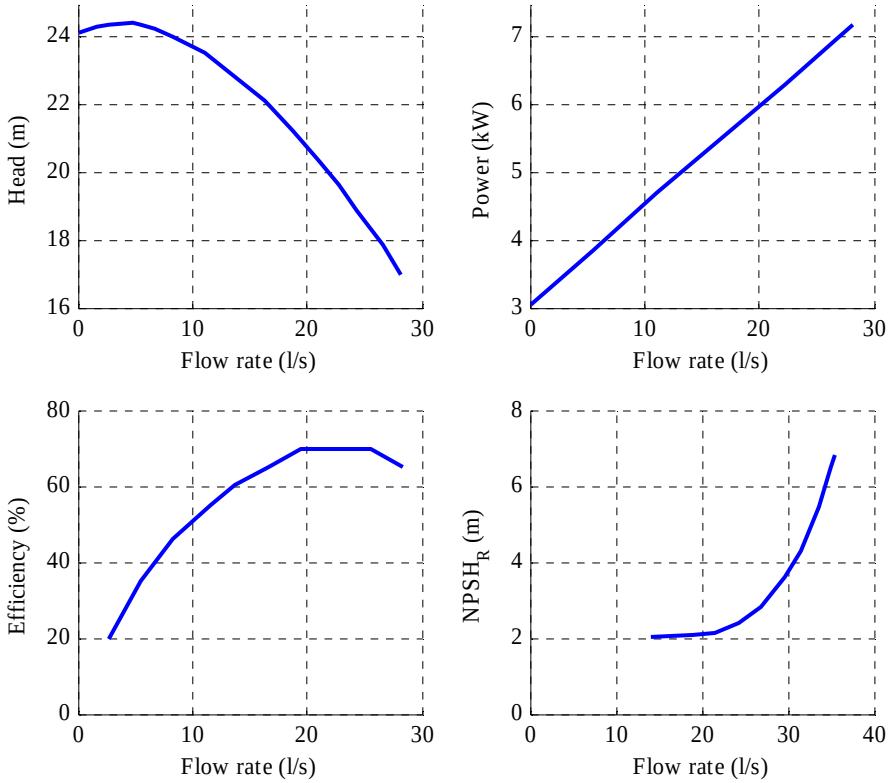

Fig. A.3: Published characteristic curves of a Serlachius DC-80/260 centrifugal pump. The curves show the pump head, shaft power requirement, efficiency and $NPSH_R$ as a function of flow rate, when the pump is driven at 1425 rpm rotational speed. The original efficiency curve has been given with the resolution of five percentage units.

Specific speed of the Serlachius pump:

$$n_q = \frac{1425 \cdot \sqrt{0.022}}{20^{0.75}} \approx 22 . \qquad \text{(A.3)}$$

Suction specific speed of the Serlachius pump:

$$n_{ss} = \frac{1425 \cdot \sqrt{0.022}}{3^{0.75}} \approx 93 . \qquad \text{(A.4)}$$

Grundfos pumping system comprises a Grundfos LP 100-125/130 centrifugal pump, a two-pole 5.5 kW Grundfos induction motor and an ABB ACS 800 frequency converter. The pump is equipped with an eight-bladed mixed-flow impeller having a diameter of 130 mm. The published characteristic curves of the pump have been measured, when the motor has been

supplied with a fixed voltage (380 V as the line-to-line voltage) and frequency (50 Hz). The nominal speed of the Grundfos motor is 2890–2910 rpm. The published characteristic curves are shown in Fig. A.4.

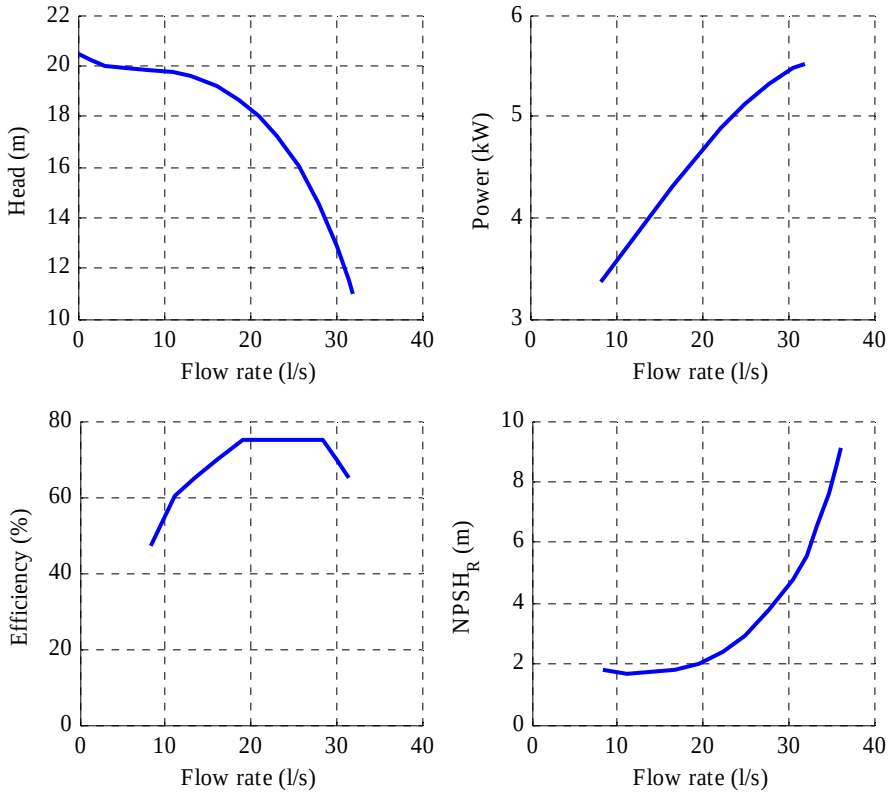

Fig. A.4: Published characteristic curves of a Grundfos LP 100-125/130 centrifugal pump. The curves show the pump head, shaft power requirement, efficiency and $NPSH_R$ as a function of flow rate, when the motor of the pumping system is driven with a fixed-voltage (380 V) and fixed-frequency (50 Hz) supply. The original efficiency curve has been given with the resolution of five percentage units.

Specific speed of the Grundfos pump:

$$n_q = \frac{2900 \cdot \sqrt{0.024}}{17^{0.75}} \approx 54 . \qquad \text{(A.5)}$$

Suction specific speed of the Grundfos pump:

$$n_{ss} = \frac{2900 \cdot \sqrt{0.024}}{2.7^{0.75}} \approx 213 . \qquad \text{(A.6)}$$

APPENDIX B

Measurement equipment

The measurement equipment used in the laboratory tests to determine the pump operating point location and shaft power consumption are presented in this Appendix. Technical details of the vibration measurements are also given here.

WIKA S-10 absolute pressure sensors were applied to determine the pump head. In the suction side of the pump, a sensor with 0–2.5 bar measurement range was applied to the measured p_s. The discharge pressure of the pump p_d was determined by a WIKA S-10 pressure sensor having 0–6 bar measurement range. The accuracy of the pressure sensors is ≤ 0.5 % of the measurement span. The accuracy of the pressure sensors was verified before the laboratory measurements by calibration.

The pump flow rate was measured by a **venturi tube** and a **Valmet DIFF-EL differential pressure sensor**. To ensure correct results, the differential pressure sensor was calibrated before the test measurements. In addition, the accuracy of the venturi system has been verified before the laboratory tests with an ISOIL MS2500 electromagnetic flow meter to be within 2 l/s over the entire pump operating region.

The temperature of the pumped water was determined with a **four-wire Pt-100 temperature sensor** installed into the suction water tank. During the measurements, temperature of the pumped water was around 20 °C.

Dataflex 22/100 torque and speed measurement shaft was used to determine the rotational speed, shaft torque and power consumption of the Sulzer pump. The accuracy of the shaft torque measurement is 1 % of the nominal torque value (100 Nm) for the sensor. The measurement shaft was connected to the Dataflex DF 1 terminal housing unit, which provides voltage signals that indicate the instantaneous rotational speed and shaft torque. In addition, DF 1 unit allows the low-pass filtering of the measured shaft torque signal. A limit frequency of 1 kHz was applied to the low-pass filtering of the shaft torque signal. A 5 kHz sampling frequency was used to store the shaft torque measurements.

Acoustic emission of the Sulzer pump was measured with a **Holroyd MHC-SetPoint unit**, which provides a dB value describing the average magnitude of the continuous AE signal around the frequency range of 100 kHz.

Radial vibration of the Sulzer pump was measured with a **SKF CMSS786A acceleration sensor** from the pump bearing. The sensor was supplied with a constant current amplifier, which has a fourth-order low-pass filter with 3 dB attenuation at 7 kHz. Vibration measurements were carried out with a 20 kHz sampling frequency.

The shaft torque and radial acceleration measurements were stored to a measurement computer by a **National Instruments PCI-6032E data acquisition card**, which allows measurements with a 100 kHz sampling frequency. The sampling resolution of the data acquisition card is 16 bits.

The pressure sensors and the voltage signal output for the pump rotational speed were connected to a **Fluke Hydra 2620A data acquisition unit** that allowed the monitoring of these

measurements. In Fig. B.1, the measurement setup applied with the Sulzer pumping system is shown.

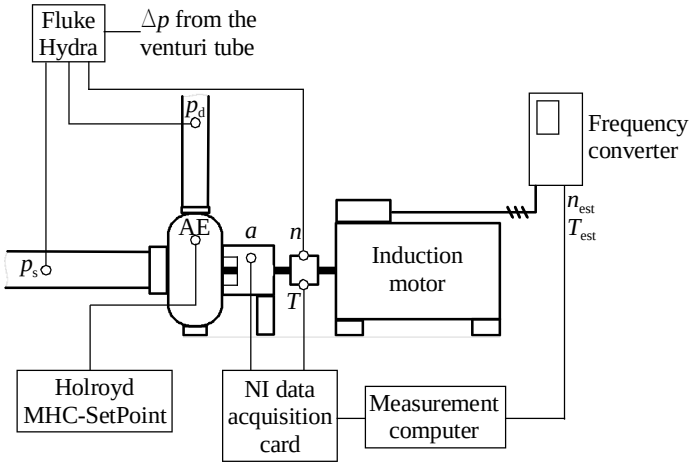

Fig. B.1: Measurement setup applied to evaluate the applicability of a frequency converter to the determination of the pump operating point location and detection of cavitation occurrence.

In the case of the Serlachius pumping system, the mean values of the rotational speed and the shaft torque were determined with an **HBM torque measurement transducer** on the motor shaft. The transducer was connected to an HBM display unit, which showed the instantaneous values for the rotational speed and that shaft torque.

ACTA UNIVERSITATIS LAPPEENRANTAENSIS

384. RITALA, PAAVO. Coopetitive advantage – How firms create and appropriate value by collaborating with their competitors. 2010. Diss.

385. RAUVANTO, IRINA. The intrinsic mechanisms of softwood fiber damage in brown stock fiber line unit operations. 2010. Diss.

386. NAUMANEN, VILLE. Multilevel converter modulation: implementation and analysis. 2010. Diss.

387. IKÄVALKO, MARKKU. Contextuality in SME ownership – Studies on owner-managers´ ownership behavior. 2010. Diss.

388. SALOJÄRVI, HANNA. Customer knowledge processing in key account management. 2010. Diss.

389. ITKONEN, TONI. Parallel-operating three-phase voltage source inverters – Circulating current modeling, analysis and mitigation. 2010. Diss.

390. EEROLA, TUOMAS. Computational visual quality of digitally printed images. 2010. Diss.

391. TIAINEN, RISTO. Utilization of a time domain simulator in the technical and economic analysis of a wind turbine electric drive train. 2010. Diss.

392. GRÖNMAN AKI. Numerical modelling of small supersonic axial flow turbines. 2010. Diss.

393. KÄHKÖNEN, ANNI-KAISA. The role of power relations in strategic supply management – A value net approach. 2010. Diss.

394. VIROLAINEN, ILKKA. Johdon coaching: Rajanvetoja, taustateorioita ja prosesseja. 2010. Diss.

395. HONG, JIANZHONG. Cultural aspects of university-industry knowledge interaction. 2010. Diss.

396. AARNIOVUORI, LASSI. Induction motor drive energy efficiency – Simulation and analysis. 2010. Diss.

397. SALMINEN, KRISTIAN. The effects of some furnish and paper structure related factors on wet web tensile and relaxation characteristics. 2010. Diss.

398. WANDERA, CATHERINE. Performance of high power fiber laser cutting of thick-section steel and medium-section aluminium. 2010. Diss.

399. ALATALO, HANNU. Supersaturation-controlled crystallization. 2010. Diss.

400. RUNGI, MAIT. Management of interdependency in project portfolio management. 2010. Diss.

401. PITKÄNEN, HEIKKI. First principles modeling of metallic alloys and alloy surfaces. 2010. Diss.

402. VAHTERISTO, KARI. Kinetic modeling of mechanisms of industrially important organic reactions in gas and liquid phase. 2010. Diss.

403. LAAKKONEN, TOMMI. Distributed control architecture of power electronics building-block-based frequency converters. 2010. Diss.

404. PELTONIEMI, PASI. Phase voltage control and filtering in a converter-fed single-phase customer-end system of the LVDC distribution network. 2010. Diss.

405. TANSKANEN, ANNA. Analysis of electricity distribution network operation business models and capitalization of control room functions with DMS. 2010. Diss.

406. PIIRAINEN, KALLE A. IDEAS for strategic technology management: Design of an electronically mediated scenario process. 2010. Diss.

407. JOKINEN, MARKKU. Centralized motion control of a linear tooth belt drive: Analysis of the performance and limitations. 2010. Diss.

408. KÄMÄRI, VESA. Kumppanuusohjelman strateginen johtaminen – Monitapaustutkimus puolustushallinnossa. 2010. Diss.

409. KARJALAINEN, AHTI. Online ultrasound measurements of membrane compaction. 2010. Diss.

410. LOHTANDER, MIKA. On the development of object functions and restrictions for shapes made with a turret punch press. 2010. Diss.

411. SIHVO, VILLE. Insulated system in an integrated motor compressor. 2010. Diss.

412. SADOVNIKOV, ALBERT. Computational evaluation of print unevenness according to human vision. 2010. Diss.

413. SJÖGREN, HELENA. Osingonjakopäätökset pienissä osakeyhtiöissä. Empiirinen tutkimus osakeyhtiölain varojenjakosäännösten toteutumisesta. 2010. Diss.

414. KAUPPI, TOMI. Eye fundus image analysis for automatic detection of diabetic retinopathy. 2010. Diss.

415. ZAKHVALINSKII, VASILII. Magnetic and transport properties of $LaMnO_{3+\delta}$, $La_{1-x}Ca_xMnO_3$, $La_{1-x}Ca_xMn_{1-y}Fe_yO_3$ and $La_{1-x}Sr_xMn_{1-y}Fe_yO_3$. 2010. Diss.

416. HATAKKA, HENRY. Effect of hydrodynamics on modelling, monitoring and control of crystallization. 2010. Diss.

417. SAMPO, JOUNI. On convergence of transforms based on parabolic scaling. 2010. Diss.

418. TURKU. IRINA. Adsorptive removal of harmful organic compounds from aqueous solutions. 2010. Diss.

419. TOURUNEN, ANTTI. A study of combustion phenomena in circulating fluidized beds by developing and applying experimental and modeling methods for laboratory-scale reactors. 2010. Diss.

420. CHIPOFYA, VICTOR. Training system for conceptual design and evaluation for wastewater treatment. 2010. Diss.

421. KORTELAINEN, SAMULI. Analysis of the sources of sustained competitive advantage: System dynamic approach. 2011. Diss.

422. KALJUNEN, LEENA. Johtamisopit kuntaorganisaatiossa – diskursiivinen tutkimus sosiaali- ja terveystoimesta 1980-luvulta 2000-luvulle. 2011. Diss.

423. PEKKARINEN, SATU. Innovations of ageing and societal transition. Dynamics of change of the socio-technical regime of ageing. 2011. Diss.

424. JUNTTILA, VIRPI. Automated, adapted methods for forest inventory. 2011. Diss.

425. VIRTA, MAARIT. Knowledge sharing between generations in an organization – Retention of the old or building the new? 2011. Diss.

426. KUITTINEN, HANNA. Analysis on firm innovation boundaries. 2011. Diss.